Characterising Saharan Dust Sources and Export using Remote Sensing and Regional Modelling

Dissertation
zur Erlangung des Doktorgrades
der Mathematisch-Naturwissenschaftlichen Fakultät
der Christian-Albrechts-Universiät
zu Kiel

vorgelegt von

Kerstin Schepanski

Kiel, Dezember 2008

Referent: Prof. Dr. A. Macke
Koreferent/in: Dr. I. Tegen
Tag der mündlichen Prüfung: 26. Januar 2009
Zum Druck genehmigt: Kiel, 26. Januar 2009

Zusammenfassung

Die vorliegende Doktorarbeit beschäftigt sich mit dem atmosphärischen Kreislauf von nordafrikanischem Wüstenstaub. Dabei wird die Ausprägung der einzelnen Stufen Emission, Transport und Deposition während verschiedener Jahreszeiten anhand von Satellitenbeobachtungen und Modellsimulationen diskutiert.

Satellitengestützte Messungen im infra-roten (IR) Bereich des Wellenlängenspektrums sind für die Erkennung von atmosphärischem Mineralstaub über im sichtbaren stark reflektierenden Flächen wie Wüsten sehr gut geeignet. Im Rahmen der vorliegenden Arbeit wurde ein Staubindex basierend auf Messungen des SEVIRI (Spinning Enhanced Visible and InfraRed Imager) Instruments auf dem geostationären Meteosat Second Generation (MSG) Satelliten im IR Wellenlängenbreich verwendet. Basierend auf den 15-minütigen Staubindexbildern wurde eine Karte der Staubquellregionen für den Zeitraum ab 03/2006 erarbeitet. Neben der räumlichen Information mit einer $1^\circ \times 1^\circ$-Auflösung ist die Uhrzeit des Zeitpunktes der ersten Staubmobilisierung in 3-stündlichen Intervallen gespeichert.

Die raum-zeitliche Information über afrikanische Mineralstaubquellen nördlich 5° N wurden hinsichtlich saisonaler Variabilität mit Blick auf räumliche und (tages)zeitliche Variabilitäten untersucht. Saisonale Verlagerungen von Regionen häufiger Staubquellen verdeutlichen den Zusammenhang zwischen jahreszeitlich unterschiedlicher Ausprägung atmosphärischer Zirkulationsmuster und Bodenbeschaffenheiten. Die örtlichen Morgenstunden weisen mit 65 % den größten Anteil an beobachteter einsetzender Staubmobilisierung (2006/03–2008/08) auf. Einsetzende Staubemission während dieser Tageszeit deutet auf den Einfluss des bis in die bodennahen Troposphärenschichten heruntergemischten Grenzschichtstrahlstroms (engl. low-level jet (LLJ)) und der damit zusammenhängenden, kurzfristig einsetzenden Zunahme der Windgeschwindigkeit. Im Rahmen der vorliegenden Arbeit wurde die Bedeutung des LLJ für die Staubmobilisierung anhand von Beobachtungsdaten, regionaler und globaler Modellsimulierung untersucht. Modellsimulationen wurden mit dem Regionalmodell LM-MUSCAT, bestehend aus dem meso-scaligen Atmosphärenmodell Lokalmodell (LM) des Deutschen Wetterdienstes (DWD), und dem Aerosolmodul MUSCAT (MUlti-Scale Chemistry Aerosol Transportmodell) erstellt.

Mit Fokus auf Staubexport und Depositionsflüsse über der Atlantikregion wurden drei jeweils einen Monat umfassende Fallstudien gerechnet. Dabei wurden die Monate (März, Juli und Januar) so gewählt, dass sie saisonal unterschiedliche atmosphärische Gegebenheiten widerspiegeln. Im Winter wird Wüstenstaub aus der Sahara in südwestliche Richtungen und in niedrigen Troposphärenschichten transportiert, im Sommer hingegen als abgehobene Schicht in westliche Richtung. Diese saisonalen Unterschiede zeichnen sich auch in den Depositionsflüssen ab.

Abstract

The present PhD thesis aims to characterise the Saharan dust cycle at different seasons using satellite remote sensing techniques and regional modelling studies.
Basically, the dust cycle is build up by mainly three steps: 1. dust entrainment into the atmosphere, 2. dust transport, and 3. dust deposition.
Satellite remote sensing techniques applied to the infrared (IR) spectrum are suitable to detect airborne dust over at visible wavelength high reflecting surfaces like deserts. Here, a dust index based on 15-minute IR measurements provided by the SEVIRI (Spinning Enhanced Visible and InfraRed Imager) flying on-board of the geostationary Meteosat Second Generation (MSG) satellite are used to infer spatio-temporal characteristics of dust sources north of 5°N over Africa since March 2006. The time and location of dust source activation are compiled in a $1° \times 1°$ map in 3-hour time slots.
Dust source activation frequencies are used to investigate on spatio-temporal distribution of active dust sources. Seasonally changing pattern of high frequencies of activated dust sources are evident, linking changing atmospheric conditions to soil conditions suitable for dust mobilisation. The spatial distribution points towards the importance of endorheic drainage systems in mountain areas as most of North African dust sources are situated over the foothills and the break-down. The distribution of the time-of-day when dust entrainment starts points towards the break-down of the nocturnal LLJ as most important meteorological feature forcing frequently recurring dust source activation. 65 % of dust source activation events during 2006/03–2008/08 observed over North Africa occur during 06-09 UTC emphasing the importance of the LLJ break-down for dust source activation.
Detailed studies on the role and ability of the LLJ break-down for dust entrainment has been investigated using wind speed observations at synoptic stations, regional and global atmospheric simulations in addition to the satellite based DSA observations. Beside the improvement of the knowledge on the relation of LLJ occurrence and dust entrainment, the ability of global and regional models is tested to represent such an important feature for dust mobilisation with the observed frequency.
To study on step two (transport of airborne dust) and three (removal of airborne dust from the atmosphere), three case studies are performed using the regional dust emission, transport and deposition model system LM-MUSCAT consisting of the atmospheric meso-scale model *Lokalmodell* (today renamed to COSMO) provided by the German weather service (DWD) and the *MUlti-Scale Chemical Aerosol Transport* model. Each case study comprised one month representing spring, summer and winter, respectively. The model results are used to describe seasonal differences concerning dust export towards the eastern North Atlantic, transport height, transport direction and deposition, showing strong seasonal differences. In winter, the dust layer is situated at lower tropospheric levels and being transported in south-westward direction. In summer, the dust layer is found as an elevated layer, moving in westward direction.

Contents

Preface

This thesis is written cumulative and includes three scientific publication:

K. Schepanski, I. Tegen, B. Laurent, B. Heinold, and A. Macke (2007), *A new Saharan dust source activation frequency map derived from MSG-SEVIRI IR-channels*, Geophys. Res. Lett., 34, L18803, doi:10.1029/2007GL030168.

K. Schepanski, I. Tegen, M. C. Todd, B. Heinold, G. Bönisch, B. Laurent and A. Macke (2008), *Meteorological processes forcing Saharan dust emission inferred from MSG-SEVIRI observations of sub-daily dust source activation*, J. Geophys. Res., revised.

K. Schepanski, I. Tegen and A. Macke (2008), *Saharan Dust Transport and Deposition towards the Tropical Northern Atlantic*, Atmos. Chem. Phys. Discuss., 8, 16061-16096, SRef-ID: 1680-7375/acpd/2008-8-16061.

The latter publication is submitted to the journal *Atmosphere Chemistry Physics*, the last stage of the peer-review publishing process for this interactive open-access journal.

Chapter 1 will introduce the reader into the scientific topic of airborne mineral dust, Chapter 6 will give a short overview on the publications. The interested reader is referred to Chapter 2 – Chapter 5, which can be seen as additional information and give a more detailed background as it is possible in these scientific publications. However, these chapters are not essential to understand the work.

Chapter 1

Introduction on Mineral Dust

Desert areas are the main sources of atmospheric mineral dust. Worldwide, global modelling studies estimate a dust emission of 1100-5000 Tg per year (*Engelstaedter et al.*, 2006), whereby the estimates of individual studies vary strongly. According to these model estimates, around 40-70% of the global dust emission is occurring in North African deserts. Strong and frequently activated sources for mineral dust are mainly situated at subtropical latitudes, where the availability of water is limited (especially west parts of continents). There the vegetation cover is sparse and gives the impression of a dust belt. As water is one of the main limiting factors for vegetation, the arid and hyperarid climate of desert areas is commonly classified by the ratio of the mean annual precipitation and the mean annual evapotranspiration. Around 7.5% of the World's total land surface is classified as hyperarid area, around 12% is classified as arid area [UNEP Report: Dust Global Outlook, available at www.unep.org]. The Sahara desert that is strongest dust source worldwide shows highest aridity next to the Chilean-Peruvian desert.

The entrainment of mineral dust to the atmosphere is linked to the surface. Wind erosion and mobilisation of soil particles is a threshold problem, whereby wind velocity and turbulent fluxes are necessary to mobilise soil particles. This erosion process depends strongly on surface conditions. Vegetation, crusting and snow cover inhibit particle mobilisation. Consequently, for dust emission, two major conditions have to be fulfilled: (1.) Soil surface conditions suitable for dust mobilisation and (2.) appropriately high wind velocities.

Mineral dust aerosol, defined as a suspension of soil particles in a gaseous medium as the atmosphere (*Pye*, 1987) plays an important role in the weather and climate system (*IPCC*, 2007). Mineral dust is the major contributor to atmospheric aerosol (*Shao*, 2000). The atmospheric radiation budget is directly and indirectly influenced by dust particles (e.g. *Miller and Tegen*, 1999; *Sokolik and Toon*, 1996; *Tegen and Lacis*, 1996). Due to their physical, optical, chemical, and mineralogical properties mineral dust particles absorb and scatter shortwave as well as they absorb, scatter and re-emit longwave radiation at characteristic wavelengths of the radiation spectrum and consequently effect the atmospheric radiation budget directly (e.g. *Sokolik et al.*, 2001). Furthermore, atmospheric dust layers

shadow the Earth's surface by scattering and absorbing solar radiation. Less solar radiation reaches the surface leading to lower surface temperatures but the radiation absorbed by the dust layer leads to a heating within the dust layer due to thermal re-emission. Hence a redistribution of the radiative energy is evident (*Perlwitz et al.*, 2001), resulting in a stabilised vertical atmospheric column (e.g. *Heinold et al.*, 2008b; *Miller and Tegen*, 1999). In particular over dust source areas where the break-down of the low-level jet (LLJ) forces dust mobilisation frequently (*Schepanski et al.*, 2008b), the enhanced atmospheric stability inhibits the downward transport of momentum from the LLJ and therefore dust mobilisation (*Heinold et al.*, 2008b). The stability affects vertical transport and exchange processes like e.g. convection, turbulence, and baroclitiy. Furthermore, airborne dust acting as an elevated heat source is able to change the surface pressure gradient. Hence, dust aerosol impacts on atmosphere dynamics and cloud formation processes (e.g. *Hoose et al.*, 2008; *Lohmann*, 2002). Size and number distribution of cloud condensation nuclei (CCN) are limiting factors for optical properties of clouds and precipitation rates (*DeMott et al.*, 2003; *Levin et al.*, 1996; *Rosenfeld et al.*, 2001; *Sassen et al.*, 2003; *Wurzler et al.*, 2000). Mineral dust aerosol is assumed to affect this distribution by changing cloud properties. As clouds play an important role for Earth's radiation budget, dust aerosol plays an important role in this context as well.

Besides radiative effects, deposited dust provides nutrients for terrestrial and oceanic ecosystems (e.g. *Mahowald et al.*, 2005). The fertilisation efficiency of dust depends on the bio-availability of micro-nutrients provided by the particles, mainly controlled by mineralogical and chemical properties as well as by processes on the particle surface during transport (*Goudie and Middleton*, 2001; *Journet et al.*, 2008; *Luo et al.*, 2003). Mineral dust as lithogenic soil particle is characterised by the same chemical and mineralogical composition as the source area. A study on soil composition by *Wedepohl* (1995) indicate an iron content of around 4 % for North Africa, so mineral dust can be considered as a transport medium for the micro-nutrient iron (*Fung et al.*, 2000; *Jickells et al.*, 2005; *Sarthou et al.*, 2003). Additionally, lithogenic dust particles originating from the soil of its place of origin represent the mineralogical source characteristics. Hence geomorphology of source areas provides the mineralogical characteristics of the soil dust particles and therefore their efficiency for fertilisation, as well as their role as CCN and their radiative behaviour. Thus, the knowledge of dust source areas concerning location, activity and geomorphology are a necessary prerequiste for an accurate estimation of dust impact on weather, climate and ecosystems.

Increasing diseases of asthma, infections, meningitis (*Griffin and Kellogg*, 2004; *Sultan et al.*, 2005) and valley fever seem to be related to dust outbreaks. Sampled dust aerosols are often accompanied by viable fungi and bacteria which my cause allergic reactions or asthma (*Griffin and Kellogg*, 2004; *Prospero et al.*, 2005). Furthermore, dust in general impact on air quality (*Gatz and Prospero*, 1996; *Prospero*, 1999) which today comes increasing in governmental focus. From economic considerations, dust impacts on aviation and ground transportation (e.g. affected by drifting sand) (*Criado and Dorta*, 2003).

Dust is observed to be transported over long distances. North Africa as strongest source area provides largest contributions to the global atmospheric dust content. Saharan dust is transported over the Atlantic Ocean (e.g. *Chiapello et al.*, 1995; *Ellis and Merrill*, 1995; *Gatz and Prospero*, 1996; *Perry et al.*, 1997; *Prospero and Lamb*, 2003; *Prospero et al.*, 1996; *Swap et al.*, 1992), towards the Mediterranean Sea (e.g. *Avila and Penuelas*, 1999; *Moulin et al.*, 1998), and farther east (e.g. *Ganor*, 1994; *Israelevich et al.*, 2002; *Kubilay et al.*, 2000). Frequently, dust is transported towards Southern Europe (e.g. *Lyamani et al.*, 2005; *Mattsson and Nihlen*, 1996; *Rogora et al.*, 2004) and farther north towards Central and North Europe (e.g. *Bücher and Dessens*, 1992; *Coen et al.*, 2004; *Psenner*, 1999; *Ryall et al.*, 2002; *Schwikowski et al.*, 1995; *Thomas*, 1982).
Besides dust export towards the Atlantic, Mediterranean and Red Sea regions, interhemispheric transport of Saharan dust is documented in the literature. *Koren et al.* (2006) and *Boy and Wilke* (2008) describe Saharan dust transport towards the Amazonian rain forest and the Andes, respectively. In ocean ecosystems, iron acts as controlling factor for marine life (e.g. phytoplankton growth) in high-nitrate, low chlorophyll (HNLC) regions (*Mahowald et al.*, 2005; *Moore et al.*, 2006; *Neuer et al.*, 2004; *Sarthou et al.*, 2007). Furthermore, iron supplied by mineral dust is assumed to enhance nitrogen fixation. Both, fertilisation and nitrogen fixation due to dust deposition ultimately influence the CO_2-cycle coupled to the climate system (*Gao et al.*, 2001; *IPCC*, 2007; *Moore et al.*, 2006, and references therein).
Over Asia, dust frequently emitted in the Taklamakan and Gobi deserts is often transported in eastward direction towards the Pacific Ocean and farther east to North America (e.g. *Jaffe et al.*, 2003; *McKendry et al.*, 2001; *Tsai et al.*, 2008; *VanCuren*, 2003; *Wilkening et al.*, 2000; *Zhang et al.*, 2003; *Zhao et al.*, 2006). Dust emission over Asia is mostly related to troughs and strong, active cold fronts (e.g. *Goudie and Middleton*, 1992; *Littmann*, 1991; *Liu et al.*, 2004; *Qian et al.*, 2002).

The atmospheric fraction of mineral dust is investigated and observed on several ways. Measurements of atmospheric dust are performed using ground and space-borne remote sensing techniques like sun-photometer, Lidar and satellite instruments. Sampling techniques (*Prospero et al.*, 1996), deposition measurements using sediment traps or ice core records (*Kohfeld and Harrison*, 2001, and related references) are used to describe dust deposition fluxes.
The AERONET (AErosol RObotic NETwork, *Holben et al.* (1998)) sun-photometer network is a good example for a long-term global network characterising atmospheric total column aerosol. But as only total column information can be retrieved, no information is gained on emission and deposition fluxes. The observations characterise transport with regard to a single station. Furthermore, weather observation stations provide information on the presence of atmospheric dust in addition to information of the general state of the atmosphere like wind, temperature, dew-point, pressure, precipitation and visibility. As dust reduces horizontal visibility, long-term station observations have been used to conclude to dust storm activity over North Africa (*Mbourou et al.*, 1997) but also worldwide (*Mahowald et al.*, 2007). Additionally, radio sonds and drop sonds (from air planes)

provide information on the height of dust layers (e.g. *McConnell et al.*, 2008; *Ott et al.*, 1991)

The dust cycle consisting of entrainment (dust emission), transport path (height and direction) and deposition (dust removal from the atmosphere) strongly depends on atmospheric conditions during each step of the cycle. Local wind regimes force dust emission if the local threshold wind speed is exceeded and determines the dust flux into the atmosphere (*Marticorena and Bergametti*, 1995; *Shao*, 2001). Local and regional atmospheric conditions like stability and wind impact on vertical mixing, transport height and direction of the emitted dust particles. Atmospheric large-scale circulation transports the dust away from source regions. Thus, stability, transport height, size distribution of the airborne dust, clouds and precipitation are major factors for dust removal from the atmosphere, also affecting the location of deposition.
Dust emission does not occur as continuous process. It rather starts and stops when the surface winds exceed threshold conditions and fall short again. Observations show an intermittent characteristic. Airborne dust does not appear as a homogeneously distributed aerosol, although a background level of dustiness is obvious at stations downwind of desert areas (e.g. *Carlson*, 1979). Sometimes it occurs as dense dust plume, sometimes as slight dust haze at varying locations which makes it difficult to estimate dust feedback on e.g. radiation budget, cloud, precipitation and ecosystems.

For an adequate estimation of dust impacts on atmospheric processes and processes of the ecosystem, an as accurate as possible description of potential dust source areas with regard to geomorphology is necessary. Furthermore, the understanding of meteorological situations leading to frequent dust emission will help to relate dust storms to typical weather conditions and improve the adjustment of e.g. land-use in a changing environment. An improved dust forecast will also help to prevent health of millions of people living in desert areas.

To characterise dust cycle and to estimate dust feedbacks, modelling and measurement approaches have been performed during the last decades. Dust schemes have been implemented in global (e.g. GOCART (Global Ozone Chemistry Aerosol Radiation Transport) model, (*Ginoux et al.*, 2001), DEAD (Dust Entrainment And Deposition) module (*Zender et al.*, 2003)) and regional scale atmospheric models (e.g. DREAM (Dust REgional Atmospheric Model) (*Nickovic et al.*, 2001; *Pérez et al.*, 2003), CHIMERE-Dust model (*Menut et al.*, 2007), LM-MUSCAT (*Heinold et al.*, 2007)) to estimate the amount of dust emission, major dust transport paths, dust residence time within the atmosphere and deposition fluxes (e.g. *Ginoux et al.*, 2001; *Tegen and Fung*, 1994; *Weaver et al.*, 2001). The radiative feedback of dust leading to either warming or cooling of the net effect is estimated in recent literature, using global (e.g. *Perlwitz et al.*, 2001; *Tegen and Lacis*, 1996) and regional scale models (e.g. *Heinold et al.*, 2007; *Pérez et al.*, 2003). Such models must be validated against a range of observational data.

To improve our understanding of dust feedback to the environment, several measurement campaigns have been performed during the last decades. E.g., the BODEX (BODélé EXperiment) in 2005 studied on the process of dust entrainment. It carried out at the Bodélé Depression in Chad, often referred as "World's dustiest place" (*Todd et al.*, 2007, 2008; *Washington and Todd*, 2005; *Washington et al.*, 2006a,b). The AMMA (African Monsoon Multidisciplinary Analysis, *Redelsperger et al.* (2006)) campaign investigates dust and monsoon relations using a wide field of measurement set-ups, modelling and remote sensing techniques with the aim to improve the knowledge on West African Monsoon circulation and its influence on a regional and global environment. Besides the SHADE (SAHaran Dust Experiment, *Haywood et al.* (2003)) campaign in September 2000, the SAMUM (SAharan Mineral dUst experiMent, Tellus Special Issue, 61B(1), 2009) project focuses on the optical properties and radiative impact of Saharan dust particles. Thereby, the SAMUM-I campaign in May 2006 in Morocco determines optical and mineralogical properties of dust particles at near source regions. SAMUM-II in January/February 2008 was located at the Cape Verde Islands, suitable to study aged dust in an environment polluted with soot from biomass burning. The mixing of dust and biomass burning aerosol was also a topic of DABEX (Dust And Biomass EXperiment, *Johnson et al.* (2008)). Thereby, measurements have been performed during January and February 2006 near Niamey over the Sahel. The DODO-Experiment (Dust Outflow and Deposition to the Ocean) investigates Saharan dust export and deposition to the Atlantic using aircraft measurements based in Dakar, Senegal (*McConnell et al.*, 2008). In addition to studies on optical properties, the role of dust within the oceanic ecosystem is investigated by the SOPRAN (Surface Ocean PRocess in the Anthroprocene, http://sopran.pangaea.de) project embedded to the SOLAS (Surface Ocean – Lower Atmosphere Study, http://www.uea.ac.uk/env/solas) project frame. Besides African dust, Asian dust is in the focus of recent experiments like the ACE-Asia (Aerosol Characterization Experiment) project in 2001 and the PACDEX campaign (PACific Dust EXperiment, http://www.eol.ucar.edu/projects/pacdex/), which investigate Asian dust and pollutants transported to the Pacific. Such field studies provide information on specific short-term dust events.

Remote sensing methods are used to characterise atmospheric dust, but also to localise dust source areas over arid and semi-arid terrain (e.g. *Prospero et al.*, 2002; *Schepanski et al.*, 2007; *Zender and Newman*, 2003) following different approaches. Spectrometers on-board low orbiting space crafts like the Franco-American A-Train chain of sun-synchronous orbiting Earth observation satellites (in 2008 consisting of Aqua, Aura, Parasol, CALIPSO and CloudSat) show high spatial resolution of a single sample, but due to its relative narrow viewing field ($13\,\mathrm{km} \times 25\,\mathrm{km}$ for OMI (Ozone Monitoring Instrument) on-board NASA Aura space craft), at least one day is needed to cover the whole Earth by composing the meridional swathes (paths) of the satellites. Compared to single-viewing instruments like OMI, MODIS (MODerate resolution Imaging Spectrometer) or SEVIRI (Spinning Enhanced VIsible InfraRed Imager), multi-viewing instruments such as MISR (Multi-angle Imaging SpectroRadiometer) or MERIS (MEdium Resolution Imaging Spectrometer) are limited for dust retrievals by a relative coarse resolution (*Kahn et al.*, 2007).

To retrieve information on the vertical structure of atmospheric dust plumes, the vertical atmospheric column can be remotely observed by e.g. sondes or LIDAR instruments. Since 2006, CALIOP (Cloud-Aerosol Lidar with Orthogonal Polarization) is flying onboard CALIPSO (Cloud Aerosol Lidar and Infrared Pathfinder Satellite Observation) measuring vertical atmospheric profiles. This profiles containing information on vertical dust distribution are also used to assimilate models or to reduce the height dependency in aerosol retrievals. Furthermore, dust export paths e.g. from the Sahara towards the Atlantic are estimated (*Liu et al.*, 2008). But for spatio-temporal dust source characterisation, CALIPSO measurements are not suitable due to its narrow viewing-field and the resulting low spatio-temporal resolution. For dust source observation covering continental scale areas, relatively high spatial and temporal resolutions are required.
Aerosol optical thickness (AOT) retrievals applied to the visible part of the spectrum cannot be used for dust source determination over bright surfaces like in arid and hyperarid areas. For dust source analysis based on space-borne dust detection, dust aerosol algorithms as the OMI Aerosol index (AI), Deep Blue and infrared (IR) techniques are applicable. But due to their daily (or less) resolution the diurnal characteristic from polar-orbiting instruments like OMI and MODIS and accurate location of dust sources is difficult for an area like the Saharan desert, where dust source activations occur during the morning hours (*Schepanski et al.*, 2008b) and the sun-synchronous orbiting satellite overpasses around noon. Daily maps of airborne dust index like the TOMS/OMI AI are often used to retrieve dust source areas (e.g. *Prospero et al.*, 2002). *Prospero et al.* (2002) and *Washington et al.* (2003) relate high frequencies of high dust index values to the location of dust source areas. *Brooks and Legrand* (2000) follow a similar approach relating high mean values of the daily Infrared Difference Dust Index (IDDI) to dust source areas. *Grini et al.* (2005) assume relation between surface reflectivity and soil types suitable to act as dust source. All these approaches are applied to satellite retrievals that are available at daily resolution at best. Furthermore, the accuracy of the applied dust detection algorithms is limited by the ability of the space-borne instrument, which is characterised by sampling interval, orbital parameter and wavelength spectrum. Therefore, daily products are used and applied to statistical methods. Sub-daily processes as dust mobilisation and variabilities in transport cannot be resolved by applying daily retrievals. To have a more detailed understanding in dust source areas and mobilisation processes, observations on a higher temporal resolution are required. When comparing to sub-daily dust index products, a strong transport component in wind direction is evident, biasing the retrieved location of assumed dust sources (*Schepanski et al.*, 2007).

Geostationary satellites provide observations on a high temporal resolution such as the European Meteosat Second Generation (MSG) satellite. Due to its geostationary location, measurements are provided for the whole viewing field at one scanning sequence. The viewing field of the MSG SEVIRI (Spinning Enhanced Visible and InfraRed Imager (*Schmetz et al.*, 2002)) instrument covers the Arabian Peninsula, the Middle East, Africa, Europe, Eurasia and the Atlantic Ocean.

The high spatio-temporal resolution of MSG SEVIRI observations motivates an analysis of Saharan dust source activity (*Schepanski et al.*, 2007). A detailed characterisation of dust source activity improves the understanding of dust source distributions. Furthermore the knowledge on temporal distribution of dust source activity helps to identify meteorological situations that may provide atmospheric conditions suitable for dust mobilisation (*Schepanski et al.*, 2008b). Satellite observations are not able to quantify dust emission process itself. Only the fact, that dust was mobilised can be indicated by satellite indices. Monitoring times-of-day when dust mobilisation starts for each source location indicate recurring atmospheric conditions leading to dust source activations at this location. To investigate such recurring meteorological conditions, meso-scale model studies are a good enhancement (*Schepanski et al.*, 2008b).

Neither ground-based measurements, remote sensing nor modelling are able to describe all aspects of the dust cycle by itself. But in combination the information from each approach can complement each other and lead to a more accurate understanding and description of the global dust cycle. In the present work, the Saharan dust cycle is described using satellite remote sensing techniques, sun-photometer data, observations of weather stations and regional modelling. The work was performed in the frame of the network project TRACES (Ocean – Atmosphere – Land Impacts on TRopical AtlantiC EcoSystems) funded by the Wissenschaftsgemeinschaft Gottfried Willhelm Leibniz. The project investigates the transport of soil lithogenic matter towards the tropical Atlantic and its role in the ecosystem.

The present thesis is structured as following: First an overview on the Saharan dust cycle in Chapter 2 including dust emission, transport and deposition processes, and an introduction in the meteorological aspects forcing mineral dust emission in Chapter 3 will be given. Then Chapter 4 and Chapter 5 and will describe the methods used in this work: Satellite remote sensing and regional modelling. Results of this work will be given in Chapter 6 by three scientific publications, comprising the third part of the thesis. This thesis will conclude with an outlook given in Chapter 7.

Following scientific papers are published in the frame of this thesis:

K. Schepanski, I. Tegen, B. Laurent, B. Heinold, and A. Macke (2007), A new Saharan dust source activation frequency map derived from MSG-SEVIRI IR-channels, Geophys. Res. Lett., 34, L18803, doi:10.1029/2007GL030168.

> This publication presents a newly developed map of Saharan dust source areas inferred from 15-minute MSG SEVIRI IR dust index observations. The dust index is validated in terms of its sensitivity to detect airborne dust. A comparison of the newly derived dust sources with the commonly used approach that relates high frequencies of a dust-indicating aerosol index to dust source areas is performed showing a strong impact of dust wind transport component in

dust source areas derived from daily dust retrievals. In addition, the new compiled map of dust sources is used in simulations of dust emission and transport with the regional model system LM-MUSCAT. An improvement of dust distribution can be shown when utilising the new map compared to earlier results.

K. Schepanski, I. Tegen, M. C. Todd, B. Heinold, G. Bönisch, B. Laurent and A. Macke (2008), Meteorological processes forcing Saharan dust emission inferred from MSG-SEVIRI observations of sub-daily dust source activation, J. Geophys. Res., revised.

Dust entrainment to the atmosphere can be considered as a wind threshold problem, linking atmospheric and soil conditions. In this publications, the meteorological role for frequent dust mobilisation is investigated using spatio-temporal dust source analysis as introduced in *Schepanski et al.* (2007), wind measurements performed at synoptic stations, global and regional scale modelling. 65 % of Saharan dust source activation events are obseved during the local morning hours, pointing towards the frequent recurring meteorological process of the break-down of the low-level jet (LLJ). Here, the ability of the LLJ break-down as mechanism for frequent dust emission is the major focus.

K. Schepanski, I. Tegen and A. Macke (2008), Saharan dust transport and deposition towards the Tropical Northern Atlantic, Atmos. Chem. Phys. Discuss., 8, 16061-16096, SRef-ID: 1680-7375/acpd/2008-8-16061.

A modelling study using the meso-scale dust emission and transport model LM-MUSCAT is performed to characterise seasonally changing strength and extension of the Saharan dust cycle. Three case studies are computed, each comprising an one month period representing different seasons (spring, summer, winter). Horizontal and vertical distributions of atmospheric dust concentrations indicate a clear seasonality concerning height and direction of dust transport. Furthermore, the contribution of dust originating from the Bodélé depression, the strongest emitting Saharan dust source area, is estimated.

The latter publication is submitted to the journal *Atmosphere Chemistry Physics*, the last stage of the peer-review publishing process for this interactive open-access journal.

Moreover, during the here presented work several publications have been written in collaboration with members of working groups at different institutes. In the following, this peer-review publications will be listed, but not discussed in detail.

W. Birmili, **K. Schepanski**, A. Ansmann, G. Spindler, I. Tegen, B. Wehner, A. Novak, E. Reimer, I. Mattis, K. Müller, E. Brüggemann, T. Gnauk, H. Herrmann, A. Wiedensholer, D. Althausen, A. Schladitz, T. Tuch, G. Löschau (2008), A case of extreme particulate matter concentrations over Central Europe caused by dust emitted over the southern Ukraine, Atmos. Chem. Phys., 8, 997-1016.

C. Cavazos, M. C. Todd, **K. Schepanski** (2008), Numerical model simulation of the Saharan dust event of March 2006, J. Geophys. Res., revised.

B. Heinold, I. Tegen, **K. Schepanski**, O. Hellmuth (2008), Dust Radiative Feedback on Saharan Boundary Layer Dynamics and Dust Mobilization, Geophys. Res. Lett., 35, L20817, doi:10.1029/2008GL035319.

L. Klüser and **K. Schepanski** (2008), Remote sensing of mineral dust with MSG inferred channels: A new Bitemporal Mineral Dust Index, submitted to Remote Sens. Environ.

F. Reinfried, I. Tegen, B. Heinold, O. Hellmuth, **K. Schepanski**, U. Cubasch, H. Huebener, P. Knippertz, Simulations of convectively-driven density currents in the Atlas region using a regional model: Impacts on dust emission and sensitivity to horizontal resolution and convection schemes, J. Geophys. Res., revised.

R. Washington, C. Bouet, G. Cautenet, E. Mackenzie, I. Ashpole, S. Engelstaedter, G. Lizcano, G. Henderson, **K. Schepanski**, I. Tegen (2008), Dust as a Tipping Element: The Bodélé Depression, Chad, PNAS, revised.

B. Heinold, I. Tegen, M. Esselborn, K. Kandler, P. Knippertz, D. Müller, A. Schladitz, M. Tesche, B. Weinzierl, A. Ansmann, D. Althausen, B. Laurent, A. Massling, T. Müller, **K. Schepanski**, A. Wiedensohler (2009), Regional Saharan Dust Modeling during the SAMUM 2006 Campaign, Tellus, 61B(1), in press.

P. Knippertz, A. Ansmann, D. Althausen, D. Müller, M. Tesche, E. Bierwirth, T. Dinter, T. Müller, W. von Hoyningen-Huene, **K. Schepanski**, M. Wendisch, B. Heinold, K. Kandler, A. Petzold, L. Schütz, I. Tegen (2009), Dust Mobilization and Transport in the Northern Sahara during SAMUM 2006 – A Meteorological Overview, Tellus 61B(1), in press.

Chapter 2

Saharan Dust Cycle

2.1 Dust Mobilisation: A Threshold Phenomenon

Dust mobilisation is limited by surface characteristics and surface wind velocity. Observations and laboratory experiments show a non-linear relation between the number and size distribution of mobilised dust and the surface wind velocity (*Bagnold*, 1941). Furthermore, dust mobilisation only occurs for wind velocities higher than a certain local threshold. Physically, dust mobilisation is described by processes setting soil particles in motion, either in horizontal or vertical direction. Therefore, momentum is transferred due to wind or collision with adjacent particles. The magnitude of transferred momentum, particle gravitation and interparticle cohesion forces comprising van der Waals, electrostatic, capillary and chemical binding forces are factors limiting whether a particle starts moving or remains at rest. In general, dust emission can be determined by the balance of gravitational, cohesive and aerodynamic forces (*Shao*, 2001). As particle mobilisation depends on the momentum transfer from the air to the erodible soil elements, energy transfer can be described by the surface wind shear stress $[kg\,m^{-1}s^{-2}]$,

$$\tau = \rho_a u_\star^2, \tag{2.1}$$

with ρ_a being the air density $[kg\,m^{-3}]$ and $u_\star$ the wind friction velocity $[m\,s^{-1}]$,

$$u^\star = U_0 \kappa \ln\left(\frac{z}{z_0}\right)^{-1}, \tag{2.2}$$

with the von Karman constant κ, the roughness length z $[m^{-1}]$, the surface roughness length z_0 $[m^{-1}]$ and the surface wind velocity U_0 $[m\,s^{-2}]$. This relationship is valid for neutral stability conditions. The threshold wind friction velocity $u_{\star,t}$ $[m\,s^{-1}]$ be exceeded for dust particle mobilisation depends on particle diameter D_p $[m]$ (Figure 2.1), particle density ρ_p and air density ρ_a, according to the equation

$$u_{\star,t} = A\sqrt{\frac{\rho_p g D_p}{\rho_a}}, \tag{2.3}$$

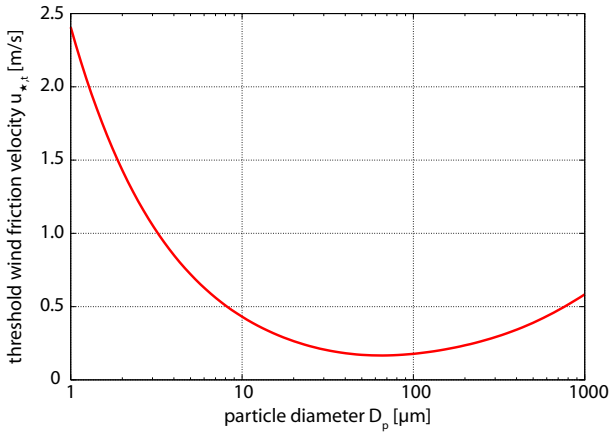

Figure 2.1: *Threshold wind velocity for particle mobilisation depending on particle size. For small particles cohesive forces are dominant and inhibit particle mobilisation for low wind friction velocities. For large particles the threshold wind friction velocity increases again due to increasing gravitational forces. After Marticorena and Bergametti (1995).*

with the gravitational constant g $[m\,s^{-2}]$ and a threshold parameter A depending on the friction Reynolds number (*Marticorena and Bergametti*, 1995). $u_{\star,t}$ is small for dry and sparse vegetated sandy surfaces. Therefore, the most important dust sources are situated over such areas. Over semi-arid and arid areas wind velocities of at least around $6\,m\,s^{-1}$ are necessary to mobilise dust particles (*Bouet et al.*, 2007; *Tegen and Lacis*, 1996; *Todd et al.*, 2007). As wind provides momentum, and soil characteristics require a minimum of transferred energy for mobilisation, both, wind and soil characteristics are the main limiting factors to describe dust mobilisation. Both, $u_{\star,t}$ and $u_{\star}$ depend on several factors such as atmospheric conditions, soil type, soil texture, and topographical forcing e.g. turbulence by windbreaks (*Shao*, 2000).

The soil surface can be described by vegetation cover, roughness elements (e.g. rocks, stones, pebbles), soil texture (e.g. coarse, medium, fine sand, silt, clay) and soil moisture content. On the one hand these parameters limit the erodibility of the surface and on the other hand the momentum flux required for particle mobilisation is a limiting factor (*Gillette*, 1979; *Marticorena and Bergametti*, 1995). Soil surfaces are a mixture of different-sized particles following a size distribution according to the local geomorphological conditions. Both, gravitational and cohesion forces are size-dependent and are described by the soil surface characteristics. Cohesion forces depend on mineralogical composition of the soil. E.g., clay particles show higher cohesion forces than quartz particles in the same size range. The progress of mobilised particles depends on buoyancy and gravitational forces, influenced by particle weight and aerodynamic drag. To describe the momentum flux from the atmosphere to the soil, relations between wind friction velocity and dust flux have been assumed. A relation between wind friction velocity and size distribution of mobilised particles is obvious (*Marticorena and Bergametti*, 1995).

Bagnold (1941) proposed to classify three main types of particle motion (Figure 2.2): *suspension* for the finest particles with diameters smaller than $60\,\mu$m, *saltation* for particles

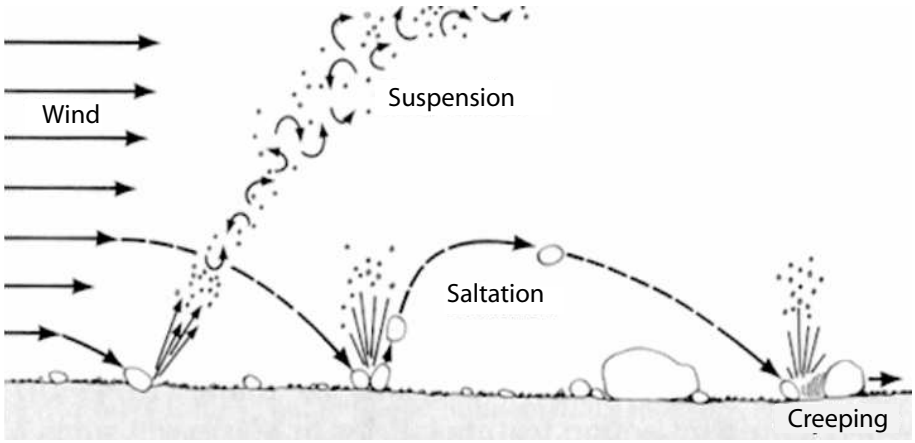

Figure 2.2: *Classification of particle motion (Bagnold, 1941), modified from http://www.lmfa.ec-lyon.fr*

larger than 60 μm but smaller than 2000 μm and *creeping* for particle elements larger than 2000 μm. Depending on particle size and factors like wind, stability, and precipitation rate, a certain residence time for dust particles can be assumed (*Duce*, 1995).

Suspension or aerodynamic entrainment
Finest particles ($< 60\,\mu$m) are small enough to be transported upward by turbulent eddies and aerodynamic forces (*Shao*, 2001). Gravity forces diminish mobilisation of particles larger than 2000 μm. Fine particles are difficult to mobilise due to interparticle cohesive forces. Dust flux due to direct aerodynamic entrainment is low (*Loosmore and Hunt*, 2000). Once mobilised, fine particles are able to remain in the atmosphere for long times and can be transported over long distances far away from their source regions by large scale circulation pattern (e.g. *Mahowald et al.*, 2003; *Prospero et al.*, 1981, 1996; *Riemer et al.*, 2006). Desert dust, associated with particle diameters smaller than 60 μm are observed to cross the oceans within elevated air layers (e.g. *Arimoto et al.*, 1997; *Barkan et al.*, 2004; *Goudie and Middleton*, 2001; *Prospero et al.*, 1981, 1996).

Saltation (bombardment)
Due to the sandblasting behaviour, a disaggregation of fine and coarse particles can be observed (*Zender et al.*, 2003). Particles with diameters in the range of 60 to 100 μm are most suitable for mobilisation (*Bagnold*, 1941; *Iversen and White*, 1982). But due to gravitational forces, the particles settle down within a few minutes or hours (*Duce*, 1995). Saltation is the main and most efficient process for dust mobilisation and due to its sandblasting behaviour also fine particles are emitted (e.g. *Grini et al.*, 2002; *Marticorena and Bergametti*, 1995; *Shao et al.*, 1993, 1996).
Particles lifted by surface winds with diameters in the rage of 60 to 2000 μm reach heights of a few decimetre up to 1-2 m (*Marticorena and Bergametti*, 1995; *Pacyna*, 1995). To remain in the atmosphere, gravitational forces related to the particle weight, and buoyancy forces impacted by upward motion and aerodynamic drag, have to be at least in

an equilibrium. Particles larger than 60 μm fall back to the ground near the source area. Momentum from the air is transferred to soil particles that are lifted and deposited down again by gravitational settling, where it may mobilise smaller particles by impaction.

Creeping
Soil particles larger than 2000 μm were too heavy for up-lifting, but wind momentum is able to set these particles in horizontal motion by shear forces. This motion is called creeping.

In the recent literature several formulations and approaches describing dust mobilisation processes mathematically exists (e.g. *Marticorena and Bergametti*, 1995; *Shao*, 2001; *Zender et al.*, 2003). Commonly, the dust flux F is separated into a horizontal and vertical component. Taking sandblasting linking the horizontal dust flux F_h $[kg\,m^{-1}\,s^{-1}]$ to the vertical flux F_v $[kg\,m^{-2}\,s^{-1}]$ into account, the dust flux can be approximated by Equation 2.4 and 2.5, representing the non-linear relation between dust flux and wind velocity (Figure 2.3). Here, the sandblasting efficiency is expressed by the soil type depending factor α $[m^{-1}]$.
Vertical dust flux:

$$F_v = \alpha F_h, \tag{2.4}$$

Horizontal dust flux:

$$F_h = \frac{\rho_a}{g} u_\star^3 \left(1 + \frac{u_{\star,t}(D_p)}{u_\star}\right)\left(1 - \frac{u_{\star,t}^2(D_p)}{u_\star^2}\right) \tag{2.5}$$

Beside $u_\star$ and $u_{\star,t}$, the dust flux is determined by the effective surface area covered by vegetation and snow and the surface soil moisture content. Vegetation and snow cover prevent dust mobilisation.
The amount of particles set into motion due to sandblasting depends on particle size distribution and the mineralogical composition. Consequently, different sandblasting efficiencies have to be assumed for different soil types as shown by wind tunnel experiments (e.g. *Gillette*, 1978) and field experiments (e.g. *Shao et al.*, 1996). Dust emission occurs when all limiting factors allow for wind erosion. However, it can be imagined that spatial and temporal variability in dust source areas is evident, mainly related to varying local soil characteristics (i.e. vegetation cover in semi-arid areas) and atmospheric conditions.

2.2 Dust Transport

Dust mixed up into the atmosphere is transported within local wind regimes, regional- and large-scale circulation pattern. Dust transport depends on, the height up to which the dust is mixed. Dust particles larger than 60 μm are removed from the atmosphere by dry deposition in less than one day (*Duce*, 1995) in the absence of precipitation and cloud interactions. Larger particles (60 - 2000 μm) fall out near the source area and particles are situated at lower tropospheric levels. Only small particles ($< 60\,\mu$m) can be mixed

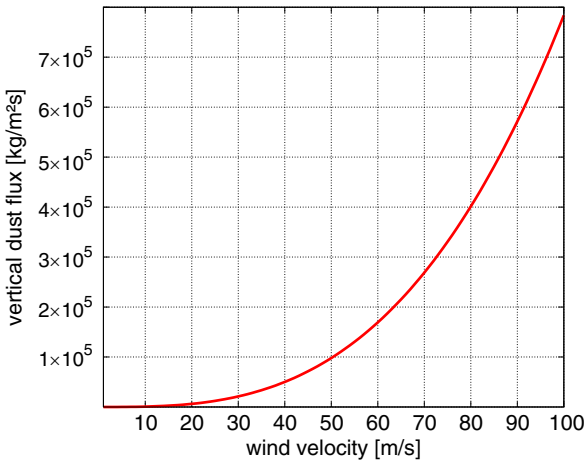

Figure 2.3: *Relation of vertical dust flux and surface wind velocity, after Marticorena and Bergametti (1995).*

over the entire boundary layer depth due to turbulent fluxes and can remain within the atmosphere for several days (*Duce*, 1995). During this time, the dust aerosol is embedded in the transport of the air mass. Vertical turbulent fluxes determine the mixing height and therefore the vertical extent of the dust layer. Local wind regimes, impacted by surface conditions like topography and roughness elements (e.g. vegetation, rocks, stones) transport the dusty air layers away from the source area. On a larger scale, local wind regimes are impacted by regional and large-scale circulation pattern, which gain influence on the dust transport. During transport, the height of the dust layer changes due to air mass properties. This leads either to elevation or subsidence, which in terms determines whether the dust layer is more impacted by larger-scale circulation pattern or local scale conditions. Particles being mixed into upper tropospheric levels are able to remain within the atmosphere for 1-2 weeks (*Duce*, 1995) and will be influenced by general circulation regimes of the atmosphere (e.g. *Mahowald et al.*, 2003; *Prospero et al.*, 1996; *Riemer et al.*, 2006).

The Sahara as World's largest dust source contributes the largest fraction to the atmospheric dust content and shows seasonal varying transport pattern with regard to amount and pathway. The wind regimes are important for transport directions, air mass characteristics like moisture content and temperature are important especially for transport height. Additionally, the seasonality of the dust source activity affects the dust export as it adjusts the local and temporal distribution of source areas and the emitting dust flux. Saharan dust export towards the tropical and subtropical North Atlantic is mainly influenced by

1. spatial distribution of activated dust source areas,
2. predominant regional wind regimes,
3. boundary layer heights, and
4. precipitable clouds controlling atmospheric wash-out and rain-out of dust.

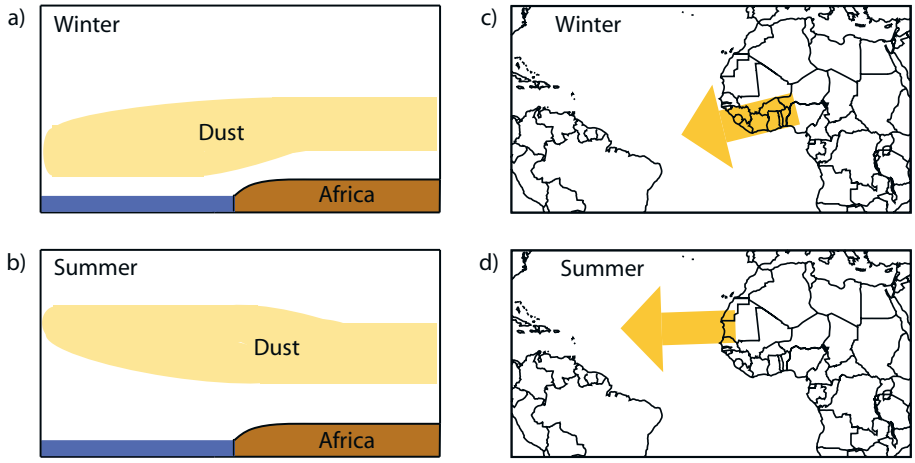

Figure 2.4: *Schematics of Sahran dust export towards the tropical North Atlantic with regard to main transport height and direction. The image is taken from Schepanski et al. (2008a). In winter, a south-westward wind regime is dominant and transport dust towards South America. In summer, westward winds transport dust towards the Caribbean. Additionally, dust source activity changes with seasons. In winter, the Bodélé area is the most activ dust source area, while West African dust sources are dominant in summer (Schepanski et al., 2007).*

After dust mobilisation, upward mixing leads to a specific vertical distribution of atmospheric dust, influenced e.g by particle size distribution and atmospheric stability. Boundary layer dynamic is responsible for the (homogeneous) vertical distribution of dust and the height of the top of the dust layer which is important for transport. First, a new dust layer is transported by local wind regimes within the boundary layer (BL) because the inversion at the top of the daytime boundary layer inhibits a vertical mixing over the entire troposphere. During night, convective turbulence due to insolation creases and a shallow boundary layer develops within the height of the former daytime boundary layer. The layer between the former top of the daytime boundary layer and the top of the nocturnal boundary layer is called residual boundary layer. In case of a strong vertical mixing during daytime and consequently a deeper daytime boundary layer, dust is trapped within the residual layer (*Kalu*, 1979). During night, a nocturnal low-level jet (LLJ) can develop under suitable conditions, at the top of the nocturnal boundary layer. This low-level wind speed maximum transports the dust layer away from the source region (e.g. *Westphal et al.*, 1987). When a strong daytime boundary layer develops dust again is mixed down from the former residual layer. Otherwise, the dust remains as an enclosed layer within the atmosphere. On the one hand, during step-wise coupling dust layer to the daytime boundary layer and decoupling to a residual layer, a dust layer can either lost dust load due to daytime turbulent downward mixing. On the other hand, it can be rapidly transported during night within the nocturnal LLJ. By reaching areas with daytime boundary layer depth below the level height of the dust layer, dust can become detached and remains for a long time in the atmosphere, and thus can be transported over long distances. Depending on the seasons, boundary layer depths change and so does the transport height of dust layers entering the tropical North Atlantic (Figure 2.4). Consequently, transport paths

of Saharan dust layers towards the Atlantic depend on the seasons (Figure 2.4), mainly related to the position of the inter-tropical convergence zone (ITCZ) and of strength and direction of the trade winds (*Engelstaedter et al.*, 2006; *Mbourou et al.*, 1997; *Moulin et al.*, 1997).
Interannual variability of dust transport across the Atlantic is proposed to be related to the North Atantic Oscillation (NAO) (*Hurrell*, 1995; *Jones et al.*, 1997) and is investigated by several studies using satellite data (e.g. *Chiapello and Moulin*, 2002; *Chiapello et al.*, 2005; *Evan et al.*, 2006; *Moulin et al.*, 1997; *Riemer et al.*, 2006), in-situ measurements (e.g. *Mahowald et al.*, 2003; *Moulin et al.*, 1997) and global modelling (e.g. *Ginoux et al.*, 2004). The NAO is build up by two centrers of action, the Icelandic Low and the Azores High. To characterise the variability of the NAO, an index is defined by from the normalised difference between atmospheric pressure at sea-level at stations near to the two centres of action: Stykkisholmur, Iceland and Lisbon, Portugal (*Hurrell*, 1995). *Jones et al.* (1997) use the standardised pressure difference between Iceland and Gibraltar instead. A strengthening of the Azores high and thus a northward shift of the westerly winds occurs for positive phases of the NAO. The trade winds are strengthened and shifted (*Chiapello and Moulin*, 2002; *Chiapello et al.*, 2005), dryer conditions (*Moulin et al.*, 1997) and strong Harmattan surges due to a strong Azores high occur (*Knippertz and Fink*, 2006) leading to increased dust mobilisation over North Africa. Furthermore, patterns of wind and precipitation related to the NAO control dust transport across the Atlantic, especially during winter.
The variability of Saharan dust outbreaks towards the tropical Atlantic during northern hemispheric summer is assumed to be modulated by African Easterly Waves (AEW) (e.g. *Jones et al.*, 2003, 2004; *Prospero and Nees*, 1986; *Prospero et al.*, 1981). AEW are synoptic-scale disturbances of the middle-level African Easterly jet (AEJ), which is build up by the thermal gradient between high temperatures over the Sahara desert and lower temperatures over the Gulf of Guinea (e.g. *Thorncroft and Blackburn*, 1999).

Enclosed Saharan dust layers propagating towards the North Atlantic are often refereed to as Saharan Air Layer (SAL) (e.g. *Dunion and Velden*, 2004) and are observed to extend over a large area of the North Atlantic far west to the West Indies (*Carlson and Prospero*, 1972). The dusty air layer can be identified by very low relative humidity, high optical opacity and high potential temperatures. The layer is separated by a strong vertical inversion. During north hemispheric summer, the SAL is located above the trade wind layer at a height of up to 5–7 km (*Chiapello et al.*, 1997; *Dunion and Velden*, 2004; *Kalu*, 1979), during winter, the SAL is embedded in the trade wind layer at levels below 1.5–2 km (*Barkan et al.*, 2004; *Chiapello et al.*, 1997). In summer, the Saharan dusty air overlays the moist, denser monsoon air, reaches the Atlantic and crosses the ocean embedded within the westward winds as enclosed layer. The marine BL is relative shallow compared to the continental BL. When reaching the warm, West Atlantic, the SAL extends downward into the marine BL due to sedimentation of dust particles (*Karyampudi et al.*, 1999). Furthermore, deep moist convection strong enough to penetrate through the BL inversion and strong vertical wind shears due to the middle-level easterly jet is able to mix dust from

the SAL downwards (*Karyampudi et al.*, 1999). To cross the Atlantic, times of around one week (5-7 days) are derived from satellite imaginary (e.g. *Carlson and Prospero*, 1972; *Ott et al.*, 1991), dust plume tracking by atmospheric soundings, and the time of arrival of dust-laden air at different stations along the transport pathway (*Prospero et al.*, 1981).
Beside dust export towards the North Atlantic, Saharan dust is transported towards the Mediterranean Sea and farther to South, Central and North Europe (e.g. *D'Almeida*, 1986; *Franzen et al.*, 1994; *Guerzoni et al.*, 1997). The Sharav Cyclone, a lee-cyclone enhanced by baroclinity counts for several dust storms observed over the Mediterranean coast and Middle East (*Alpert and Ziv*, 1989; *Alpert et al.*, 1990).

Dust transport paths give information on areas where the dust can be expected to settle down, which is e.g. important for economical (e.g. aviation and ground transportation), governmental (e.g. air-quality restrictions), health and fertilisation aspects. During atmospheric transport, dust particle surface may change concerning physical, optical and chemical characteristics. (Photo)-chemical processes under dry or aqueous (e.g. in presence of clouds or moist air) conditions as well as reactions due to adsorption of soot and pollutants (e.g. sulphur) occurs, depending on the transport path in relation to clouds or emitted pollutants (e.g. biomass burning, industry, aviation, shipping) (e.g. *Erel et al.*, 2006; *Meskhidze et al.*, 2003). Changing particle characteristics may change particle–radiation interactions, the bio-availability of micro-nutrients delivered by dust or the hygroscopic properties important for particle–cloud interactions (e.g. *Fan et al.*, 2006; *Johansen et al.*, 2000; *Meskhidze et al.*, 2005).

2.3 Dust Deposition

The removal of dust from the atmosphere is described by the deposition, separated into dry and wet deposition. The former is related to turbulent diffusion and gravitational settling. The latter is described by scavenging processes like rain wash-out or in-cloud scavenging (removal of dust particles by cloud droplets).
Whether dust particles remain in the atmosphere or settle down can be described by the relation of particle upward and downward motions. Due to their weight, gravitational forces lead to a downward motion. Turbulent eddies as well as Brownian diffusion have either upward or downward components of vertical motions intensifying or diminishing buoyancy effects of drag forces. Turbulent transfer, Brownian diffusion, impaction, interception, gravitation and particle rebound have to be considered. A simple description of the forces acting on aerosol particles within a fluid like the atmosphere are given by Newton's gravitation law (left term of Equation 2.6) for friction consideration and the Stokes equation describing the flow within a viscose medium with relation to drag, viscosity and particle velocity (right term of Equation 2.6). Equilibrium between gravitational and frictional forces leads to the equation

$$\frac{g\pi D_p^3 \left(\rho_p - \rho_a\right) C_c}{6} = 3\pi\eta D_p v_g, \tag{2.6}$$

with the gravitational constant g $[m\,s^{-2}]$, particle diameter D_p $[m]$, particle density ρ_p $[kg\,m^{-3}]$, air density ρ_a $[kg\,m^{-3}]$, Cunningham slip correction factor C_c, dynamic viscosity of air η $[kg\,m^{-1}\,s^{-1}]$ and the gravitational settling velocity v_g $[m\,s^{-1}]$. Gravitational settling is commonly described by the terminal settling velocity v_g, derived from Equation 2.6 describing the terminal fall velocity of a particle

$$v_g = \frac{(\rho_p - \rho_a)\, g D_p^2 C_c}{18\eta}. \tag{2.7}$$

The Stokes law considers the velocity of the air surrounding the dust particles relative to the particle itself as zero. This assumption is correct in continuum but not for particles larger than the mean free path λ of air molecules. So the Cunningham slip correction factor C_c is used to apply the Stokes law for larger particles. The experimentally determined relation

$$C_c = 1 + \frac{2\lambda}{D_p}\left[1.142 + 0.558\exp\left(-\frac{0.4995 D_p}{\lambda}\right)\right] \tag{2.8}$$

is a function of the particle diameter D_p and the mean free path λ $[m]$ of air molecules and is proposed by *Allen and Raabe* (1982, 1985). The quotient $\frac{2\lambda}{D_p}$ expresses the Knudsen Number, a measure for the density of the flow. Mineral dust particles are the product of soil erodible processes and consequently non-spherical particles with irregular surface structures. To take different settling velocities of spherical and irregular particles into account, an equivalent aerodynamic diameter, Stokes diameter or volume equivalent diameter is defined, adjusted to Stokes Equation by a shape factor. The aerodynamic diameter is described by the diameter of a spherical particle with the density of $\rho_0 = 1000\,kg\,m^{-3}$. The artificially created particle is characterised by the same sedimentation velocity v_g as the particle of interest. The Stokes diameter denote the diameter of a spherical particle having the same density and sedimentation velocity as the particle of interest. Finally, the volume equivalent diameter indicates the diameter of a spherical particle with the same volume as the non-spheric particle of interest.

Dry deposition is separated for large particles ($D_p > 2\,\mu m$) and small particles ($D_p < 2\,\mu m$). Large particle deposition is dominated by the gravitational settling, small particles are additionally affected by the surface resistance R_s and aerodynamic resistance R_a accounting for turbulent deposition. The aerodynamic resistance determines the heat and water vapour transport due to evaporation from the surface into the air layers above the canopy layer, whereby neutral stability conditions are assumed. Transpiration by crops and evaporation by the soil surface both impact on the vapour flow and are described by the surface resistance depending on their part on the stomatal resistance and the sunlit leaf area index. Furthermore, to describe deposition accurately, turbulent transfer, Brownian diffusion, impaction, interception, gravitationally settling, and particle rebound have to be taken into account. Deposition is affected by particle size, density and meteorological condition as well. The dry deposition is commonly parametrised using the deposition velocity v_d $[m\,s^{-1}]$ following (*Zhang et al.*, 2001):

$$v_d = \frac{1}{R_a + R_s + R_a R_s v_g} + v_g \tag{2.9}$$

Especially for particles with diameters $D_p < 2\,\mu$m, atmospheric small-scale dynamics (e.g. turbulent elements) deflect particle deposition path. Close to the surface, roughness elements and vegetation effect the turbulent processes.

Wet deposition describes the particle removal by scavenging due to rain-out (sub-cloud scavenging by falling rain drops collecting dust particles) and wash-out (in-cloud scavenging either by nucleation scavenging by activation and growth of dust particles to cloud droplets or by collecting the non-activated fraction of a particle by coagulation with cloud droplets). The wet deposition rate is mainly controlled by the precipitation rate and the scavenging efficiency of the rain drops related to the rain-drop size distribution. Wet deposition by rain-out and wash-out can be parametrised following e.g. *Berge* (1997) and *Jacobson et al.* (1997).
The wet deposition rate Ω $[kg\,m^{-2}\,h^{-1}]$ is controlled by the precipitation rate Λ $[mm\,h^{-1}]$, the scavenging coefficient σ $[m^2\,kg^{-1}]$:

$$\Omega = -\sigma \cdot \Lambda \tag{2.10}$$

with

$$\sigma = \frac{A \cdot E}{v_r}. \tag{2.11}$$

The scavenging coefficient σ is related to the rain drop fall velocity v_r $[m\,s^{-1}]$, an empirical factor $A = 5.2\ m^3\,kg^{-1}\,s^{-1}$, and the collection efficiency of the rain drops E. Both factors A and E are related to the Marshall-Palmer size distribution (Equation 2.12), describing the best-fit exponential approximation of observed rain-drop size distributions (*Marshall and Palmer*, 1948),

$$N(D_r) = N_0 e^{-\Lambda D_r}, \tag{2.12}$$

with diameter D_r $[m]$. The slope factor of the fitted exponential function is found to be the precipitation rate Λ, the intercept parameter N_o can be given as constant $N_0 = 8{\cdot}10^6\,m^{-4}$ (*Marshall and Palmer*, 1948).
Dry and wet deposition show seasonal varying pattern, depending on the state of the atmosphere and transport path (*Schepanski et al.*, 2008a). Of course, the location of source areas also affect the deposition area, as it is the result of emission and transport path.

Dust deposition towards the oceans is estimated using global modelling (e.g. *Ginoux et al.*, 2001; *Luo et al.*, 2003; *Zender and Newman*, 2003). Different modelling studies estimate a deposition flux of 180-260 $\mathrm{Mt\,yr^{-1}}$ for the North Atlantic basin (*Mahowald et al.*, 2005).

Chapter 3

Meteorological Aspects of Saharan Dust Emission

For arid areas, where vegetation cover is sparse, meteorological conditions are the main factors determining whether a dust source becomes active or not. In the following, an introduction into the role of the boundary layer as interface between dust emitting surface and dust transporting free troposphere will be given.

3.1 The Atmospheric Boundary Layer

The atmospheric or planetary boundary layer (BL) is commonly defined as the lowest atmospheric air layer which is impacted by surface structure via friction, and heat fluxes (*Garratt*, 1992). Surface elements decelerate air flows close to the surface. Turbulence forced by thermal convection and mechanical turbulence due to wind shear characterise the nature of the BL. As the BL is coupled to the surface, exchange processes concerning the conserved quantities mass (e.g. precipitation and evaporation, emission and deposition of aerosols), energy (e.g. latent and sensible heat flux, radiation) and momentum (e.g. friction) between atmosphere and geosphere occur.
The inertial sublayer (Prandtl-Layer) is situated above the interfacial sublayer comprising the first few millimetres above the surface. This layer is characterised by a strongly increasing wind velocity and turning wind direction due to decreasing impact of the surface elements. In contrast to the interfacial sublayer, the flow above becomes turbulent and is often characterised by a Reynolds number (measure of the ratio of inertial and viscose forces) $Re > 5000$. Air flow within the inertial sublayer can be expressed by the equilibrium of pressure gradient force and turbulent friction force, often termed antitriptic wind. Wind, turbulence and turbulent exchange are closely related. So the vertical flux of momentum is described by the turbulent exchange coefficient K $[m^2\,s^{-1}]$ related to the turbulent viscosity and the vertical gradient of momentum. Prescribing a thermal neutral atmospheric stratification, the turbulent exchange coefficient K increases with height z $[m]$:

$$K = \kappa u_\star z, \tag{3.1}$$

with the empiric von Karman constant κ and the wind friction velocity $u_\star$ $[m\,s^{-1}]$. However, within the inertial sublayer, the vertical momentum flux is assumed to be constant with height. Consequently, the vertical momentum flux, the density of air and the von Karman constant κ can be considered as constant and for the vertical wind $v(z)$ profile $[m\,s^{-1}]$ follows:

$$v(z) = \frac{u_\star}{\kappa} \ln\left(\frac{z}{z_0}\right), \tag{3.2}$$

with the surface roughness length z_0 $[m^{-1}]$ and the vertical height z $[m]$.

For a logarithmic wind profile to occur, thermal neutral stratification of the atmosphere is one of the preconditions. In case of non-thermal neutral stratification, the wind shear dv/dz does not change with the reciprocal height z^{-1}. Furthermore, the decrease is empirically related to the Monin-Obukhov length $\mathrm{L}_\star$ $[m]$. The Monin-Obukhov length describes the height at which turbulence produced by vertical shear is balanced by negative buoyancy. In case of stably stratified atmosphere, the surface wind velocity is low and increases stronger than the logarithmic profile with height. For unstable atmospheric conditions, the surface wind velocity is higher than in the neutral case but the increase with height is weaker.

Above the inner region (interfacial and inertial sublayer) lies the outer region (*Garratt*, 1992). The transition from inner to outer region is characterised by an overlap region. Within the outer region, often referred to as Ekman layer, the air flow is just little affected by the surface characteristics and the impact to the Coriolis force due to the Earth's rotation is obvious. Mainly three forces determine the wind flow and its direction: the propulsive pressure force, the deflecting Coriolis force and the decelerating turbulent friction force. The equilibrium between these forces results in the geotriptic wind. A major characteristic of the Ekman layer is the turning wind direction with height and coinstantaneously increasing wind velocities due to decreasing deceleration effect of surface elements. Under ideal conditions (flat, homogeneous terrain, no advection, predominant mechanic turbulence (wind shear)), the hodograph of the wind vectors will show the so called Ekman spiral.

With regard to the vertical wind profile, the top of the Ekman layer is reached when the geotriptic wind equals the geostrophic wind, described by the equilibrium of pressure gradient force and Coriolis force.

The structure and height of the BL depends strongly on the turbulence development, mainly affected by diurnal heating and cooling of the surface (*Thorpe and Guymer*, 1977). During daytime, the BL is dominated by convective turbulence elements due to inhomogeneous heating and resulting buoyancy effects leading to thermal instability or convection. At near-surface layers, a super-adiabatic lapse-rate is observed. In this case of unstable BL condition, the outer region or Ekman layer is often termed mixed-layer in the literature. Under neutral atmospheric conditions, buoyancy effects that would be a prerequisite for convective turbulence are absent. Static stable conditions, typically occurring during night, are characterised by a surface inversion.

The top of the BL under convective conditions is often marked by a stably stratified layer, the so called capping inversion. This layer decouples the turbulence within the BL from

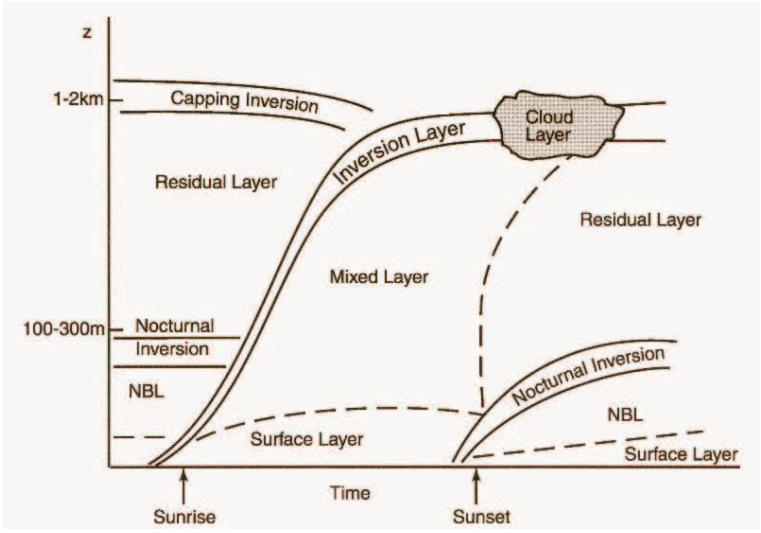

Figure 3.1: *Structrue of atmopsheric boundary layer development, Wyngaard 1992*

the free troposphere above. Turbulent motion and elements of raising air, e.g. thermal plumes and latent heat conversion, are able to erode this capping inversion layer. Over deserts, the BL regularly reaches depths around 5 km, but also depth up to 10 km have been observed over heated desert surfaces. Under stable condition, the top of the BL is not so well defined because the turbulence is weaker. Consequently the stable BL is shallow, often just a few hundred meters deep. Assuming an Ekman layer, wind speed should be zero at surface due to friction. But turbulent momentum mixing leading to a homogeneous BL causes sub-geostrophic wind speeds within the BL.

After sunset, surface heating stops and convective turbulence diminishes due to weakening buoyancy. As surface and lower atmosphere cool, the BL breaks down to a shallow nocturnal BL (NBL) within a stably stratified layer, and a surface temperature inversion develops. Above the surface inversion, a weak residual layer still exists as the rest of the daytime BL (*Garratt*, 1992).
The NBL is generally defined as a shallow, turbulent layer above which the mean shear stress and heat flux are negligibly small (e.g. *Garratt*, 1992; *Hoxit*, 1975; *Mahrt*, 1999; *Mauritsen and Svensson*, 2007).
The NBL depth is highest under clear-sky conditions with moderate to high wind speeds over horizontal terrain. The lower the surface wind speed, the shallower the NBL. In that case, intermittent turbulence occurs: turbulent mixing due to high wind shear at top of the NBL occurs abruptly and decreases the shear to a sub-critical value (*Van de Wiel et al.* (2003) and references therein, *Mahrt* (1985)). Mainly turbulent and radiative effects influence the temperature inversion and since turbulence is not a precondition, its height is mostly found to be higher than the NBL extension. In the upper part of the inversion, sharp density gradients can occur and gravity waves can be forced (*Garratt*, 1992; *Sorbjan*, 2006, and related references).

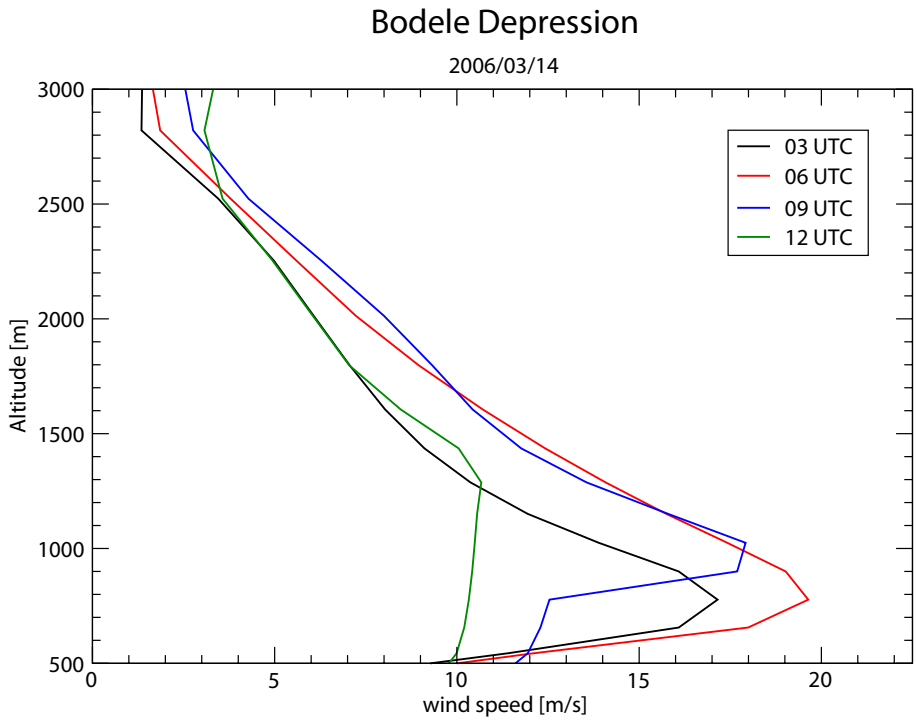

Figure 3.2: *Temporal evolution of the nocturnal low-level jet (LLJ) over the Bodélé depression on March 14 2006. The wind speed maximum of the nocturnal LLJ develops during 03-06 UTC and is present until the daytime BL depth reaches the height of the LLJ (morning hours after sunset). Then downward mixing of the momentum of the LLJ starts, indicated by increasing surface wind speeds and decreasing wind speed maximum.*

3.2 The Nocturnal Low-Level Jet

Examining the vertical wind profile (Figure 3.2), a low-level jet (LLJ) can be identified by a horizontal wind speed maximum occurring in the lowest few kilometres of the atmosphere (e.g. *Banta et al.*, 2006; *Blackadar*, 1957; *Holton*, 1967). It should not be confused with the jet streams at the top of the troposphere reaching length of thousands of kilometres, width of hundreds of kilometres and high wind speeds of about 100 $\mathrm{m\,s^{-1}}$ (*Davis*, 2000; *Lenschow and Stankov*, 1979; *Stensrud*, 1996).

Measurement campaigns like the CASES-99 (Cooperative Atmosphere-Surface Exchange Study-1999) campaign (*Poulos et al.*, 2002) and the Wangara experiment (south-east Australia) and model studies (e.g. *Brost and Wyngaard*, 1978; *Enger et al.*, 1993; *McNider et al.*, 1993; *Thorpe and Guymer*, 1977) have shown that there are several possible causes for the LLJs (e.g. *Blackadar*, 1957; *Bonner*, 1968; *Bonner and Paegle*, 1970; *Brost and Wyngaard*, 1978; *Chimonas*, 2005; *Davis*, 2000; *Enger et al.*, 1993; *Ha and Mahrt*, 2001; *Holton*, 1967; *Hoxit*, 1975; *Mahrt*, 1985; *Mahrt et al.*, 1998; *McNider and Pielke*, 1981; *Thorpe and Guymer*, 1977): synoptic-scale baroclinity associated with weather patterns, baroclinicity associated with sloping terrain, fronts, advective acceleration, splitting, ducting and confluence around mountain barriers, land and sea breezes, mountain and valley

winds, and inertial oscillation (*Kraus et al.*, 1985). In general there are two different types of LLJs: on the one hand those which occur in disturbed conditions within the troposphere associated with stationary rain bands on a cold front (*Browning and Bryant*, 1975) as well as the East African jet (*Findlater*, 1972), and on the other hand those which are related to fine weather conditions with clear skies and low surface wind speeds over land (e.g. *Thorpe and Guymer*, 1977). The latter can be explained by frictional decoupling at night due to radiative cooling performing a nocturnal temperature inversion at the top of the static stably stratified layer of cooled air (e.g. *Banta et al.*, 2003, 2002; *Blackadar*, 1957; *Mahrt*, 1999; *Nappo*, 1991).
Within the residual layer above the nocturnal BL, the decoupled air accelerates due to geostrophy. As the degeneration of the BL to the NBL occurs relatively fast, the air aloft is accelerated to super-geostropic wind velocities and a LLJ can develop (Figure 3.2). During the next morning, turbulent processes couple the LLJ layer to the surface and momentum of the LLJ is mixed downward leading to suddenly increasing surface wind speeds frequently strong enough to mobilise dust. The LLJ often reaches super-geostrophic wind speeds, which are high enough to mobilise dust in case of downward mixing during the next morning (Figure 3.2). *Mahrt* (1999) has found a high night-to-night variability of height and strength of the nocturnal LLJ, but low variability within the same night. The characteristics of a LLJ can be observed over all continents (*Stensrud*, 1996, and related references). LLJs can occur during daytime and night time over flat and complex terrain and shows often length of tens to hundreds of kilometres (*Davis*, 2000).
To physically describe the retardation from the sub-geostrophic wind speeds during day to the super-geostrophic velocities during night, three present approaches have been proposed and will be presented in the following: inertial oscillation (*Blackadar*, 1957), thermal wind (*Holton*, 1967), and shallow baroclinity (*Stensrud*, 1996).

Inertial Oscillation
The first approach introduced by *Blackadar* (1957) can explain both diurnal variability of wind speed intensity (higher wind speed at night time) like an oscillation, their day-to-day and night-to-night variability, respectively, and the super-geostrophic velocities.
Near nightfall, the lowest air layers cool due to radiative cooling. Hence they become static stably stratified and turbulence is reduced except within the shallow NBL: a surface temperature inversion develops and decouples the air above the inversion from the surface layer (e.g. *Banta et al.*, 2006; *Nappo*, 1991). The decoupled air becomes nearly frictionless and turbulence free, and accelerates to geostrophic conditions. At the beginning, there is an imbalance between pressure gradient $\underline{F}_p = -\frac{1}{\rho}\nabla_h p$ and Coriolis forces $\underline{F}_c = f\underline{k} \times \underline{v}$, inducing an inertial oscillation ($\underline{F}_p$ pressure gradient force, ρ density, p pressure, $\underline{F}_c$ Coriolis force, $f = 2\Omega \sin\phi$ Coriolis parameter with Ω the angular speed of Earth' rotation and ϕ the latitude, $\underline{k}$ unit vector along z-axis, $\underline{v}$ wind vector)(Figure 3.3 and Equation 3.5). Applying the equation of horizontal motion ($\underline{v}_h$ denotes the horizontal wind vector and $\underline{F}_R$ the friction drag force)

$$\frac{\partial \underline{v}}{\partial t} + (\underline{v}_h \cdot \underline{\nabla}_h)\,\underline{v}_h + f\underline{k} \times \underline{v}_h = -\frac{1}{\rho}\nabla_h p + \underline{F}_R \tag{3.3}$$

to the conditions above the boundary layer where the horizontal pressure gradient $-\frac{1}{\rho}\nabla_h p$ can be assumed as zero, the horizontal motion as homogeneous (no advective acceleration $(\underline{v}_h \cdot \underline{\nabla}_h)\,\underline{v}_h$) and no turbulence (Reynold stress) is evident,

$$\frac{\partial \underline{v}}{\partial t} = -f\underline{k} \times \underline{v}_h \tag{3.4}$$

describes the geostrophic conditions above the boundary layer. To describe the inertial oscillation, the difference between occurring wind $\underline{v}$ and geostrophic wind $\underline{v}_g$, often termed as ageostrophic wind $\underline{v}_{ag} = \underline{v} - \underline{v}_g$ is considered. The differentiation with respect to time leads to the equation of oscillation:

$$\frac{\partial^2}{\partial t^2}\left(\underline{v}_{ag}\right) = f^2\left(\underline{v}_{ag}\right). \tag{3.5}$$

The solutions are sinusoidal oscillations with a frequency T $[s^{-1}]$ depending on latitude:

$$T = \frac{2\pi}{f} \tag{3.6}$$

Considering the geostrophic wind speed as stable case, turbulent mixing and friction cause sub-geostrophic wind speeds as during daytime. This oscillation between increase and decreases of wind speed from the sub-geostrophic case to the super-geostrophic case and back has a period of 15 hours at subtropic latitudes, 17 hours at mid-latitudes. Shortly after sunrise the BL develops exceeding the height of nocturnal surface inversion and the inertial oscillation breaks down. Finally the approach of an inertial oscillation relying on

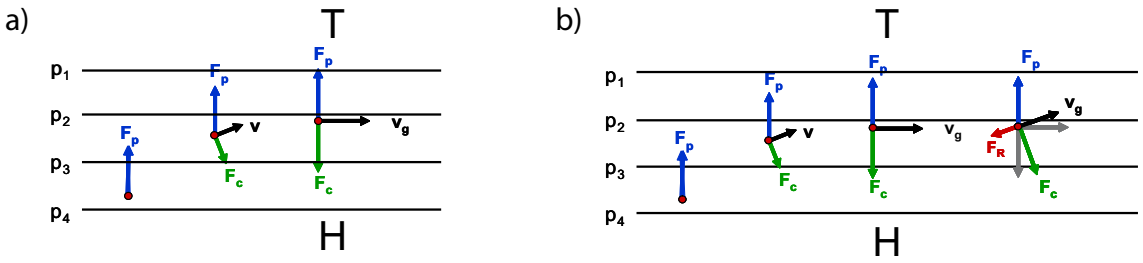

Figure 3.3: *Derivation of inertial oscillation from geostrophy. a) Describes the development of the geostropic state of equilibrium for an air parcel accelerated by the pressure gradient. In case of equilibrium, the air parcel is characterised by motion parallel to the isobars. The right-most vector diagram in b) shows the impact of frictional drag at surface reducing the wind velocity while backing wind direction and leading to sub-geostrophic wind velocities.* $\underline{F}_c$ *Coriolis force,* $\underline{F}_p$ *pressure gradient force,* $\underline{v}$ *wind,* $\underline{v}_g$ *geostrophic wind,* $\underline{F}_R$ *frictional drag force.*

the retardation to sub-geostrophic wind speeds during daytime and a frictional decoupling during night time, explains the LLJ occurrence at synoptic scale conditions allowing surface inversions and its wind speed variations. Thus, a wind speed maximum will be generated at round about 8 hours after sunset (*Hoxit*, 1975). However, this approach does not take sloping terrain into account.

Thermal Wind

The NBL is sensitive to some minor influences (*Sorbjan*, 2006) as terrain slopes (e.g. *Brost and Wyngaard*, 1978; *Holton*, 1967; *McNider and Pielke*, 1981) and heterogenities of surface characteristics (e.g. *Mahrt et al.*, 1998; *Nappo*, 1991). As the approach by *Blackadar* (1957) does not account for complex terrain, two more approaches have been proposed: first by *Holton* (1967) basing on thermal wind and second on *Stensrud* (1996) basing on shallow baroclinity. Diurnal heating and cooling of sloping terrain result in a periodic

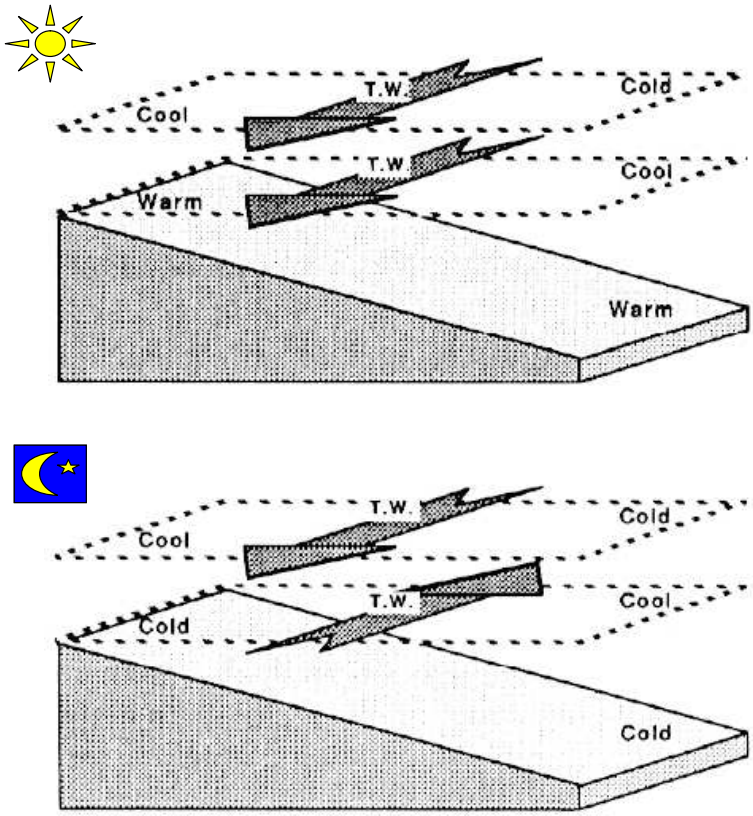

Figure 3.4: *Thermal wind (T. W.) and shallow baroclinity at mountain hills (Stull, 1988).*

variation of thermal wind and consequently in wind speed oscillation (thermal wind + geostrophic wind on the one side and thermal wind - geostrophic wind on the other side) (e.g. *Bonner and Paegle*, 1970; *Holton*, 1967; *McNider and Pielke*, 1981). At daytime, solar radiation warms up the surface and a mixed layer with near-adiabatic laps rate develops. Considering a horizontal slice within sloping terrain, a temperature gradient $\underline{\nabla}_h T$ develops from warm surface to cool surrounding air at the same horizontal slice. This temperature gradient is evident at surface and at higher levels as well (Figure 3.4). Referring to the simplified thermal wind equation

$$\frac{\partial \underline{v}_g}{\partial z} = \frac{g}{fT}\underline{k} \times \underline{\nabla}_h T, \tag{3.7}$$

a balancing flow should occur. Turbulent mixing during daytime weakens this flow. At night time, the surface cools more quickly than the air. Hence considering a slice starting

at near surface levels at one point, the temperature gradient is reversed compared to the daytime value. But considering a horizontal slice starting above the thermal inversion, the temperature gradient may be the opposite as below the inversion. The stably stratified layers below the inversion layer subpress motion so that calm or nearly calm conditions appear near the surface. Above the inversion, no friction retard the thermal wind and a jet can develop. The thermal wind is described by the equation 3.8 describing the change of the geostrophic wind components $\underline{v}_g$ with height. For a horizontal layer between two given geopontential levels Φ_0 and Φ_1, the thermal wind vector $\underline{v}_T$ is given by:

$$\underline{v}_T = \frac{1}{f}\underline{k} \times \underline{\nabla}(\Phi_1 - \Phi_0). \tag{3.8}$$

Summarising, the following equation system can be formed:

$$\text{day time :} \qquad \frac{\partial T}{\partial x} \leq 0, \qquad \frac{\partial \underline{v}_T}{\partial z} \leq 0 \tag{3.9}$$

$$\text{night time :} \qquad \frac{\partial T}{\partial x} \geq 0, \qquad \frac{\partial \underline{v}_T}{\partial z} \geq 0 \tag{3.10}$$

This approach alone cannot explain the super-geostrophic wind, but it may work together with the approach of inertial oscillation. Accordingly, both approaches together can explain the development and occurrence of nocturnal LLJ over sloping and complex terrain (*Holton*, 1967).
Furthermore, mountain sides can block and channel low-level flows of cold, stably stratified air mass to flow along the deepest path downward. Due to the high density of cold air, it is trapped in mountain valleys and forces a temperature gradient oriented normal to the mountains. This gradient can be assumed to be persistent during geostrophic balance of wind flows as described above, and a LLJ with mountain-parallel flow develops (*Stensrud*, 1996, and related references).

Shallow Baroclinity
This approach mainly takes horizontal differences due to surface variability into account (*Stensrud*, 1996). Significant changes in surface characteristics such as land-sea contrast in coastal regions, land/sea-ice contrasts or rock-sand contrasts leads to horizontal changes of sensible and latent heat fluxes (*Murphy et al.*, 1982). The resulting gradients produce strong low-level baroclinity within the BL and LLJs through strong geostrophic forcing, whereby the LLJ develops parallel to the low-level horizontal temperature gradient (*Stensrud*, 1996, and related references). Shallow baroclinity can explain constant LLJ occurrences throughout the day but, however, in regions where the surface fluxes have a diurnal component, significant diurnal changes in the strength of the LLJ occur.
LLJs produced by shallow baroclinity due to surface characteristic changes are observed in coastal region, the Antarctica, in shelf ice regions, in desert areas with sharp rock/sand or mountain/salt lake contrasts.
Topography influences the wind flow in direction and speed as it blocks and modifies the flow (*Peagle et al.*, 1984). Consequently, on a meso-scale, mountains can accelerate flows above a mountain ridge due to increasing transport through a horizontal slice, within a

valley due to channelling effect, and edging effect as sharp topographical gradients which forces development of eddies. On the lee-ward side of mountains, lee-waves can be generated and lead to turbulent mixing down of momentum resulting in gusts at surface level. On a large scale, lee-cyclones can develop and generate their own dynamic.
Over the Bodélé depression, located surrounded by the Tibesti Mountains in the North and the Ennedi Mountains in the East, a topographically forced LLJ occurs frequently (*Engelstaedter and Washington*, 2007; *Todd et al.*, 2008; *Washington and Todd*, 2005; *Washington et al.*, 2006a,b). Thereby, the mountains accelerate wind with south-westward direction and provide a LLJ. During daytime, convective turbulence mixes momentum downward and the LLJ disappears on most days, except the BL does not extend to the height of the LLJ. Then the LLJ remain above the daytime BL. After sunset, the LLJ develops fast. The Bodélé LLJ occurs very frequent and is able to explain the high frequency of dust events originating from the Bodélé depression.

Dust source observations indicate that 65% of all Saharan dust source activations occur during the morning hours (*Schepanski et al.*, 2008b). For dust mobilisation, the down-ward transport of the LLJ's momentum leads to high surface wind speeds (*Schepanski et al.*, 2008b), when the LLJ layer becomes coupled to the near-surface air layers by turbulence. As calm night-time BL conditions are required for LLJ development, the local frequency of LLJ occurrences also change with seasons (*Schepanski et al.*, 2008b).

3.3 Hadley Circulation

The Hadley circulation describes the distribution and location of high and low pressure systems forcing general atmospheric circulation patter over the tropics and subtropics. The variability of the Hadley circulation is linked to the variability of dust source areas and their activities because the Hadley circulation impacts on air mass circulation in which single synoptic scale atmospheric features are embedded. Also the LLJ development is effected by the strength and characteristic of the Hadley circulation because it affects BL dynamics.

Rather stationary high pressure systems are situated over the subtropical ocean on both hemispheres (Azores high, St. Helena high, Indic-Mascarean high and the high pressure system due to the Asian Ferrel-Circulation, Figure 3.5). Surface conditions, in particular ocean currents, determine the stability of these high pressure systems. Cold ocean currents caused by up-welling along the east shores of the oceans stabilise the lower troposphere leading to more stationary conditions. Along the oceans west shores, warm water currents destabilise the lower troposphere leading to frequent convective interruptions and thereby less stable conditions.

These high pressure systems are part of the Hadley circulation, describing the meridional circulation between the thermal equator and the subtropics. The Hadley cell consists of

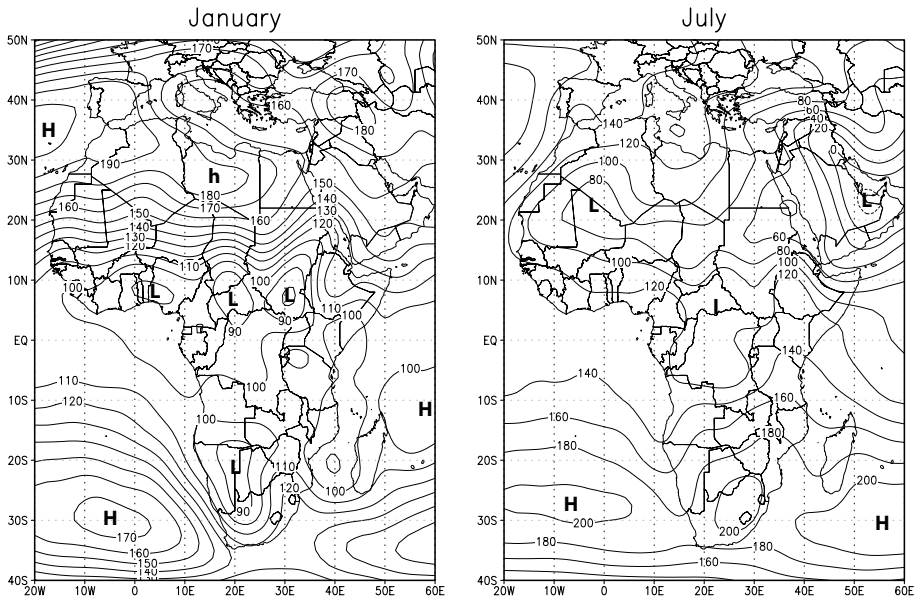

Figure 3.5: *CDAS-NCEP/NCAR Reanalysis geopotential [gpdm] at 1000 hPa level. Climatological mean of 1979-1995.*

the equatorial trough related to the thermal equator, where air masses heated by solar insolation ascend. Ascending air leads to low pressure at surface levels and high pressure zone in the upper troposphere. As consequence of the mass balance, upper tropospheric air masses spread out to the north and south (anti-trade winds). The air cools due to the conversion of latent heat, and descends leading to upper-tropospheric low pressure and an area of high pressure at surface levels: the subtropical high. Within the lower troposphere, an equilibrium air flow from the zone of high pressure to the equatorial trough occurs: the trade wind, over the Sahara often named Harmattan.

Due to significant seasonal changes in surface pressure distribution caused by changing solar inclination over the large continental area of the Sahara, the northern hemisphere has different high and low pressure distribution for summer and winter. At lower tropospheric levels, the Azores high over the subtropical North Atlantic shifts northward and the Saharan heat low (SHL) develops south of the Atlas Mountain chain. At the upper tropospheric levels, high pressure is evident over the SHL. Heat lows are normally related to strong precipitation events due to ascending air motions. But in case of the SHL, very dry desert air inhibits precipitation. Furthermore, the upper tropospheric high pressure area suppress the ascending motion of the SHL. Thus an inversion layer (trade wind inversion), is formed by descending air due to the subsiding branch of the Hadley circulation and the ascending air from the surface SHL. The height of the inversion layer increases from the SHL towards the equatorial trough, accompanied by deep convection, which is at maximum at the location of the inter-tropical convergence zone (ITCZ), located at around 10 to 15° N during northern hemispheric summer. From the centre of the SHL to the equatorial trough atmospheric moisture content increases inhomogeneously. A strong gradient of atmospheric moisture content occurs where dry desert air meets moist mon-

soon air at the inner-tropical discontinuity (ITD). The combination of a raising inversion layer height and an increasing atmospheric moisture content indicates convective clouds towards the equatorial trough. Figure 3.6 illustrates different air mass characteristics of desert and monsoon air between surface heat trough (SHL) and region of strongest precipitation (ITCZ).

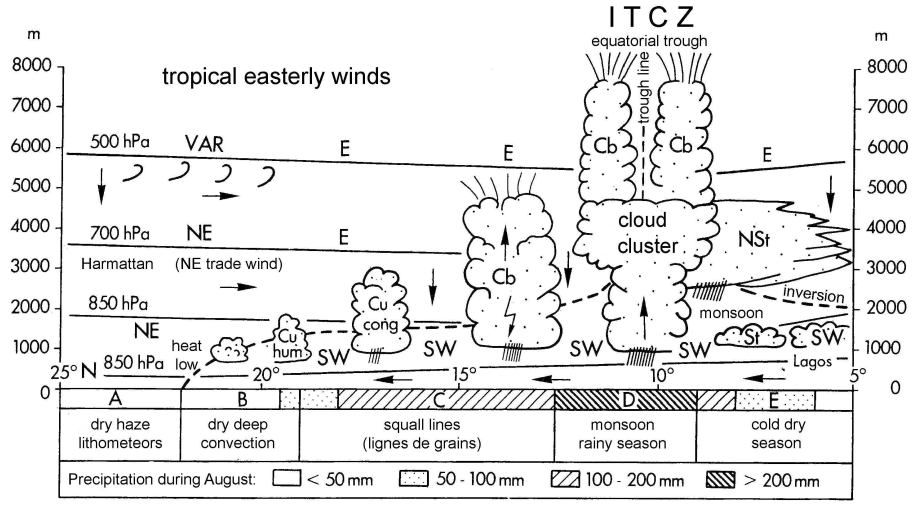

Figure 3.6: *Meridional transect of weathering zones over West Africa between the Sahel zone and the coast of Guinea, modified after Weischet and Endlicher (2000). Air mass characteristics and the trade wind inversion are illustrated. For a detailed explanation on the five weathering zones see text. Cu denotes cumulus, Cb cumulonimbus, and NSt nimbostratus*

Five weather zones are defined, originally based on studies of *Hamilton and Warchbold* (1945); *Leroux* (1983); *Solot* (1959); *Walker* (1958). *Zone A* located far north of the ITCZ is dominated by the Harmattan. The atmospheric conditions are stable and dry haze reduces the horizontal surface visibility. Here, stable atmospheric conditions are suitable for nocturnal LLJ development (*Schepanski et al.*, 2008b) providing sudden high surface wind velocities during the morning. *Zone B* is characterised by the ITD. As over the desert the Harmattan (north-east trade wind) is dominant and the monsoon air is transported by the south-west monsoon winds, the ITD is further characterised by a conversion of both wind regimes (Figure 3.7). There, the moisture gradient at surface levels is strongest, often dew-point difference of 15 K and more are observed accompanied by a strong shift in wind direction. Near the surface, the denser monsoon air is evident while at higher tropospheric levels the dry north-east trade winds are still dominant. Both, monsoon and trade wind layer are separated by the trade wind inversion. The height of the inversion increases with decreasing distance towards the ITCZ. Due to strong vertical wind shear within the trade wind inversion and the dry trade wind air mass, only shallow convective clouds can develop. Occasional convective events are able to penetrate the inversion layer. However, the evaporation rate is too high to allow for precipitation reaching the soil surface. Compared to zone B, *zone C* is characterised by a deeper monsoon air layer (1500-2000 m) allowing for deep moist convection and strong thunderstorms. Over this

region, convective clouds are often observed to be characterised by an organised structure (e.g. *Houze et al.*, 1990; *Parker and Johnson*, 2000). This cloud complexes, so-called meso-scale convective systems (MCS) or meso-scale convective complex (MCC) show a longer life-time and a more complex dynamic than individual convective elements. MCSs are characterised by a contiguous precipitation area of more than 100 km and up to 500 km in at least one horizontal direction. They have life-times of about 20 hours. Horizontal extent and life-time of MCSs are limited by the Coriolis parameter and ageostrophic advection. MCSs are accompanied by strong rainfall events which are assumed to account for 75% of the annual sub-Saharan precipitation (*Laurent et al.*, 1998). Most precipitation evaporates before reaching the surface, and a pool of cold, dense air is generated sinking rapidly downwards. Such downward flow of cold air generated by evaporative cooling is often termed "gravity current" or "density current" (e.g. *Flamant et al.*, 2007). High surface wind speeds associated with such gravity currents reaching the surface are able to force dust emission. Dust storms, so called Haboobs, associated with such cold outflows develop and spread radially out (10-15 $m\,s^{-1}$) forming an arcus-like front-edge. Haboobs are a typical phenomenon for this region. *Zone D* marks the location of the ITCZ characterised by deep convection forming cloud clusters and strong precipitation. The depth of the monsoon air mass is deepest with 2.5-3 km. The trade wind inversion layer is not evident due to the missing presence of the subtropical high. Southward of the ITCZ, the vertical characteristics of the troposphere are impacted by the St. Helena high. Again, in upper tropospheric levels, subsidence dominates and reducing the level height of trade wind inversion. Besides the anti-cyclonic subsidence, the cold Benguela current stabilises the atmosphere as well. Furthermore, the transition of south-east trade winds to south west monsoon winds at near surface levels while the south-east trade winds are persistent at higher tropospheric levels leads to vertical wind shear, which prevents deep convection. Stratifom clouds with occasionally drizzle (nimbostratus) are evident.

The Hadley circulation is probably the major element of general atmospheric circulation impacting on the North African dust source activation during north-hemispheric summer. In winter, when the equatorial trough and thereby the axis of the Hadley circulation is shifted to the south, extra-tropical disturbances related to the southward shifted polar jet force cyclogenetic activities, which disturb the predominant Harmattan winds. Furthermore, all meteorological elements are embedded within the Hadley circulation on different scales. With regard to dust source activation, the strength and centre of the Hadley circulation effects the distribution of activated dust sources as well as the strength of occurring dust storms on the one hand, but decrease dust mobilisation by precipitation and increasing vegetation cover on the other hand (*Engelstaedter et al.*, 2006).

3.4 West African Monsoon Circulation

The West African Monsoon (WAM) circulation is a predominant characteristic over West Africa during the northern hemisphere summer. Due to its ageostrophic meridional flow it

is associated with the advection of moist air from the Gulf of Guinea towards the Sahara (Figure 3.7, *Parker et al.* (2005); *Sultan et al.* (2006)). It is assumed to be affected by the combination of geostrophy and convection, both interacting on a diurnal time scale. Due to peaking solar inclination in northern hemisphere summer, the SHL south of the

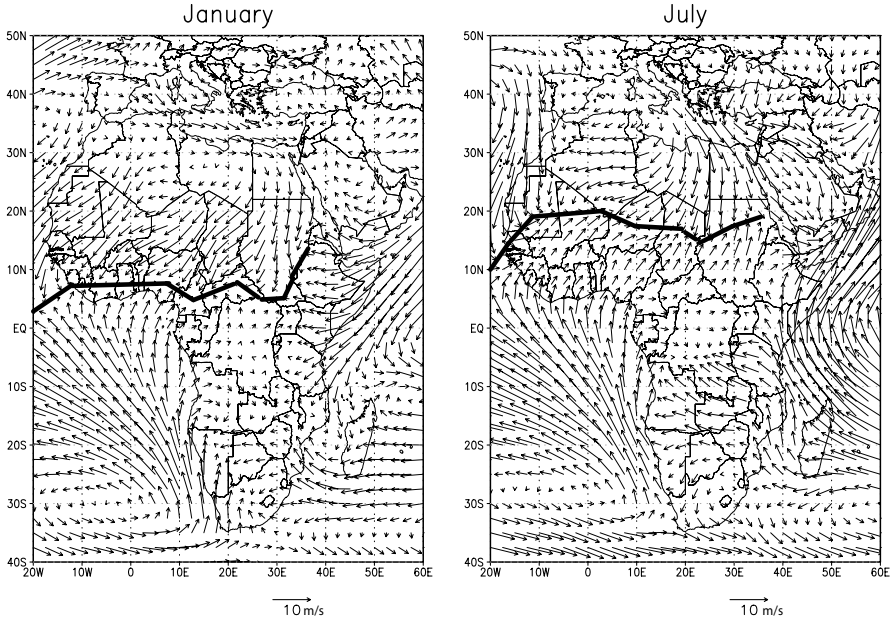

Figure 3.7: *CDAS-NCEP/NCAR Reanalysis climatological mean wind distribution at 1000 hPa for January and July 1979-1995. The convergence line of NE trade and SE monsoon flow is associated with the ITD over the North African continent (black line).*

Atlas Mountains develops (Figure 3.5). Moist air from the Gulf of Guinea is advected towards the Sahara. This transport is driven by the pressure gradient between the Gulf of Guinea and the SHL, supported by the temperature and moisture gradient between desert and monsoon region (Figure 3.7). However, the SHL is assumed to contribute to the strength of the WAM (*Drobinski et al.*, 2005; *Parker et al.*, 2005; *Ramel et al.*, 2006; *Sijikumar et al.*, 2006; *Sultan and Janicot*, 2003). In contrast to the pressure minimum of the SHL during afternoon due to maximum thermal heating, the wind velocity within the lower troposphere is observed to be lowest. With regard to atmospheric boundary layer dynamics, the afternoon wind velocity minimum can be explained by strong vertical mixing due to convective turbulence leading to a homogeneous vertical distribution of momentum. However, the ageostrophic wind (geostrophic wind adjusted by the surface friction drag) does not occur during day time. At dawn, insolation as driving factor for convective BL turbulence and therefore for the diminished ageostrophic wind, ceases and the pressure gradient force of the SHL becomes more dominant.

The WAM acts as major contributor to transport of moist air towards the Sahel, where it is involved into moist convection and the development of MCSs. Thus the WAM is one of the controlling processes for Sahel precipitation, a limiting factor for human agricultural activity in this region. Dust emission is influenced by the WAM in different ways. Besides

triggering dust emission by forcing the development of strong surfaces winds in convective events (Haboobs), precipitation related to the WAM also inhibits dust mobilisation due to increasing soil moisture and vegetation cover. Furthermore, the geostrophic wind related to the WAM has a major contribution to the nocturnal LLJ development (e.g. *Parker et al.*, 2005) and therefore to morning time dust source activation (*Schepanski et al.*, 2008b).

Because of clouds, precipitation and evaporation the air temperature is relatively low over equatorial regions. Thus a strong temperature gradient between the Sahara and the equatorial area occurs (*Burpee*, 1972; *Cook*, 1999; *Thorncroft and Blackburn*, 1999). From this gradient an easterly thermal wind results leading to a strong wind speed maximum of 10-20 $m\,s^{-1}$ at around 650 hPa over 16° N in summer (August) (*Burpee*, 1972; *Parker et al.*, 2005). This mid-tropospheric wind speed maximum is termed African Easterly jet (AEJ). As the strength of the AEJ depends on the thermal and thereby on the moisture gradient between the Sahara and the coast of Guinea, seasonal variability occurs. The AEJ is located close to the ITD. Thus disturbances related to the flow dynamics of the AEJ, or initiated by hindrances like mountains, may lead to baroclinic or barotropic instabilities (*Burpee*, 1972, 1974). Co-located to the ITD, strong gradients with regard to moisture and temperature force the development of strong deep convection, which is able to organise itself as MCS. These convective elements lead to a synoptic-scale wave-like perturbation of the AEJ (e.g. *Berry and Thorncroft*, 2005). This wave-structures are the so-called African Easterly waves (AEW) are observed during summer (June to September) with wavelengths of 2000 to 4000 km (*Burpee*, 1972, 1974; *Carlson*, 1969) and a propagating velocity of about 8 $m\,s^{-1}$ in westward direction. AEWs are observed westward of 30° E and are assumed to modulate Sub-Saharan rainfall (e.g. *Payne and McGarry*, 1977).
African Easterly Waves are characterised by zones of convergence and divergence along a zonal flow, which can be identified well on isobaric weather charts. They are a common phenomenon during north-hemispheric summer over the African continent and the tropical North Atlantic (e.g. *Berry et al.*, 2007; *Burpee*, 1972). They are associated with Saharan dust outbreaks towards the tropical East Atlantic (e.g. *Jones et al.*, 2003, 2004; *Prospero and Nees*, 1986; *Prospero et al.*, 1981) that occur every 3-5 days (e.g. *Jones et al.*, 2003). Under suitable conditions like sea surface temperatures above 26-27°C and less horizontal wind shear, AEWs entered towards the tropical North Atlantic can act as seeding for strong gales (named as Cape Verde gale) or Hurricanes (e.g. *Thorncroft and Hodges*, 2001).

Chapter 4

Remote Sensing of Mineral Dust

In this thesis, infrared (IR) measurements taken from the geostationary MSG satellite are used to characterise Saharan dust emission areas and events in space and time. The Sahara desert is the World's most important dust source (e.g. *Goudie and Middleton*, 2001; *Middleton and Goudie*, 2001; *Prospero et al.*, 2002; *Washington et al.*, 2003). To study Saharan dust source location and characteristics with regard to time of activity, dust flux, and transport, remote sensing methods are required due to the spatial and temporal limits of ground-based observations. During previous studies, estimations on mineral dust sources have been made based on dust retrievals with at best daily resolution. In this chapter, the basics of the IR dust remote sensing technique and its limits of application will be discussed.

4.1 Meteosat Second Generation (MSG) Satellite

Low Earth orbiting meteorological satellites have a higher spatial resolution of their field-of-view due to lower orbital height, but their temporal resolution is, at best, daily. The field of view of geostationary satellites does not change with time as their orbit requires a similar angle velocity as the Earth. The temporal resolution of measurements taken by geostationary satellites is limited by the ability of the scanning interval of the instrument. The here used SEVIRI (Spinning and Enhanced Visible and InfraRed Imager) instrument on-board the Meteosat Second Generation (MSG) space craft is characterised by a return-interval of 15 minutes for single measurements on a resolution of 3×3 km at nadir (*Schmetz et al.*, 2002). The spatial resolution decreases with distance from the sub-satellite point due to the curvature of the earth surface (Figure 4.1). The satellite is located at 3.5° W over the equator (Gulf of Guinea), the images are entered at 0° longitude.
The SEVIRI instrument measures radiances at 11 different narrow-band wavelength (channels) covering the visible and IR spectrum between 0.6 μm and 13.4 μm and one high resolution broadband channel, listed in Tabel 4.1. As the instrument is designed for meteorological purpose, the channels fulfill different objectives in weather and climate monitoring. The atmosphere of the Earth shows different radiative characteristics at different wavelength of the solar and thermal spectrum. As it is not possible to measure at sin-

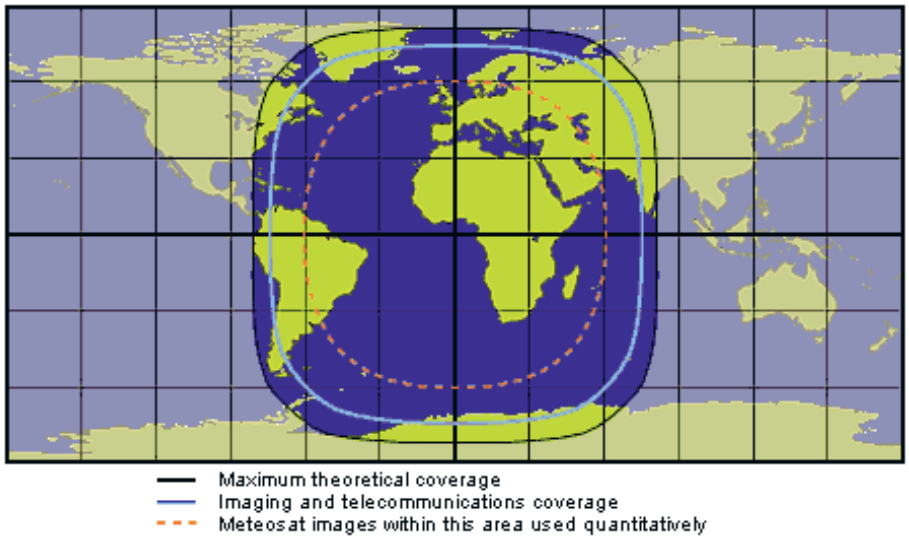

Figure 4.1: *Coverage area of MSG satellite (http://www.eumetsat.int).*

gle, discrete wave length, spectro-radiometer are designed to detect at narrow wavelength bands. Specific, wavelength dependent characteristics of atmospheric objects and the atmosphere itself can be remotely sensed at best with as narrow as possible wavelength bands. Then the spectral contribution of other atmospheric objects is lowest.

Channel	Alternative Name	Central Wavelength	Primary Objectives
Ch01	VIS 0.6	0.64 μm	surface, clouds, wind field
Ch02	VIS 0.8	0.81 μm	surface, clouds, wind field
Ch03	NIR 1.6	1.64 μm	surface, cloud phase
Ch04	IR 3.9	3.90 μm	surface, clouds, wind field
Ch05	WV 6.2	6.25 μm	water vapour, high-level clouds, atmospheric instability
Ch06	WV 7.3	7.35 μm	water vapour, atmospheric instability
Ch07	IR 8.7	8.70 μm	surface, clouds, atmospheric instability
Ch08	IR 9.7	9.66 μm	ozone
Ch09	IR 10.8	10.80 μm	surface, clouds, wind fields, atmospheric instability
Ch10	IR 12.0	12.00 μm	surface, clouds, atmospheric instability
Ch11	IR 13.4	13.40 μm	cirrus cloud height, atmospheric instability
Broadband:			
Ch12	HRV	0.4 - 1.1 μm	cirrus cloud height, atmospheric instability

Table 4.1: *MSG SEVIRI channels and its objectives, after EUMETSAT.*

The atmosphere is characterised by so-called atmospheric windows, wavelength bands at which the transmittance is highest and the atmosphere is relatively transparent. With regard to the wavelength spectrum remotely sensed by the MSG-SEVIRI, three major important windows exists (Figure 4.2): the visible window, the 3.7 μm window, the and the 8.5–12.5 μm IR-window (intermitted by the ozone (O_3) absorption band at 9.6 μm) (*Kidder and Vonder Haar*, 1995). The relatively high or low spectral transmittance of the atmosphere is due to absorption and emission characteristics of atmospheric gases, especially water vapour (H_2O), carbon dioxide (CO_2) and ozone (O_3).

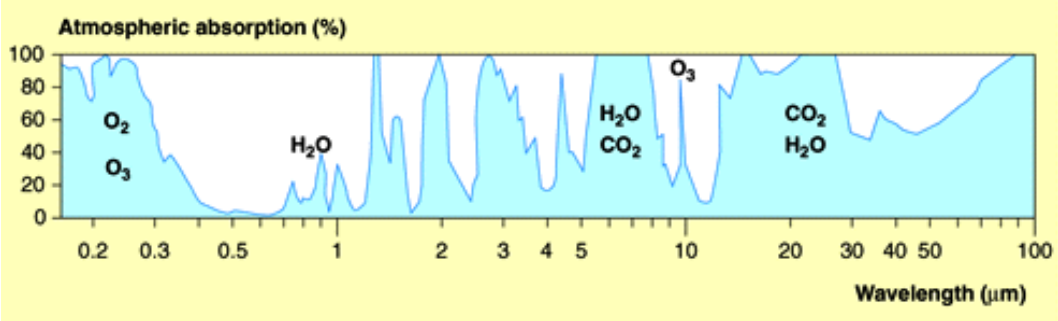

Figure 4.2: *Spectral distribution of atmospheric absorption [%]. High absorption means low transmittivity of radiation and thereby a strong impact of the atmosphere. Low absorption indicates a relatively low impact of the atmosphere. The image is taken from www.eduspace.esa.int.*

As the impact of the atmosphere is relatively low at the atmospheric window wavelength bands, non-gaseous atmospheric elements like clouds or dust can be remotely sensed. The combination of several wavelength band at which the element of interest shows spectral different characteristics, provides additional information. An example is the red-green-blue (RGB) composite technique (Figure 4.4 and 4.6).

4.2 Dust Detection Method

In case of airborne mineral dust, at visible wavelengths solar radiation is scattered back. Compared to ocean's surfaces, vegetated surfaces or generally dark surfaces, dust layers appear as bright area due to intense back-scattering (Figure 4.4a). Bare soil surfaces show high back-scattering rates and bright dust layers cannot be clearly distinguished from the surrounding over such high-reflecting surfaces. Thus, dust detection using visible wavelength bands shows good results over dark surfaces such as oceans, but is very difficult over bright surfaces like the Saharan desert (*Fraser*, 1997). Additionally, dust detection at the visible part of the spectrum is constricted to daylight and limited by sun-glint areas over the ocean.
Ackerman (1997) proposes a tri-spectral algorithm for dust detection using IR wavelength band centred at around 8.5 μm, 11 μm and 12 μm. The 11 and 12 μm wavelength bands are termed as "split-window" (e.g. *Chesters et al.*, 1983) as the brightness temperature differ-

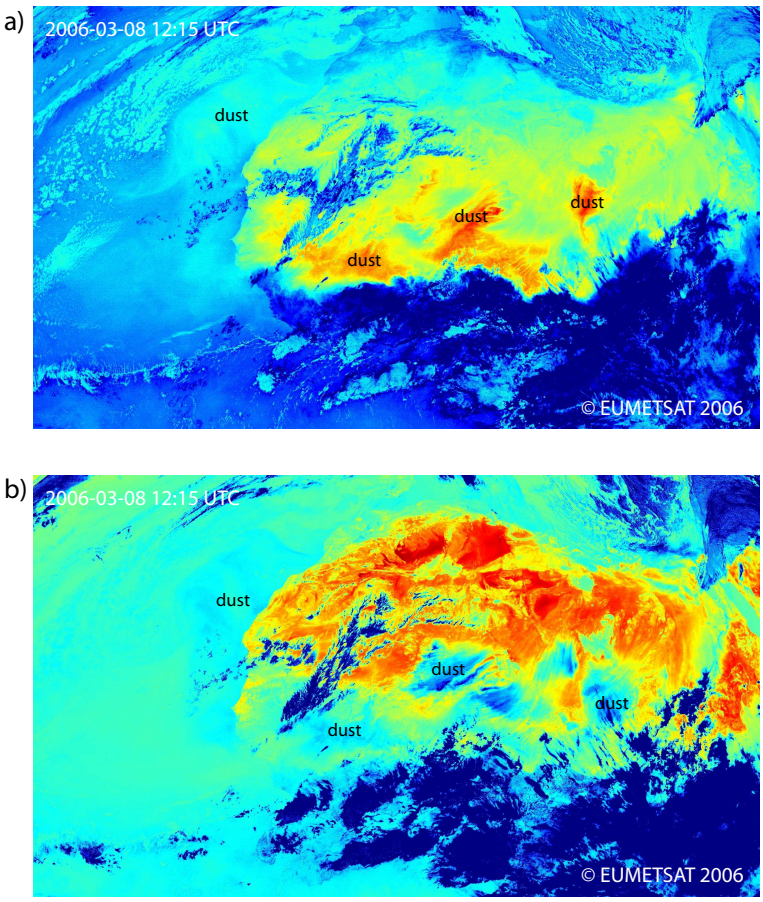

Figure 4.3: *a) The thermal signature of airborne mineral dust can be separated from the signature of the surface by applying the split-window technique. Thereby the BTD of the two adjacent wavelength channels entered at 10.8 and 12 μm is able to indicate the presence of airborne dust. b) Besides BTD of the split-window channels, BTD of 10.8 and 8.7 μm is able to indicate the presence of airborne dust as well. Both BTD imaginaries are shown for March 08 2006, 12:15 UTC. Compare also to Figure 4.4b.*

ence (BTD) of measurements at two adjacent wavelength channels can be used in order to separate atmospheric and surface signature. The split-window technique at IR wavelength has primarily been applied to remote sensing of volcanic ash aerosols (e.g. *Barton et al.*, 1992; *Prata*, 1989), but studies e.g. by *Shenk and Curran* (1974) and *Legrand et al.* (1989) pointed towards the potential of thermal IR split-window techniques for remote sensing of airborne dust, especially over land (Figure 4.3). Dust aerosol shows a strong variation in the 8-10 μm and 10-12 μm part of the spectrum, a wavelength region where the atmosphere is fairly transparent (*Ackerman*, 1997) (Figure 4.2).

For monochromatic radiation, transmittance due to the aerosol and transmittance due to the clean atmosphere lead to the transmittance of the real atmosphere. In case of mineral dust aerosol, the radiative absorption is strong for wavelength of 8-9 μm and 10-12 μm as well. At these wavelength regions, absorption due to atmosphere gases is weak (Figure 4.2). Thus the split-window technique is a potential tool to detect airborne dust by separating

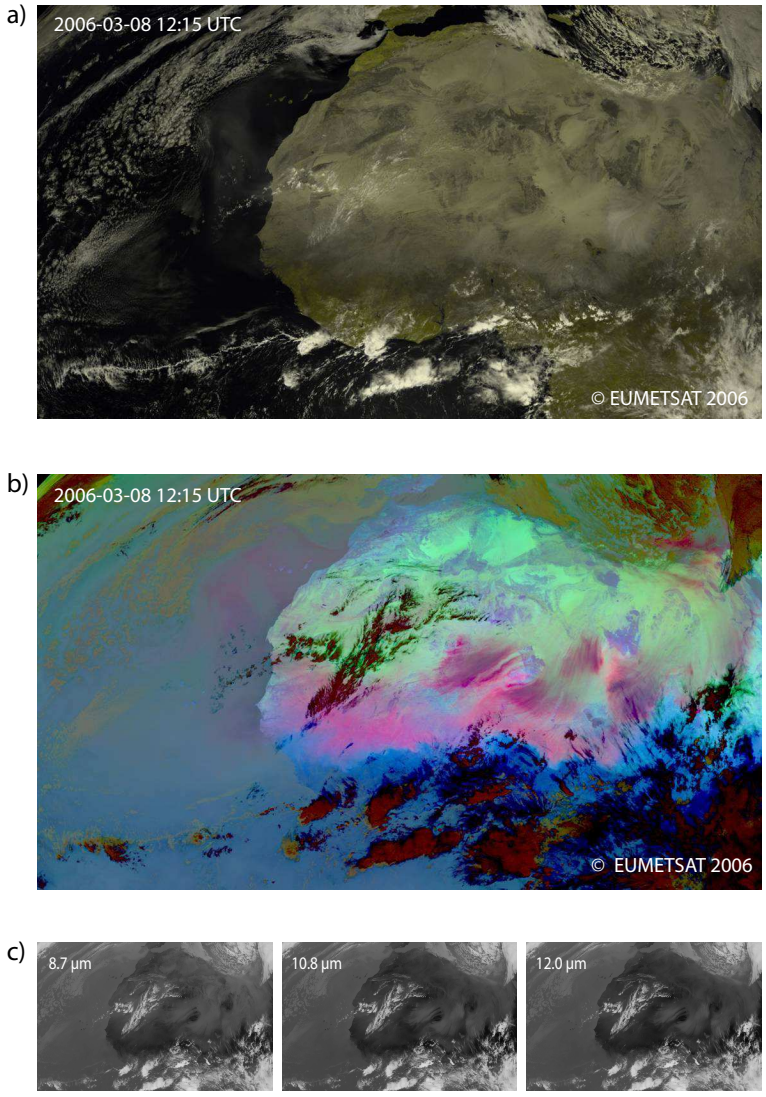

Figure 4.4: *Remote sensing of airborne dust: a) RGB-composite using VIS 0.6 VIS 0.8 and NIR 1.2 b) RGB composite images using tri-spectral BTD. In Figure 4.4b the magenta colour indicates airborne dust. c) Brightness temperature imaginary for the IR channels chosen for the tri-spectral composite image indicating airborne dust. All images are shown for March 08 2006, 12:15 UTC.*

the atmospheric (dust) and surface radiance contribution. Furthermore, applying different wavelengths account for the spectral radiative properties of dust particles.
To detect dust aerosol a few parameters have to be known (*Ackerman*, 1997): (1.) atmospheric structure, (2.) extinction coefficient (integrated over path it describes the optical depth, a measure for the attenuation of radiation by an aerosol volume), (3.) single-scattering albedo (1 for a non-absorbing medium and 0 for a fully absorbing and non-scattering medium) and (4.) phase function describing the direction of the scattered energy.

Both, real and imaginary part of the refractive index of dust particles show a strong

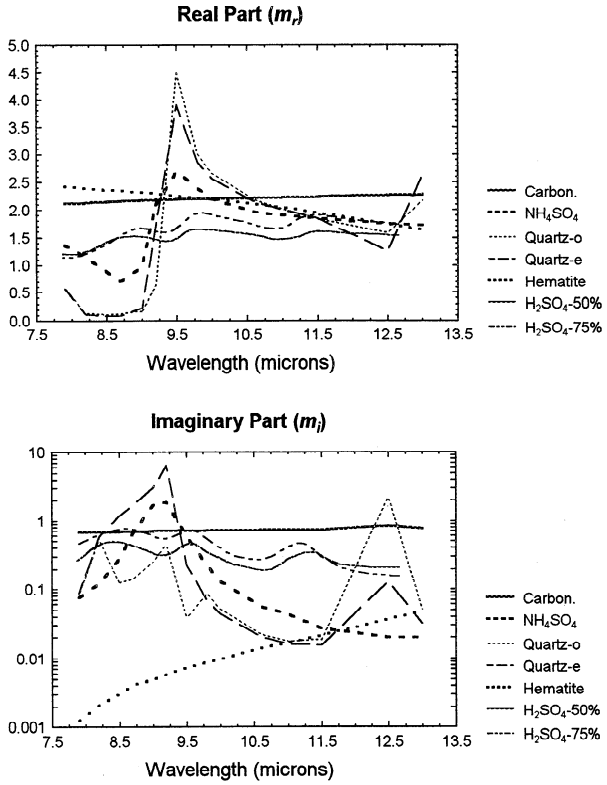

Figure 4.5: *Refractive index for the 8 to 12 μm wavelength region, shown for elemental components common in atmospheric aerosols. The figure is taken from Ackerman (1997).*

spectral dependency, encouraging the application of the split-window techniques (e.g. *Ackerman*, 1997; *Sokolik*, 2002; *Wald et al.*, 1998). As the refractive index for dust and ice or water clouds are different, multi-spectral IR techniques are a potential tool to separate dust plumes and clouds (*Ackerman*, 1997). Compared to clear-sky conditions, the presence of dust aerosol decrease the BTD between the 10.8 μm and the 12 μm wavelength band (BTD(10.8, 12)) (e.g. *Sokolik*, 2002).

Beside physical characteristics, mainly impacted by chemical and mineralogical constitution of the particle, size affects the radiative characteristic of a particle (*Ackerman*, 1997; *Wald et al.*, 1998). In addition to the spectral variability of dust and clear atmosphere, spectral particle size dependencies and temperature differences between desert surface and airborne dust provide additional a criterion for thermal dust detection. The thermal emissivity of airborne dust is less than the desert surface emissivity at wavelength around 11 μm (*Wald et al.*, 1998). This can be explained by the fact, that surface emissivities are decreased by particle size distribution (granulometry of soil aggregates) and packing effects (particle – particle distance). Considering wavelength around 8.5 μm, the emissivity increases for decreasing particle sizes.

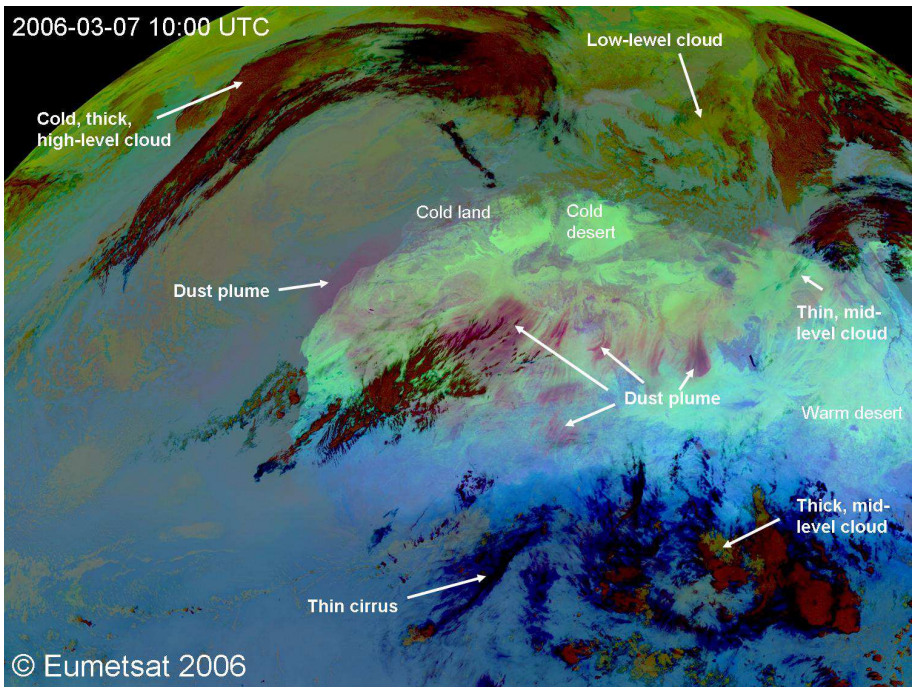

Figure 4.6: *MSG-SEVIRI tri-spectral thermal IR RGB-composite picture: red = 12 μm - 10.8 μm, green = 10.8 μm - 8.7 μm and blue = 8.7 μm. The composite image is shown for March 07 2006, 10:00 UTC.*

However, different spectral dependencies of absorption and emissivity due dust aerosol and surface, and high transmittance in case of pure atmosphere due to the atmospheric window characteristic, the thermal wavelength region 8-13 μm is well suitable for airborne dust detection as well as for applying the split-window technique to distinguish the spectral signature of airborne dust from the surface signature. According to the thermal channels provided by the MSG-SEVIRI instrument, in the context of this work a dust detection algorithm based on to brightness temperature (BT) converted radiances measured at the wavelength bands centred at 8.7 μm, 10.8 μm and 12 μm (Figure 4.4c) as provided by EUMETSAT is used. Due to applying BTs, the radiative signature of airborne dust and the surface can be separated, which is more difficult for BT of single wavelength channels (compare Figure 4.4b and c). The spectrally different characteristics of dust at 8.7 μm and 9.7 μm are quit significant, but due to the ozone absorption band at 9.7 μm, the IR9.7-channel is not suitable for dust detection.
Figure 4.6 shows a scene of MSG-SEVIRI dust index. This index is a colour index combining BTD(12, 10.8) (Figure 4.3a) for the red part, BTD(10.8, 8.7) (Figure 4.3b) for the green part and BT(8.7) for the blue part of the digital information. Atmospheric elements like clouds, dust plumes, and surfaces are represented by different colours indicating different spectral behaviours at the used wavelength bands. A similar index is applied to MODIS (Moderate-resolution Imaging Spectroradiometer) IR channels (*Zhang et al.*, 2006), that has been recently used to characterise Australian dust sources (*Bullard et al.*, 2008).
Thermal wavelength bands have been used for dust detection before. *Legrand et al.* (2001)

presented the IDDI (IR difference dust index) using first generation Meteosat measurements. Based on the broad-band IR channel (10.5-12.5 μm), a daily noon-time index for dust detection is designed by comparing cloud free noon-time scenes to a reference image build up on a 15-day reference period (*Brooks and Legrand*, 2000). Meteosat first generation (1977-2004, at 0° over the equator) does not provide the ability to apply the split-window technique. The comparison to a reference scene limits the index to a daily time resolution. Furthermore, the cloud free reference scene representing the highest BT values measured during the reference period is affected by long-lasting dust events (*King et al.*, 1999), persistent clouds, or by biomass burning aerosol (*Brooks and Legrand*, 2000).

4.3 Dust Detection Algorithm at UV and Visible Wavelengths

Dust detection algorithm also exists at other regions of the wavelength spectrum. Measurements at the short part of the visible spectrum like the deep-blue part or at the ultra-violet (UV) part of the spectrum are successfully applied to dust detection objectives, able to infer airborne dust over desert land surfaces.

Product	Characteristic						
	bright surf.	global	long-term	night	sub-daily	height depend.	quant.
VIS AOT		x	x		x		x
Deep Blue AOT	x	x					x
TOMS/OMI AI	x	x	x			x	
Meteosat IDDI	x		x			x	
MSG IR dust	x			x	x	x	

Table 4.2: *Characteristics of commonly used space-borne dust retrievals.*

Herman et al. (1997) defined an Absorbing Aerosol Index (AI) using the UV part of the spectrum measured by the Total Ozone Mapping Spectrometer (TOMS). TOMS was flying on-board several polar orbiting space crafts (Nimbus 7, ADEOS (Advanced Earth Observing Satellit), Meteor 3 and Earth-Probe) covering the measuring period 1979-2005. The AI algorithm is also applied to the Ozone Monitoring Instrument (OMI), since September 2004 on-board the low-orbiting Aura satellite (*Veihelmann et al.*, 2007). At UV wavelength, the surface reflectivity is low (*Eck et al.*, 1987) and UV-absorbing aerosols are detected due to their spectral contrast at 0.34 μm and 0.38 μm concerning backscattering effects (Mie-scattering) (*Herman et al.*, 1997). Since both mineral dust and soot are absobing at UV wavelength bands, the index does not distinguish between mineral dust aerosol and soot which becomes important especially over the Sahel and further south during the winter (*McConnell et al.*, 2008).
During the last years, *Hsu et al.* (2004) develop a new algorithm, Deep Blue, using a mul-

tiple narrow-channel technique applied to the deep-blue part of the shortwave spectrum (0.412, 0.47 and 0.65 μm for MODIS). The Deep Blue algorithm is able to detect absorbing aerosol over bright surfaces and provides information on the aerosol optical thickness (AOT). Compared to the IR aerosol detection algorithm, the Deep Blue algorithm uses look-up tables of a radiative transport model to retrieve aerosol information. At the moment, the retrieval is applied to MODIS on-board Terra spacecraft and SeaWiFS (Sea Wide Field-of-view Sensor) measurements, yielding to a daily resolution.

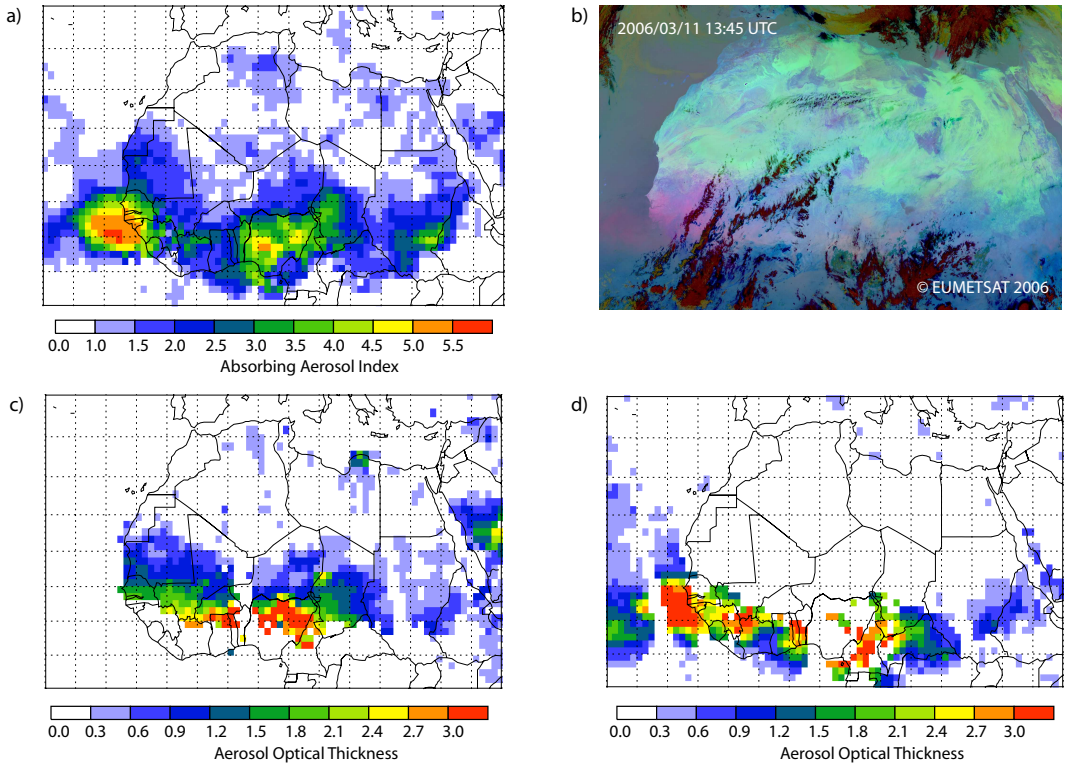

Figure 4.7: *Commonly used satellite retrievals to indicate the presence of airborne dust. All retrievals are applied to different wavelengths. a) OMI AI (UV, semi-quantitative index), b) MSG SEVIRI IR dust index (qualitative, magenta colour indicates airborne dust), c) MODIS Aqua Deep Blue AOT (deep-blue part of the visible spectrum, quantitative index) and d) MODIS Aqua AOT (visible wavelength, quantitative). All images are of the same event on March 11 2006 and taken at noon-time. The data for a), c) and d) are available at http://disc.sci.gsfc.nasa.gov/giovanni.*

A comparison of commonly used dust detection algorithms is shown in Table 4.2 with regard to dust source characterisation ability. Each algorithm is mainly limited by the measurement conditions provided by the used instrument. Instruments flying on-board a polar-orbiting satellite provide a low temporal resolution for a fixed surface location, but a high spatial resolution at each swath. Geostationary satellites are characterised by a high temporal resolution over an enlarged region compared to low, polar-orbiting satellites. Due to higher orbit level, spatial resolution is lower, but with e.g. 3 km at nadir for the MSG SEVIRI high enough to detect individual dust sources. Observations at wavelength of the

UV and IR are able to detect airborne dust over bright surfaces. Only IR based retrievals are able to detect airborne dust during day and night as thermal emittance is evident during all times. However, emissivity and scattering of airborne dust particles may change during transport (vertical and horizontal): The particles get cooler with increasing height and e.g. photo-chemical reactions or soot adsorption may change surface properties. Both affect the spectral signature of mineral dust particles at the measured radiance scene.
Figure 4.7 shows a comparison of results from commonly used retrievals to detect airborne dust, observed at noon time on March 11 2006. As discussed above, the retrievals are applied to different parts of the wavelength spectrum allowing dust retrieval over bright surfaces (e.g. AI, Deep Blue, IR retrievals) or not (e.g. MODIS VIS AOT). On March 05 a synoptic-scale density current was initiated along the Atlas Mountain chain by an upper-level disturbance. The density current, and dust emitted by high surface wind speeds, spread out radially and cross the entire Sahara towards the Sahel and the North Atlantic (*Tulet et al.*, 2008). The dust plume over the Sahel and West Africa shown by the scenes on Figure 4.7 is related to this extraordinary dust event. Thus the dust layer over the Sahel and southward is aged and mixed upward by boundary layer dynamics. All four aerosol indices show maximum dust concentrations over the Sahel and West Africa, but the images differ in detail. MODIS Deep Blue and VIS AOT retrieve high AOT values over Ghana, where OMI AI and MSG SEVIRI IR do not indicate high dust concentrations. Furthermore, MSG SEVIRI IR dust index does not indicate comparable high dust loadings over the Sahel and West Africa as it is indicated by the other retrievals. MSG SEVIRI IR dust index is based on thermal differences and thus is affected by the height and age of the dust plume, which limits the significance of this index to qualitative information on the presence of airborne dust. The MSG IR scene indicates active dust sources over the Akhdar Massif (Libya) and the Atlas mountains, both well represented by the MODIS Deep Blue retrieval. OMI AI shows some difficulties with regard to place of maximum (Atlas) and the maximum (Akhdra), which might be due to the height dependency of the retrieval leading to an underestimation of dust plumes at lower levels (*Israelevich et al.*, 2002).
OMI AI and former TOMS AI images have been used to identify dust sources (e.g. *Prospero et al.*, 2002). From this point of view of using airborne dust retrievals for dust source identification, the figure point towards difficulties in assuming high index values as being related to dust source areas. On the one hand, daily noon time images do not represent the place of origin as most dust plumes are initiated during the local morning hours (*Schepanski et al.*, 2007, 2008b). On the other hand, height dependencies strength aged, elevated dust plumes (*Israelevich et al.*, 2002). Hence high index values detected by those daily retrievals are the result of the strength of dust emission, the transport path affected by the present wind field, and the height of the dust layer. This have to be considered when relating high index values to dust source areas.
Beside radiances measurements performed by such single-viewing instruments, multi-viewing instruments like MISR are able to provide information on atmospheric dust content, including information on particle size and height of particle layer, also using visible wavelength (*Kahn et al.*, 2007). But the coverage of observations is lower than those

provided by single-viewing instruments.

However, for dust source detection a high temporal resolution is a prerequisite. Therefore, the MSG IR technique on 15-minute time resolution are the best method to detect and study on individual dust sources.

Chapter 5

Meso-Scale Modelling

First three-dimensional (3D) global dust simulations comprising the whole dust cycle (emission, transport and deposition) have been computed at the beginning of the 1990s by *Joussaume* (1990), assuming the semi-arid, arid and hyper-arid areas as dust source. Earlier modelling studies used one-dimensional (1D) and two-dimensional (2D) mixed-layer models (*Berkofsky*, 1982; *Lee*, 1983), 2D steady state models (*Schütz*, 1980) or 2D time dependent grid point models (*Westphal et al.*, 1987) to simulate Saharan dust events.
Here, the meso-scale atmospheric model system LM-MUSCAT including a dust emission, transport and deposition scheme (*Heinold et al.*, 2007) is used to investigate meteorological features forcing dust emission (*Schepanski et al.*, 2008b) and to characterise Saharan dust export and deposition towards the tropical North Atlantic. In addition, the model is used to test the newly derived map of North African dust sources in the frame of the dust emission scheme implemented in the model system (*Schepanski et al.*, 2007).
The model system consists of the regional-scale meteorological model LM (LokalModell, now called COSMO, Version 3.19), provided by the Deutscher Wetterdienst (German Weather Service, DWD) *Steppler et al.* (2003)) and the MUlti-Scale Chemical Aerosol Transport model (MUSCAT, *Wolke et al.* (2004a)). In addition, a dust emission scheme based on *Tegen et al.* (2002) is implemented in MUSCAT.

5.1 Meteorological Part: Lokal-Modell

The LM as atmospheric frame component of the here used model system LM-MUSCAT computes meteorological and hydrological fields used for the simulation of dust emission, transport and deposition by the MUSCAT.
The non-hydrostatic meteorological model LM is developed as a "meso-to-micro scale prediction and simulation system" for tasks in scientific research and weather forecast (http://www.cosmo-model.org). The LM, since 2007 renamed as COSMO, is part of the national numerical weather prediction (NWP) system of the DWD, running operationally since 1999. The model is able to simulate atmospheric flow dynamics at the meso-γ (2 km – 20 km,), meso-β (20 km – 200 km), and meso-α (200 km – 2000 km), e.g. clouds, fog, frontal systems, meso-scale convective systems (MCS), small-scale weather events like cellular

convection and thunderstorms and local wind systems due to e.g. orographic or thermic effects. Such as atmospheric, thermo-hydrodynamic processes are simulated solving the hydro-thermodynamical equations (*Steppler et al.*, 2003). The advantage of the usage of this dynamical equations are the possibility to describe compressible non-hydrostatic processes within the moist atmosphere without assumed scale approximations. Only the difference-fields between simulated and a reference state of the atmosphere are saved. As reference state of the atmosphere, a horizontal homogeneous, time-independent dry neutral atmosphere (vertically stratified, hydrostatic balanced) is assumed. For numerical computations with the finite difference method, the primitive equations are used in their advective form, the prognostic equation is used instead of the continuity equation. For time integration, the default Leapfrog (3 time-level) scheme is used, and modified by *Skammarock and Klemp* (1992). An Arakawa-C grid with a Lorenz vertical grid staggering is used, for spatial discretisation a second-order horizontal and vertical differencing is applied.
Processes which are not accurately resolved by either the equations or the spatio-temporal resolution have to be parametrised. The prognostic (time-dependent) and diagnostic (time-independent) variables computed by the LM are listed in Tabular 5.1.

Prognostic Variables	horizontal and vertical wind components (u, v, w)
	temperature (T)
	pressure perturbation (p'): deviation from the reference state
	specific humidity (q_v)
	specific cloud water content (q_c)
Diagnostic Variables	total air density
	precipitation flux of rain and snow
Parametrised Processes	grid-scale clouds and precipitation
	subgrid-scale clouds
	moist convection (following *Tiedtke* (1989))
	radiation
	turbulent diffusion
	surface layer
	soil processes

Table 5.1: *Prognostic and diagnostic variables computed by the LM, (http://www.cosmo-model.org).*

Here, the LM runs on an artificial horizontal grid with a horizontal resolution of $28\,km \times 28\,km$ ($0.25° \times 0.25°$). For stereographic map projections, grid cells near the equator are approximately rectangular, grid-cell close to the poles are quite skewed due to the conformity. An artificial, rotated grid is defined for the model simulations to reduce that skewing. Therefore, new pole coordinates are defined in a way that maximises the rectangularity of most of the grid cells. That means, the equator of the artificial, rotated grid bisects the modelling domain. As the LM is a regional-scale model, its domain cov-

ers just a part of the global mesh. The vertical resolution is described by a generalised terrain-following height-coordinate grid (σ-p coordinate grid). Here, 40 σ-p levels are used to simulate meteorological process up to 23 km height. The first layer is situated at around 38 m above ground level.
Atmosphere and surface interact at diverse scales. So surface prescribing data sets, the so called "external data" are used for e.g. accurate parametrisation of physical processes. Table 5.2 refers to the external data sets required by the LM.

External Parameter	Source
mean topographical height	GTOPO30 data set (30" × 30"), USGS
roughness length	GTOPO30 and CORINE dataset
soil type	DSM data set (5' × 5') of FAO
vegetation cover	CORINE data set
land fraction	CORINE data set
root depth and leaf area index	CORINE data set

Table 5.2: *External parameters used by the LM, http://www.cosmo-model.org). CORINE stands for Coordination of information on the environment and was initiated in 1985 by the European Commission. GTOPO30 stands for a Global Topographical data set which is available at a horizontal resolution of 30". It is provided by the United States Geological Survey, USGS. Information on soil type are given by the Digital Soil Mapping (DSM), provided by the Food and Agricultural Organisation (FAO), United Nations Educational.*

The external data are described on a higher-resolved grid than the model simulations will be done, so the external data are interpolated on the model grid. Thereby, fine elements are smoothed and the complexity of the topography is reduced.

5.2 Tracer Transport Model MUSCAT

The MUlti-Scale Chemical Aerosol Transport model MUSCAT (*Wolke et al.*, 2004a) is developed at the Leibniz Institute for Tropospheric Research (IfT) in Leipzig, Germany, with main focus on the simulation of emission, transport, and deposition processes of European aerosol species (*Wolke et al.*, 2004a,b). Adaptions made by *Heinold et al.* (2007) and the implementation of a dust emission scheme basing on *Tegen et al.* (2002) allow for the application of the model system LM-MUSCAT to simulate the mineral dust cycle (*Heinold et al.*, 2007, 2008a; *Schepanski et al.*, 2007, 2008a,b; *Tegen et al.*, 2006). Thereby, dust particles are transported as tracer at five independent size classes.

Dust emission depends on surface properties like vegetation cover, surface roughness, soil texture, and soil moisture content and atmospheric conditions like wind and stability. So dust emission can be described as threshold phenomenon, whereby the friction wind velocity has to exceed a certain, local threshold $u_\star \geq u_{\star,t}$ depending on local soil characteristics. The friction velocity threshold $u_{\star,t}$ is computed following the approach of *Iversen*

and White (1982), modified by *Marticorena and Bergametti* (1995) (Equation 2.3). To compute the actual wind friction velocity $u_\star$ following Equation 2.2 wind fields provided by the LM are used and aerodynamic roughness length given by *Prigent et al.* (2005) for arid and semi-arid areas and *Marticorena et al.* (2004) for the Sahara domain. To consider soil characteristics strongly impacting on $u_\star$, soil data bases describing soil size distribution, soil texture and vegetation cover are required. The soil size distribution for the dust emission scheme implemented in the MUSCAT classifies four different soil size classes according to *Tegen et al.* (2002): clay, silt, medium/fine sand and coarse sand. As the size distribution does not follow the same proportion at each location, a local distribution is derived from a soil map including soil texture classes of the top 30 cm of the dominant soil type on a $0.5° \times 0.5°$ grid, provided by the Food and Agriculture Organization (FAO) (*Zobler*, 1986). Wind tunnel experiments show a particle size dependent sandblasting efficiency (*Gillette*, 1978). According to *Marticorena et al.* (1997) and *Tegen et al.* (2002) saltation efficiencies based on the wind tunnel experiments by *Gillette* (1978) have been assumed as $10^{-5}\,\mathrm{cm}^{-1}$ for silt, $10^{-6}\,\mathrm{cm}^{-1}$ for fine and medium sand and $10^{-7}\,\mathrm{cm}^{-1}$ for coarse sand (*Heinold et al.*, 2007). Beside the particle weight related to particle diameter as included in the soil size distribution, cohesion forces affect the sandblasting efficiency. Due to there mineralogical structure, clay shows high cohesion force between adjacent particles. An increasing clay content decreases the sandblasting efficiency. With regard to dust emission parametrisation, the sandblasting efficiency is set to $10^{-6}\,\mathrm{cm}^{-1}$ for clay content $< 45\,\%$ and $10^{-7}\,\mathrm{cm}^{-1}$ for a clay content $> 45\,\%$, taking the effect of variable clay contents for soils into account. The vegetation cover limits dust emission by decelerating surface wind velocities and therefore reducing the momentum transport from the air towards the soil particles, and by covering bare soils. Both limiting effects depend mainly on vegetation type and vegetation cover. E.g. a grass-like vegetation is assumed to be related to more effective dust sources than shrub-like vegetation. Shrub-like vegetation due to standing biomass elements lead a stronger decrease in surface wind velocity even if the leaf cover is low. For LM-MUSCAT, vegetation types are derived from simulations of the equilibrium terrestrial biogeography model BIOME4 (*Kaplan*, 2001). The simulation provides 27 potential vegetation types (biomes) on a $0.5° \times 0.5°$ grid. As dust emission occurs over non-forest areas, the following biomes are assumed to be important for dust mobilisation description: barren land, desert, tropical xerrophytic shrubland, temperate xerophytic shrubland, tropical grassland, temperate grassland, graminoid and forb tundra, erect dwarf-shrub tundra, prostrate dwarf-shrub tundra, and cushion-forb tundra. As mentioned above, vegetation cover is a limiting factor for dust emission beside the vegetation typ. The normalised difference vegetation index (NDVI) based on AVHRR (Advanced Very High Resolution Radiometer) difference reflectances R between $0.6\,\mu$m (visible) and $0.8\,\mu$m (near-IR) (Equation 5.1) describes the fraction of absorbed photosynthetically active radiation,

$$\mathrm{NDVI} = \frac{R_{0.8} - R_{0.6}}{R_{0.6} + R_{0.8}}. \tag{5.1}$$

Thereby high NDVI values indicate a high vegetation cover. Here, the GIMMS (Global Inventory Modelling and Mapping Studies) NDVI data set (*Pinzon*, 2002; *Pinzon et al.*,

2005; *Tucker et al.*, 2005) is used. For modelling, an empirical relationship between vegetation cover and dust emission following *Knorr and Heimann* (1995) is assumed. Therefore, an effective surface area is determined based on seasonal varying vegetation covers.
Soil moisture content reduces the soil erodibility as it impacts on cohesion forces between adjacent particles. So for a surface soil moisture content $> 99\,\%$, dust mobilisation is inhibited (*Heinold et al.*, 2007).
For modelling aspects, the emitted particles representing the original soil size spectrum with regard to surface wind velocities are distributed to five independent size bins with radii limiting at $0.1\,\mu$m, $0.3\,\mu$m, $0.9\,\mu$m, $2.6\,\mu$m, $8\,\mu$m and $24\,\mu$m (*Heinold et al.*, 2008a). These five independent size bins are transported as tracers described by the time-dependent, 3D advection-diffusion-reaction equation

$$\frac{dc}{dt} = \frac{\partial}{\partial w}\left(\rho_a K_z \frac{\partial v/\rho}{\partial w}\right) + Q(c) + D_s(c). \tag{5.2}$$

Thereby, the time-dependent dust concentration c is related to the vertical diffusion coefficient K_z, to the time-dependent emission term $Q(c)$, and to the deposition term D_s(c). Deposition, the removal of airborne dust particles from the atmosphere, is parametrised separately for dry and wet removal. The dry deposition is commonly parametrised using the deposition velocity v_d following *Zhang et al.* (2001). Wet deposition by rain-out and wash-out is parametrised following e.g. *Berge* (1997) and *Jacobson et al.* (1997) with details described in *Tsyro and Erdman* (2000).

5.3 Coupling: LM-MUSCAT

In the coupled model system LM-MUSCAT, the LM provides meteorological and hydrological fields, updated at every advection time step comprising 80 s. For radiative feedback considerations, the MUSCAT provides size-resolved dust concentration fields to the LM allowing on-line feedback mechanisms on e.g. temperature fields and atmospheric stability (*Heinold et al.*, 2007, 2008a). In MUSCAT, dust is transported as a tracer using meteorological fields up to 12 km height.
The spin-up period comprises 24 hours for the LM part, every 6 hours meteorological boundary conditions are updated using analysis field from the global weather forecast model (GME), provided by the DWD. After the spin-up period, the MUSCAT is coupled to the LM. A re-initialisation of the meteorological fields is done after a period of 24 hours.

Chapter 6

Publications

6.1 Summary of Publications

Within the present work seasonal changes of atmospheric Saharan dust cycle are characterised. Potential dust source areas and meteorological conditions suitable to force dust particle mobilisation are focussed. For this satellite remote sensing techniques (Spinning Enhanced VIsible and InfraRed Imager (SEVIRI) onboard the geostationary Meteosat Second Generation (MSG) satellite and atmospheric modelling (LM-MUSCAT, ECMWF ERA-40 reanalysis) are used. The transport of atmospheric dust depends on height, direction and atmospheric conditions during transport (e.g. the presence of clouds). The dust particles are finally removed from the atmosphere. Both, transport and deposition of mineral dust are investigated using results of the regional model system LM-MUSCAT. The model system consists of the meso-scale atmosphere model LM (Lokalmodell, *Steppler et al.* (2003)) provided by the German weather service DWD (Deutscher Wetterdienst) and the MUlti-Scale Chemistry Aerosol Transport model (MUSCAT, *Wolke et al.* (2004a)).
Modelling studies are limited by the accuracy of models, uncertainties due to parameterisation schemes and input parameters. Thus, observations are needed to improve our knowledge on processes as well as for model validation. Here, satellite remote sensing is used for observation of airborne dust as well as dust emission in terms of increasing dust indices. A $1^\circ \times 1^\circ$ map on dust source areas and the time-of-day of starting emission is compiled for the area covering Africa north of 5° N from MSG SEVIRI satellite data since March 2006. Thereby individual dust events are tracked back to the point of their first appearance (*Schepanski et al.*, 2007). The high temporal resolution at which the dust index is available is a prerequisite for this method. The movement of the dust index pattern enables distinctions from underground given in a similar colour. Additionally, dust mobilisation events directly linked to convective cloud dynamics are labelled. As dust events beneath clouds cannot be observed, only dust plumes leaving the area covered by the cloud can be detected.
Cloud cover is the main limit of this detection method. Additionally mobilisations along a dust plume track cannot be detected because of the overlying dust layer. As the dust source activation detection is done by visual observation, the dust detection is limited

to the ability of the eyes to distinguish between the colour of the surface, impacted by the surface temperature and texture, and airborne dust. This is especially the case for diffuse dust plumes or over mountainous terrain and off the west coast of the Sahara where the warm ocean inhibit the application of the infrared (IR) dust index to thin dust plumes. Nevertheless, the estimated errors of this visual observations are lower than errors that would been made due to automatically assumed thresholds for dust presence. A comparison of dust indicating IR product and AErosol RObotic NETwork (AERONET, *Holben et al.* (1998)) aerosol optical thickness (AOT) at an African station (Banizoumbou, 13° 32' N; 2°39' E) is shown in Figure 6.1. The agreement between AOT measurements and the brightness temperature difference (BTD) used in the dust index supports the assumption that the dust index is a measure for the presence of dust.

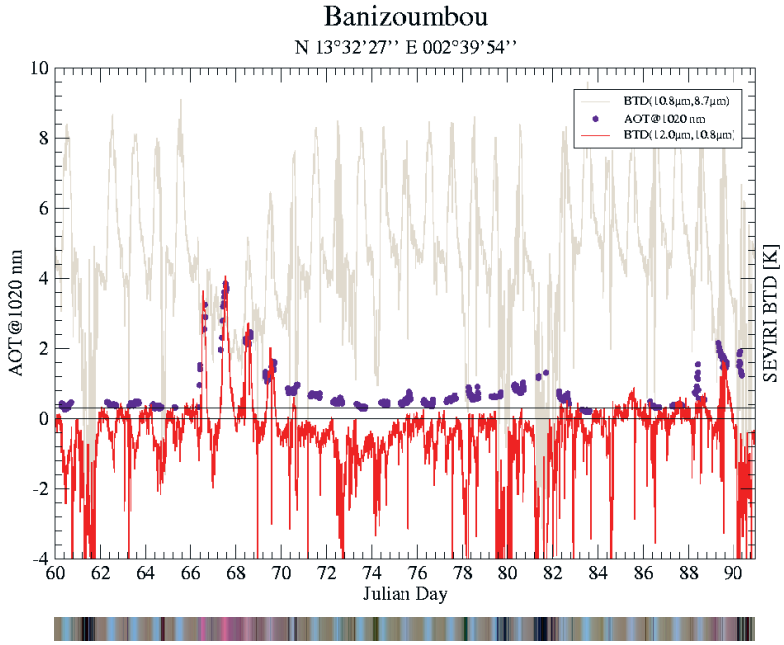

Figure 6.1: *Timeseries of AERONET AOT and MSG-SEVIRI BTD indicating dust. Bottom scale indicates the colour of the MSG-SEVIRI dust index. blue: daytime surface, gray: nighttime surface, magenta: dust, black: cloud.*

The new Saharan dust source map compiled from the dust index contains spatio-temporal information and enables for the first time the direct localisation of dust source areas, to characterise the sources by time-of-day of dust mobilisation and the frequency of dust source activation. Earlier remote sensing studies on Saharan dust sources based on daily dust retrievals, and were affected by dust transport due to the time-lag between dust source activation and dust detection. This map, named Dust Source Activation Frequency (DSAF), inferred from MSG observations is a new way to validate Saharan dust emissions computed by regional dust models. Alternatively, the map can be used as a mask for po-

tential dust source areas in such models. The simulation of dust emission is only allowed where active dust sources have been observed by MSG-SEVIRI. No specific emission fluxes are prescribed. Atmospheric conditions determine the location of dust emission and its strength (dust emission flux) Seasonal changes in the pattern of active dust sources have to be represented by the dependence of dust emission and atmospheric conditions, e.g. wind fields. First studies show that the use of this mask improves the model performance when compared with an independent dataset (*Cavazos et al.*, 2008; *Schepanski et al.*, 2007, 2008b).

The DSAF dataset is used to investigate on the spatial distribution of dust source areas highlighting endorheic drainage systems like wadis located in the mountain foothills as frequent source areas. Furthermore, seasonally changing pattern of "hot spot" areas in terms of high frequencies of active dust sources are evident: During summer, the West Sahara becomes more active than in winter when the Bodélé depression is the most active dust source area. Beside spatial distribution and variability of dust source activation frequencies, the distribution of the time-of-day when dust emission starts is analysed. The morning hours between 06-09 UTC are characterised by the maximum dust source activation frequency, 65 % for the entire North African sector during an observation period of 2006/03–2008/08.

The time-of-day distribution of dust source activations has been used to relate dust en-

Time [UTC]	**Fraction of observed DSAF**	**Meteorological conditions**
00-03	2%	Haboob
03-06	5%	Haboob
06-09	65%	LLJ break-down
09-12	16%	LLJ break-down
12-15	8%	density currents in term of *Knippertz et al.* (2007), lee-cyclolysis like the Sharave-Cyclone
15-18	1%	density currents in term of *Knippertz et al.* (2007), Haboob
18-21	2%	Haboob
21-00	1%	Haboob

Table 6.1: *Attribution of time-of-day of observed DSAF [%] over the entire Saharan and Sahelian sector including Mahgreb, and probably most important meteorlogical situation forcing DSA (Schepanski et al., 2008b). Keep in mind, that over the entire desert from the Red Sea to the Atlantic a time difference of 4 hours.*

trainment to meteorological features (*Schepanski et al.*, 2008b). Thereby, two conditions were considered: (1.) The ability to provide atmospheric condition suitable for dust mobilisation (i.e. high wind speed) and (2.) the return frequency of such feature compared to the DSAF observations (Table 6.1). Wind speed observations provided by synoptic stations and modelling studies using LM-MUSCAT and global ERA-40 reanalysis fields were investigated because the dust emission process itself cannot be resolved by satellite

remote sensing. The break-down of the nocturnal LLJ is identified to account for most of dust source activations during the morning hours and can be seen as most important meteorological feature for dust emission over North Africa in terms of frequency of emissions.
Dust source activations occurring during the afternoon and evening hours are often related to gusts generated by dry or wet convection. Density currents (also termed gravity currents) and Haboobs are generated by evaporative cooling, occurring mostly during this time of day. The relatively low number of DSA occurring during afternoon and evenings point towards a lesser role of those convective events in terms of dust activation frequency, although the emission fluxes per event may be much higher than for the dust events occurring during morning hours.
Especially over the northern part of the Sahara and the Mediterranean coast, lee-cyclones (so called Saharav cyclone) develop on the lee-ward side of the Atlas Mountain chain especially during spring and early summer, enhanced by baroclinity. During noon and afternoon hours the convective activity and related gustiness of the wind is strongest. The active warm front of these cyclones is mostly accompanied by a dust storm moving in eastward direction.
Atmospheric conditions related to typical meteorological conditions do not occur with the same frequency for all areas. Seasonal changing meteorological conditions providing atmospheric conditions suitable for dust mobilisation are the main mechanism to force or inhibit the activation of individual dust sources over desert terrain.

Dust export form the Sahara becomes important especially for regions down-wind of dust sources because dust delivers micro-nutrients for terrestrial and oceanic ecosystems, and affects modern human life. Dust transport can be observed by satellite retrievals. To determine dust transport paths (height and direction), export and deposition fluxes, three case studies representing three different seasons (winter, spring and summer) have been performed using LM-MUSCAT. Strong seasonal variabilities regarding the amount of export and deposition, but also regarding transport height and transport direction influenced by atmospheric conditions such as wind regimes and air mass characteristics are shown by the simulations (*Schepanski et al.*, 2008a). In winter, dust is transported in near-surface levels in south-westward direction. In summer, dust transport shows a clear westward direction and takes place within elevated layers, mostly above the trade wind inversion. Nevertheless, emission, transport and deposition are linked to atmospheric conditions and circulation. Parameters like wind speed, stability, temperature and moisture impact on the vertical and horizontal distribution of the dust layer. The atmospheric circulation impacts on transport direction and velocity. Also the presence of clouds and the transport into cloudy regions, respectively, impact on deposition fluxes.

Publications:

K. Schepanski, I. Tegen, B. Laurent, B. Heinold, and A. Macke (2007), *A new Saharan dust source activation frequency map derived from MSG-SEVIRI IR-channels*, Geophys. Res. Lett., 34, L18803, doi:10.1029/2007GL030168.

K. Schepanski, I. Tegen, M. C. Todd, B. Heinold, G. Bönisch, B. Laurent and A. Macke (2008), *Meteorological processes forcing Saharan dust emission inferred from MSG-SEVIRI observations of sub-daily dust source activation*, J. Geophys. Res., revised.

K. Schepanski, I. Tegen and A. Macke (2008), *Saharan dust transport and deposition towards the tropical northern Atlantic*, Atmos. Chem. Phys., 9, 1173-1189, 2009.

Due to copyright this publications are not included in the present version. Therefore, please note that page numbers differ from the original thesis.

Chapter 7

Outlook

The present work bases on observation data and model simulations. It is shown, that the usage of both leads to a more complete description of the Saharan dust cycle than each single dataset will give. The complementary usage of such datasets facilitate the improvement of the knowledge on atmospheric dust and its effects on the environment. Nevertheless, future studies have to be done.

Modelling studies are limited e.g. by the accuracy of parametrisations, input variables, and fields. To estimate the magnitude of errors made by necessary assumptions for parametrisation ensemble runs will be a good possibility. Thereby, several similar model runs but with slightly varying input parameters will be computed, approximating the most realistic case by the probability of occurrence of a specific evolution. In the case of dust modelling, e.g. several different particle characteristics concerning their optical properties and size distribution could be assumed. Dust particles act on the atmospheric conditions due to their direct and indirect radiative effect, that ensemble runs of different particle characteristics will improve the approximation of the real case. This ensembles for atmospheric models will also account for the effect of radiative feedback mechanisms on meteorological conditions and thereby allow for a feedback on processes forcing or limiting dust emission. This would not be possible with stand-alone radiative transport models.
Long-term observations of dust storm frequencies and dust optical thickness point towards strong interannual variability of atmospheric dust. The improvement of our knowledge of meteorological conditions responsible for dust emission, transport and deposition, but also teleconections to remote atmospheric and oceanic circulation pattern will help to understand interannual variability, also with regard to a changing environment. To address this question modelling studies as well as long-term observations (ground- and space-borne) are required.
Interactions of atmospheric dust and monsoon circulations as well as the development of tropical cyclones (up to Hurricanes and Typhoons) are the topic of recent modelling and measurement studies. Improved knowledge on the interaction of tropical atmospheric elements (e.g. African Easterly Jet, West African Monsoon circulation) and dust emission as well as interactions of dust particles and cloud development, convection or stability,

will help to improve forecasts and climate projections.
In the present work dust source activities over North Africa are investigated and characterised on a sub-daily scale. An extension of this study with such a comparably high temporal resolution to other hyper-arid, arid and semi-arid areas will be of interest. There, differences concerning geomorphology and atmospheric circulation are evident. Furthermore, the identification of individual source area and an improved knowledge of meteorological conditions during dust emission will help to understand dust feedback mechanisms which depend on the characteristics of dust source areas (e.g. mineralogy), transport path (e.g. chemical reactions on particle's surface) and the deposition fluxes (fertilisation of remote areas).
Besides the effect of mineral dust on the atmosphere, dust impacts on oceanic and terrestrial biosphere. Dust as transport medium for micro-nutrients act on the biological productivity of remote areas, and thereby on the atmospheric CO_2-cycle and the climate system. Furthermore, iron and phosphorous transported to the Ocean by mineral dust particles enhance nitrogen fixation, an important process for the global nitrogen cycle. The precise knowledge of dust source conditions may help to characterise the mineralogical and chemical composition of dust, providing improved estimates of their deposition fluxes. This may provide useful input for models describing microbiological processes in the surface ocean.

An improved knowledge on the spatio-temporal distribution of dust sources and its activation will help to give a more accurate estimation of interactions of mineral dust and the environment. Furthermore, an improved understanding of dust feedback mechanisms will help to describe the role of airborne dust for a changing environment.

List of Abbreviations

AEJ	African easterly jet
AERONET	AErosol RObotic NETwork
AEW	African easterly wave
AI	Absorbing Aerosol Index
AOT	Aerosol Optical Thickness
BL	Boundary Layer
BT	Brightness temperature
BTD	Brightness temperature difference
CALIPSO	Cloud-Aerosol Lidar and Infrared Pathfinder Satellite Observations
CCN	Cloud condensation nuclei
CH	Channel
DSA	Dust source activation
DSAF	Dust source activation frequency
DWD	Deutscher Wetterdienst, German Weather Service
ECMWF	European Center for Medium-Range Weather Forecast
ERA-40	ECMWF 45-year reanalysis data
EUMETSAT	European Organisation for the Exploitation of Meteorological Satellites
HNLC	High-nitrate, low chlorophyll
IDDI	Infrared Difference Dust Index
IR	Infrared, wavelength spectrum
ITCZ	Inter-tropical convergence zone
ITD	Inner-tropical discontinuity
LLJ	Low-level jet
LM	Lokalmodell, meso-scale model of German Weather Service (DWD)
MCS	Meso-scale convective system
MUSCAT	MUlti Scale Chemistry and Aerosol Transport Model
MSG	Meteosat Second Generation
NAO	North Atlantic Oscillation
NASA	National Aeronautics and Space Agency, United States
NBL	Nocturnal boundary layer
NIR	Near-infrared
OMI	Ozone Monitoring Instrument
SAL	Saharan Air Layer

SEVIRI	Spinning and Enhanced Visible and InfraRed Imager
TOMS	Total Ozone Mass Spectrometer
TRACES	Ocean – Atmosphere – Land Impacts on TRopical Atlantic EcoSystems
UTC	Universal time, coordinated
UV	Ultraviolet, wavelength spectrum
VIS	Visible
WV	Water vapour

Bibliography

Ackerman, S. A. (1997), Remote sensing aerosol using satellite infrared observations, *J. Geophys. Res.*, *102*(D14), 17,069–17,079.

Allen, M. D., and O. G. Raabe (1982), Re-evaluation of Millikan's oil drop data for the motion of small particles in air, *Journ. of Aerosol Sci.*, *13*(6), 537–547, doi:10.1016/0021-8502(82)90019-2.

Allen, M. D., and O. G. Raabe (1985), Slip correction measurements of spherical solid aerosol-particles in an improved Millikan apparatus, *Aerosol Science and Technology*, *4*(3), 269–286.

Alpert, P., and B. Ziv (1989), The Sharav Cyclone - observations and some theoretical considerations, *J. Geophys. Res.*, *94*, 18,495–18,514.

Alpert, P., B. I. Neeman, and Y. Shay-el (1990), Climatological analysis of Mediterranean cyclones using ECMWF data, *Tellus*, *42A*, 65–77.

Arimoto, R., B. J. Ray, N. F. Lewis, U. Tomaza, and R. A. Duce (1997), Mass particle size distribution of atmospheric dust and the dry deposition of dust to the remote ocean, *J. Geophys. Res.*, *102*, 15,867–15,874.

Avila, A., and J. Penuelas (1999), Increasing frequency of Saharan rains over northeastern Spain and its ecological consequences, *The Science of the Total Environment*, *228*(2-3), 153–156.

Bagnold, R. A. (1941), *The Physics of Blown Sand and Desert Dunes*, 265 pp., Methuen, New York.

Banta, R., Y. L. Pichugina, and R. K. Newsom (2003), Realtionship between Low-Level Jet Properties and Turbulence Kinetic Energy in the Nocturnal Stable Boundary Layer, *J. Atmos. Sci.*, *60*, 2549–2555.

Banta, R. M., R. K. Newsom, J. K. Lundquist, Y. L. Pichugina, R. L. Coulter, and L. J. Mahrt (2002), Nocturnal low-level jet characteristics over Kansas during CASES-99, *Bound.-Layer Meteor.*, *105*, 221–252.

Banta, R. M., Y. L. Pichugina, and W. A. Brewer (2006), Turbulent Velocity-Variance Profiles in the Stable Boundary Layer Generated by a Nocturnal Low-Level Jet, *J. Atmos. Sci.*, *63*, 2700–2719.

Barkan, J., H. Kutiel, P. Alpert, and P. Kishcha (2004), Synoptics of dust intrusion days from the African continent into the Atlantic Ocean, *J. Geophys. Res.*, *109*, D08,201, doi:10.1029/2003JD004416.

Barton, I. J., A. J. Prata, I. G. Watterson, and S. A. Young (1992), Identification of the mount Hudson volcanic cloud over SE Australia, *Geophys. Res. Lett.*, *19*(12), 1211–1214.

Bücher, A., and J. Dessens (1992), Saharan dust over France and England, 6-9 March 1991, *J. Meteor.*, *17*, 226–233.

Berge, E. (1997), Transboundary air pollution in Europe, *MSC-W Status Rep. 1997, Part 1 and 2, EMEP/MSC-W Rep. 1/97*, Norwegian Meteorol. Inst. Oslo, Norway.

Berkofsky, L. (1982), A heuristic investigation to evaluate the feasibility of developing a desert dust prediction model, *Mon. Wea. Rev.*, *110*, 2055–2062.

Berry, G., and C. Thorncroft (2005), Case study on an intense African easterly wave, *Mon. Wea. Rev.*, *133*, 752–766, doi:10.1175/MW2884.1.

Berry, G., C. Thorncroft, and T. Hewson (2007), African Easterly Waves during 2004 - Analysis Using Objective Techniques, *Mon. Wea. Rev.*, *135*, 1251–1267, doi: 10.1175/MWR3343.1.

Blackadar, A. K. (1957), Boundary Layer Wind Maxima and Their Significance for the Growth of Nocturnal Inversion, *Bull. Amer. Meteor. Soc.*, *38*(5), 283–290.

Bonner, W. D. (1968), Climatology of the Low Level Jet, *Mon. Wea. Rev.*, *96*(12), 833–850.

Bonner, W. D., and J. Paegle (1970), Diurnal Variations in Boundary Layer Winds over the South-Central United States in Summer, *Mon. Wea. Rev.*, *98*(10), 735–744.

Bouet, C., G. Cautenet, R. Washington, M. C. Todd, B. Laurent, B. Marticorena, and G. Bergametti (2007), Mesoscale modeling of aeolian dust emission during the BoDEx 2005 experiment, *Geophys. Res. Lett.*, *34*(7), L07,812, doi:10.1029/2006GL029184.

Boy, J., and W. Wilke (2008), Tropical Andean forest derives calcium and magnesium from Saharan dust, *Global Biogeochem. Cycles*, *22*, GB1027, doi:10.1029/2007GB002960.

Brooks, N., and M. Legrand (2000), Dust variability over northern Africa and rainfall in the Sahel, in *Linking Climate Change to Landsurface Change*, edited by S. J. McLaren and D. Kniveton, pp. 1–25, Kluwer Academic Publishers, Dordecht, The Netherlands.

Brost, R. A., and J. C. Wyngaard (1978), A Model Study of the Stably Stratified Planetary Boundary Layer, *J. Atmos. Sci.*, *35*(8), 1427–1440.

Browning, K. A., and G. W. Bryant (1975), An example of rainbands associated with stationary longitudinal circulations in the planetary boundary layer, *Quart. J. R. Met. Soc.*, *101*, 893–900.

Bullard, J., M. Baddock, G. McTainsh, and J. Leys (2008), Sub-basin scale dust source geomorphology detected using MODIS, *Geophys. Res. Lett.*, *35*(15), L15,404, doi: 10.1029/2008GL033928.

Burpee, R. W. (1972), The origin and structure of easterly waves in the lower troposphere of North Africa, *J. Atmos. Sci.*, *29*, 77–90.

Burpee, R. W. (1974), Characteristics of North African easterly waves during the summers of 1968 and 1969, *J. Atmos. Sci.*, *31*, 1556–1570.

Carlson, T. N. (1969), Some remarks on African disturbances and their progress over the tropical Atlantic, *Mon. Wea. Rev.*, *97*, 716–726.

Carlson, T. N. (1979), Atmospheric Turbidity in Saharan Dust Outbreaks as Determined by Analyses of Satellite Brightness Date, *Mon. Wea. Rev.*, *107*, 322–335.

Carlson, T. N., and J. M. Prospero (1972), The Large-Scale Movement of Saharan Air Outbreaks over the Northern Equatorial Atlantic, *J. Appl. Meteor.*, *11*, 283–297.

Cavazos, C., M. C. Todd, and K. Schepansi (2008), Numerical model simulation of the saharan dust event of march 2006, *J. Geophys. Res.*, revised.

Chesters, D., L. W. Uccellini, and W. D. Robinson (1983), Low-Level Water Vapor Fields from the VISSR Atmospheric Sounder (VAS) "Split Window" Channels, *J. Climate Appl. Meteor.*, *22*, 725–743.

Chiapello, I., and C. Moulin (2002), TOMS and METEOSAT satellite records of the variability of Saharan dust transport over the Atlantic during the last two decades (1979-1997), *Geophys. Res. Lett.*, *29*(8), L1176.

Chiapello, I., G. Bergametti, L. Gomes, B. Chatenet, F. Dulac, J. Pimenta, and E. S. Suares (1995), An additional low layer transport of Sahelian and Saharan dust over the North-Eastern Tropical Atlantic, *Geophys. Res. Lett.*, *22*(23), 3191–3194.

Chiapello, I., G. Bergametti, B. Chatenet, P. Bousquet, F. Dulac, and E. S. Soares (1997), Origins of African dust transported over the northeastern tropical Atlantic, *J. Geophys. Res.*, *102*(D12), 13,701–13,709.

Chiapello, I., C. Moulin, and J. M. Prospero (2005), Understanding the long-term variability of African dust transport across the Atlantic as recorded in both Barbados surface concentrations and large-scale Total Ozone Mapping Spectrometer (TOMS) optical thickness, *J. Geophys. Res.*, *110*, D18S10.

Chimonas, G. (2005), The Nighttime Accelerations of the Wind in the Boundary Layer, *Bound.-Layer Meteor.*, *116*, 519–531, doi:10.1007/s10546-005-0609-x.

Coen, M. C., E. Weingartner, D. Schaub, C. Hueglin, C. corrigan, S. Henning, M. Schwikowski, and U. Baltensperger (2004), Saharan dust events at the Jungfraujoch:

detection by wavelength dependence of the single scattering albedo and first climatology analysis, *Atmos. Chem. Phys.*, *4*, 2465–2480.

Cook, K. H. (1999), Generation of the African easterly jet and its role in determining West African precipitation, *J. Climate*, *12*, 1165–1184.

Criado, C., and P. Dorta (2003), An unusual "blood rain" over the Canary Islands (Spain). The storm of January 1999, *Journ. Arid Environm.*, *55*, 765–783.

D'Almeida, G. A. (1986), A Model for Saharan Dust Transport, *J. Climate Appl. Meteor.*, *25*, 903–916.

Davis, P. A. (2000), Development and mechanisms of the nocturnal jet, *Meteorol. Appl.*, *7*(3), 239–246.

DeMott, P. J., K. Sassen, M. R. Poellot, D. Baumgardner, D. C. Rogers, S. D. Brooks, A. J. Prenni, and S. M. Kreidenweis (2003), African dust aerosols as atmospheric cloud ice nuclei, *Geophys. Res. Lett.*, *30*(14), L1732.

Drobinski, P., B. Sultan, and S. Janicot (2005), Role of the Hoggar Masif in the West African monsoon onset, *Geophys. Res. Lett.*, *32*(1), L01,705, doi: 10.1029/2004GL020710.

Duce, R. A. (1995), Sources, Distributions, and Fluxes of Mineral Aerosols and Their Relationship to Climate, in *Dahlem Workshop on Aerosol Forcing of Climate*, edited by R. J. Charton and J. Heintzenberg, pp. 43–72, John Wiley, Chichester, U. K.

Dunion, J. P., and C. S. Velden (2004), The Impact of the Saharan Air Layer on Atlantic Tropical Cyclone Activity, *Bull. Amer. Meteor. Soc.*, pp. 353–365.

Eck, T. F., P. K. Bhartia, P. H. Hwang, and L. L. Stowe (1987), Reflectivity of the Earth's surface and clouds in ultraviolet from satellite observations, *J. Geophys. Res.*, *92*, 4287–4296.

Ellis, W. G., and J. T. Merrill (1995), Trajectories for Saharan dust transported to Barbados using Stokes Law to describe gravitational settling, *J. Appl. Meteor.*, *34*(7), 1716–1726.

Engelstaedter, S., and R. Washington (2007), Atmospheric controls on the annual cycle of North African dust, *J. Geophys. Res.*, *112*, D03,103.

Engelstaedter, S., I. Tegen, and R. Washington (2006), North African dust emission and transport, *Earth-Science Reviews*, *79*, 73–100, doi:10.1016/j.erscirev.2006.06.004.

Enger, L., D. Koračin, and X. Yang (1993), A Numerical Study of Boundary Layer Dynamics in a Mountain Valley, *Bound.-Layer Meteor.*, *66*, 357–394.

Erel, Y., U. Dayan, R. Rabi, Y. Rudich, and M. Stein (2006), Trans Boundary Transport of Pollutants by Atmospheric Mineral Dust, *Environ. Sci. Technol.*, *40*, 2996–3005.

Evan, A., A. K. Heidinger, and P. Knippertz (2006), Analysis of winter dust activity off the coast of West Africa using a new 24-year over-water advanced very high resolution radiometer satellite dust climatology, *J. Geophys. Res.*, *111*, D12,210, doi: 10.1029/2005JD006336.

Fan, S.-M., W. J. Moxim, and H. Levy (2006), Aeolian input of bioavailable iron to the ocean, *Geophys. Res. Lett.*, *33*(7), L07,602, doi:10.1029/2005GL024852.

Findlater, J. (1972), Aerial explorations of the low-level cross-equatorial current over Eastern Africa, *Quart. J. R. Met. Soc.*, *98*, 274–289.

Flamant, C., J.-P. Chaboureau, D. J. Parker, C. M. Taylor, J.-P. Cammas, O. Bock, F. Timouk, and J. Pelon (2007), Airborne observations of the impact of a convective system on the planetary boundary layer thermodynamics and aerosol distribution in the inter-tropical discontinuity region of the West African Monsoon, *Quart. J. R. Met. Soc.*, *133*, 1175–1189, doi:10.1002/qj.97.

Franzen, L. G., J. O. Mattson, and U. Martensson (1994), Yellow snow over the Alps and sub-Arctic from dust storm in Africa, March 1991, *Ambio*, *23*(3), 233–235.

Fraser, Y. J. K. R. S. (1997), The effect of smoke particles on clouds and climate forcing, *Science*, *227*, 1573–1728.

Fung, I., S. Meyn, I. Tegen, S. C. Doney, J. John, and J. K. B. Bishop (2000), Iron supply and demand in the upper ocean, *Global Biogeochem. Cycles*, *14*, 281–296.

Ganor, E. (1994), The frequency of Saharan dust episodes over Tel Aviv, Israel, *Atmos. Environ.*, *28*(17), 2867–2871.

Gao, Y., Y. J. Kaufman, D. Tanré, D. Kolber, and P. G. Falkowski (2001), Seasonal Distribution of Aeolian Iron Fluxes to the Global Ocean, *Geophys. Res. Lett.*, *28*(1), 29–32.

Garratt, J. R. (1992), *The atmospheric boundary layer*, Cambridge University Press.

Gatz, D. F., and J. M. Prospero (1996), A large silicon-aluminium aerosol plume in central Illinois: North African desert dust?, *Atmos. Environ.*, *30*(22), 3789–3799.

Gillette, D. (1978), A wind tunnel simulation of the erosion of soil: Effect of soil texture, sandblasting, wind speed, and soil consolidation on dust production, *Atmos. Environ.*, *12*, 1735–1743.

Gillette, D. A. (1979), Environmental factors affecting dust emission by wind erosion, in *Saharan Dust*, edited by C. Morales, pp. 71–94, John Wiley, New York.

Ginoux, P., M. Chin, I. Tegen, J. M. Prospero, B. Holben, O. Dubovik, and S.-J. Lin (2001), Sources and distributions of dust aerosols simulated with the GOCART model, *J. Geophys. Res.*, *106*(D17), 20,255–20,273.

Ginoux, P., J. M. Prospero, O. Torres, and M. Chin (2004), Long-term simulation of global dust distribution with the GOCART model: correlation with North Atlantic Oscillation, *Environment Modelling & Software*, *19*(10.1016/S1364-8152(03)00114-2), 113–128.

Goudie, A. S., and N. J. Middleton (1992), The changing frequency of dust storms through time, *Clim. Change*, *20*, 197–225.

Goudie, A. S., and N. J. Middleton (2001), Saharan dust storms: nature and consequences, *Earth-Science Rev.*, *56*, 179–204.

Griffin, D. W., and C. A. Kellogg (2004), Dust Storms and Their Impact on Ocean and Human Health: Dust in Earth's Atmosphere, *EcoHealth*, *1*, 284–295.

Grini, A., C. S. Zender, and P. R. Colarco (2002), Saltation sandblasting behaviour during mineral dust aerosol production, *Geophys. Res. Lett.*, *29*(18), 1868, doi: 10.1029/2002GL015248.

Grini, A., G. Myhre, C. S. Zender, and I. S. A. Isaksen (2005), Model simulations of dust sources and transport in the global atmosphere: Effects of soil erodibility and wind speed variability, *J. Geophys. Res.*, *110*, D02,205, doi:10.1029/2004JD005037.

Guerzoni, S., E. Molinaroli, and R. Chester (1997), Saharan dust inputs to the western Mediterranean Sea: depositional patterns, geochemistry and sedimentological implications, *Deep-Sea Research II*, *44*(3-4), 631–654.

Ha, K.-J., and L. Mahrt (2001), Simple Inclusion of z-less Turbulence within and above the Modeled Nocturnal Boundary Layer, *Mon. Wea. Rev.*, *129*, 2136–2143.

Hamilton, R. A., and J. W. Warchbold (1945), Meteorology of Nigeria and adjacent territory, *Quart. J. R. Met. Soc.*, *71*, 231–265.

Haywood, J., P. Francis, S. Osborne, M. Glew, N. Loeb, E. Highwood, D. Tanré, G. Myhre, P. Formenti, and E. Hirst (2003), Radiative properties and direct radiative effect of Saharan dust measured by the C−130 aircraft during SHADE: 1. Solar spectrum, *J. Geophys. Res.*, *208*(D18), 8577, doi:10.1029/2002JD002687.

Heinold, B., J. Helmert, O. Hellmuth, R. Wolke, A. Ansmann, B. Marticorena, B. Laurent, and I. Tegen (2007), Regional Modeling of Saharan Dust Events using LM-MUSCAT: Model Description and Case Studies, *J. Geophys. Res.*, *112*, D11,204, doi: 10.1029/2006JD007443.

Heinold, B., I. Tegen, M. Esselborn, K. Kandler, P. Knippertz, D. Müller, A. Schladitz, M. Tesche, B. Weinzierl, A. Ansmann, D. Althausen, B. Laurent, A. Massling, T. Müller, A. Petzhold, K. Schepanski, and A. Wiedensohler (2008a), Regional Saharan Dust Modelling during the SAMUM 2006 Campaign, *Tellus*, *61B*, doi:10.1111/j.1600-0889.2008.00387.x.

Heinold, B., I. Tegen, K. Schepanski, and O. Hellmuth (2008b), Dust Radiative Feedback on Saharan Boundary Layer Dynamics and Dust Mobilization, *Geophys. Res. Lett.*, *35*, L20,817, doi:10.1029/2008GL035319.

Herman, J. R., P. K. Bhartia, O. Torres, C. Hsu, C. Seftor, and E. Celarier (1997), Global distribution of UV-absorbing aerosols from Nimbus 7/TOMS data, *J. Geophys. Res.*, *102*(D14), 16,922–16,922.

Holben, B. N., T. F. Eck, I. Slutsker, D. Tanre, J. P. Buis, A. Setzer, E. Vermote, J. A. Reagan, Y. J. Kaufman, T. Nakajima, F. Lavenu, I. Jankowiak, and A. Smirnov (1998), AERONET - A Federated Instrument Network and Data Archive for Aerosol Characterization, *Remote Sens. Environ.*, *66*, 1–16.

Holton, J. R. (1967), The diurnal boundary layer wind oscillation above sloping terrain, *Tellus*, *19*(2), 199–205.

Hoose, C., U. Lohmann, R. Erdin, and I. Tegen (2008), The global influence of dust mineralogical composition on heterogeneous ice nucleation in mixed-phase clouds, *Environ. Res. Lett.*, *3*(2), 025,003, doi:10.1088/1748-9326/3/2/025003.

Houze, R. A. J., S. A. Rutledge, B. F. Smull, and P. Doge (1990), Mesoscale organization of springtime rainstorms in Oklahoma, *Mon. Wea. Rev.*, *118*, 613–654.

Hoxit, L. R. (1975), Diurnal Variations in Planetary Boundary-Layer Winds over Land, *Bound.-Layer Meteor.*, *8*, 21–38.

Hsu, N. C., S. C. Tsay, M. D. King, and J. R. Herman (2004), Aerosol Properties Over Bright-Reflecting Source Regions, *IEEE Trans. Geosci. Remote Sens.*, *42*(3), 557–569.

Hurrell, J. W. (1995), Decadal trend in the North Atlantic Oscillation: Regional temperatures and precipitations, *Science*, *269*, 676–679.

IPCC (2007), *Climate Change 2007: The Physical Science Basis.*, Contribution of Working Group I to the Forth Assessment Report of the Intergovernmental Panel on Climate Change, edited by S. Solomon, D. Quin, M. Manning, Z. Chen, M. Marquis, K. B. Averyt, M. Tignor, and H. L. Miller, Cambridge, United Kingdom and New York, NY, USA.

Israelevich, P. L., Z. Levin, J. H. Joseph, and E. Ganor (2002), Desert aerosol transport in the Mediterranean region as inferred from the TOMS aerosol index, *J. Geophys. Res.*, *107*(D21), 4572, doi:10.1029/2001JD002011.

Iversen, J. D., and B. R. White (1982), Saltation threshold on Earth, Mars and Venus, *Sedimentology*, *29*, 111–119.

Jacobson, H. A., J. E. Jonson, and E. Berge (1997), The multi-layer Eulerian model: Model description and evaluation of transboundary fluxes of sulphur and nitrogen species for one year, *EMEP/MSC-W Note 2/97*, Norwegian Meteorol. Inst., Oslo, Norway.

Jaffe, D., J. Snow, and O. Cooper (2003), the April 2001 Asian dust events: transport and substantial impact on surface particulate matter concentrations across the United States, *EOS transactions*.

Jickells, T. D., Z. S. An, K. K. Andersen, A. R. Baker, G. Bergametti, N. Brooks, J. J. Cao, P. W. Boyd, R. A. Duce, K. A. Hunter, H. Kawahata, N. Kubilay, J. LaRoche, P. S. Liss, N. Mahowald, J. M. Prospero, A. J. Ridgwell, I. Tegen, and O. Torres (2005), Global Iron Connections Between Desert Dust, Ocean Biogeochemistry, and Climate, *Science*, *308*(5718), 67–71.

Johansen, A. M., R. L. Siefert, and M. R. Hoffmann (2000), Chemical composition of aerosols collected over the tropical North Atlantic, *J. Geophys. Res.*, *105*(D12), 15,227–15,312.

Johnson, B. T., S. R. Osborne, and J. M. Haywood (2008), Aircraft measurements of biomass burning aerosol over West Africa during DABEX, *J. Geophys. Res.*, *113*(D00C06), doi:10.1029/2007JD009741.

Jones, C., N. Mahowald, and C. Luo (2003), The role of easterly waves on African desert dust transport, *J. Climate*, *16*(22), 3617–3628.

Jones, C., N. Mahowald, and C. Luo (2004), Observational evidence of African desert dust intensification of easterly waves, *Geophys. Res. Lett.*, *31*(17), 17,208.

Jones, P., T. Jünsson, and D. Wheeler (1997), Extension to the North Atlantic Oscillation using early instrumental pressure observations from Gribaltar and south-west Iceland, *Int. J. Climatol.*, *17*, 1433–1450.

Journet, E., K. V. Desboeufs, S. Caquineau, and J.-L. Colin (2008), Mineralogy as a critical factor of dust iron solubility, *Geophys. Res. Lett.*, *35*, L07,805, doi: 10.1029/2007GL031589.

Joussaume, S. (1990), Three-Dimensional Simulations of the Atmospheric Cycle of Desert Dust Particles Using a General Circulation Model, *J. Geophys. Res.*, *95*(D2), 1909–1941.

Kahn, R., W.-H. Li, C. Moroney, D. J. Diner, J. V. Martonchik, and E. Fishbein (2007), Aerosol source plume physical characteristics from space-based multiangle imaging, *J. Geophys. Res.*, *112*(D11), D11,205, doi:10.1029/2006JD007647.

Kalu, A. E. (1979), The African dust plume: Its characteristics and propagation across west Africa in winter, *SCOPE*, *14*, 95–118.

Kaplan, J. O. (2001), Geophysical applications of vegetation modeling, Ph.D. thesis, Dep. of Ecol., Lund Univ., Lund, Sweden.

Karyampudi, V. M., S. P. Palm, J. A. Reagen, H. Fang, W. B. Grant, R. M. Hoff, C. Moulin, H. F. Pierce, O. Torres, E. V. Browell, and S. H. Melfi (1999), Validation of the Saharan Dust Plume Conceptual Model Using Lidar, Meteosat, and ECMWF Data, *Bull. Amer. Meteor. Soc.*, *80*(6), 1045–1075.

Kidder, S. Q., and T. H. Vonder Haar (1995), *Satellite meteorology: an introduction*, Academic Press, San Diego, California.

King, M. D., Y. J. Kaufman, D. Tanre, and T. Nakajima (1999), Remote Sensing of Tropospheric Aerosol from Space: Past, Present, and Future, *Bull. Amer. Meteor. Soc.*, *80*(11), 2229–2259.

Knippertz, P., and A. H. Fink (2006), Synoptic and dynamic aspects of an extreme springtime Saharan dust outbreak, *Quart. J. R. Met. Soc.*, *132*, 1153–1177, doi: 10.1256/qj.05.109.

Knippertz, P., C. Deutscher, K. Kandler, K. Müller, T. Schulz, and L. Schütz (2007), Dust mobilization due to density currents in the Atlas region: Observations from the SAMUM 2006 field campaign, *J. Geophys. Res.*, *112*, D21,109, doi:10.1029/2007JG008774.

Knorr, W., and M. Heimann (1995), Impact of drought stress and other factors on seasonal land biosphere CO_2 exchange studied through and atmospheric tracer model, *Tellus, Ser. B*, *47*, 471–489.

Kohfeld, K. E., and S. E. Harrison (2001), DIRTMAP: the geological record of dust, *Earth-Science Rev.*, *54*(1-3).

Koren, I., Y. Kaufman, R. Washington, M. C. Todd, Y. Rudich, J. V. Martins, and D. Rosenfeld (2006), The Bodélé depression: a single spot in the Sahara that provides most of the mineral dust to the Amazon forest, *Environ. Res. Lett.*, *1*, 014,005, doi: 10.1088/1748-9326/1/1/014005.

Kraus, H. J., J. Malcher, and E. Schaller (1985), Nocturnal low-level jet during PUKK, *Bound.-Layer Meteor.*, *38*, 1–22.

Kubilay, N., S. Nickovic, C. Moulin, and F. Dulac (2000), An illustration of the transport and deposition of mineral dust onto the eastern Mediterranean, *Atmos. Environ.*, *34*(8), 1293–1303.

Laurent, H., N. D'Amato, and t. Lebel (1998), How important is the contribution of the mesoscale convective complexes to the Sahelian rainfall?, *Phys. Chem. Earth*, *23*, 629–633.

Lee, I. (1983), Simulation of transport and removal processes of Saharan dust, *J. Climate Appl. Meteor.*, *22*, 632–639.

Legrand, M., J. J. Nertrand, M. Desbois, L. Menenger, and Y. Fouquart (1989), The potential of infrared satellite data for the retrieval of Saharan dust optical depth over Africa, *J. Climate Appl. Meteor.*, *28*, 309–318.

Legrand, M., A. Plana-Fattori, and C. N'Doume (2001), Satellite detection of dust using the IR imagery of Meteosat 1. Infrared difference dust index, *J. Geophys. Res.*, *106*(D16), 18,251–18,274.

Lenschow, D. H., and B. Stankov (1979), The Rapid Morning Boundary-Layer Transition, *J. Atmos. Sci.*, *36*, 2108–2124.

Leroux, M. (1983), *Le climate de l'Afrique tropicale*, 633 pp., Editions Champion, Paris.

Levin, Z., E. Ganor, and V. Gladstein (1996), The Effects of Desert Particles Coated with Sulfate on Rain Formation in the Eastern Mediterranean, *J. Appl. Meteor.*, *35*, 1511–1523.

Littmann, T. (1991), Dust strom frequency in Asia: Climatic control and variablity, *Int. J. Climatol.*, *11*, 393–412.

Liu, D., Z. Wang, Z. Liu, D. Winker, and C. Trepte (2008), A height resolved global view of dust aerosols from the first year CALIPSO lidar measurement, *J. Geophys. Res.*, *113*(D14), D16,214, doi:10.1029/2007JD009776.

Liu, X., Z.-Y. Yin, X. Zhang, and Y. Yang (2004), Analyses of the spring dust storm frequency of northern China in relation to antecedent and current wind, precipitation, vegetation, and soil moisture conditions, *J. Geophys. Res.*, *109*, D16,210, doi: 10.1029/2004JD004615.

Lohmann, U. (2002), Possible aerosol effects on ice clouds via contact nucleation, *J. Atmos. Sci.*, *59*, 647–656.

Loosmore, G. A., and J. R. Hunt (2000), Below-threshold, non-abraded dust resuspension, *J. Geophys. Res.*, *105*, 20,663–20,671.

Luo, C., N. Mahowald, and J. del Corral (2003), Sensitivity study of meteorological parameters on mineral aerosol mobilization, transport, and distribution, *J. Geophys. Res.*, *108*(D15), 4447, doi:10.1029/2003JD003483.

Lyamani, H., F. J. Olmo, and L. Alados-Arboledas (2005), Saharan dust outbreak over southeastern Spain as detected by sun photometer, *Atmos. Environ.*, *39*(38), 7276–7284.

Mahowald, N., R. G. Bryant, J. del Corral, and L. Steinberger (2003), Ephemeral lakes and desert dust sources, *Geophys. Res. Lett.*, *30*(2), 1074, doi:10.1029/2002GL016041.

Mahowald, N. M., A. R. Baker, G. Bergametti, N. Brooks, R. A. Duce, T. D. Jickells, N. Kubilay, J. M. Prospero, and I. Tegen (2005), Atmospheric global dust cycle and iron inputs to the ocean, *Global Biogeochem. Cycles*, *19*, GB4025, doi: 10.1029/2004GB002402.

Mahowald, N. M., J. A. Ballantine, J. Feddema, and N. Ramankutty (2007), Global trends in visibility: implications for dust sources, *Atmos. Chem. Phys.*, *7*, 3309–3339.

Mahrt, L. (1985), Vertical Structure and Turbulence in the Very Stable Boundary Layer, *J. Atmos. Sci.*, *42*(22), 2333–2349.

Mahrt, L. (1999), Stratified Atmospheric Boundary Layers, *Bound.-Layer Meteor.*, *90*, 375–396.

Mahrt, L., J. Sun, W. Blumen, T. Delany, and S. Oncley (1998), Nocturnal Boundary-Layer Regimes, *Bound.-Layer Meteor.*, *88*, 255–278.

Marshall, J. S., and W. M. Palmer (1948), The distribution of raindrops with size, *J. Meteor.*, *5*, 165–166.

Marticorena, B., and G. Bergametti (1995), Modeling the atmospheric dust cycle: 1. Design of a soil-derived dust emission scheme, *J. Geophys. Res.*, *100*(D8), 16,415–16,430.

Marticorena, B., G. Bergametti, B. Aumont, Y. Callot, C. N'Doume, and M. Legrand (1997), Modeling the atmospheric dust cycle: 2. Simulation of Saharan dust sources, *J. Geophys. Res.*, *102*(D4), 4387.

Marticorena, B., P. Chazette, G. Bergametti, F. Dulac, and M. Legrand (2004), Mapping the aerodynamic roughness length of desert surface from the POLDER/ADEOS bi-directional reflectance product, *Int. J. Remote Sens.*, *25*(3), 603–626.

Mattsson, J. O., and T. Nihlen (1996), The transport of Saharan dust to southern Europe: a scenario., *Journal of Arid Environments*, *32*(2), 111–119.

Mauritsen, T., and G. Svensson (2007), Observations of Stably Stratified Shear-Driven Atmospheric Turbulence at Low and High Richardson Numbers, *J. Atmos. Sci.*, *64*(2), 645–655, doi:10.1175/JAS3856.1.

Mbourou, G. N., J. J. Bertrand, and S. E. Nicholson (1997), The Diurnal and Seasonal Cycles of Wind-Borne Dust over Africa North of the Equator, *J. Appl. Meteor.*, *36*, 868–882.

McConnell, C. L., E. J. Highwood, H. Coe, P. Formenti, B. Anderson, S. Osborne, S. Nava, K. Desboeufs, G. Chen, and M. A. J. Harrison (2008), Seasonal variations of the physical and optical characteristics of Saharan dust: results from the Dust Outflow and Deposition to the Ocean (DODO) experiment, *J. Geophys. Res.*, *113*(D14), D14S05, doi:10.1029/2007JD009606.

McKendry, I. G., J. P. Hacker, and R. Stull (2001), Long-range transport of asian dust to the Lower Fraser Valley, British Columbia, Canada, *J. Geophys. Res.*, *106*, 18,361–18,370.

McNider, R. T., and R. A. Pielke (1981), Diurnal Boundary-Layer Development over Sloping Terrain, *J. Atmos. Sci.*, *38*(10), 2198–2212.

McNider, R. T., M. Singh, and J. T. Lin (1993), Diurnal Wind-Structure Variations and Dispersion of Pollutants in the Boundary Layer, *Atmos. Environ.*, *27A*, 2199–2214.

Menut, L., G. Forêt, and G. Bergametti (2007), Sensitivity of mineral dust concentrations to the model size distribution accuracy, *J. Geophys. Res.*, *112*, D10,210, doi: 10.1029/2006JD007766.

Meskhidze, N., W. L. Chameides, A. Nenes, and G. Chen (2003), Iron mobilization in mineral dust: Can anthropogenic SO_2 emission affect ocean productivity?, *Geophys. Res. Lett.*, *30*(21), 2085, doi:10.1029/2003GL018035.

Meskhidze, N., W. L. Chameides, and A. Nenes (2005), Dust and pollution: A recipe for enhanced ocean fertilization?, *J. Geophys. Res.*, *110*(D3), D03,301, doi: 10.1029/2004JD005082.

Middleton, N. J., and A. S. Goudie (2001), Saharan dust: sources and trajectories, *Trans. Inst. Br. Geogr.*, *26*, 165–181.

Miller, R., and I. Tegen (1999), Radiative Forcing of a Tropical Direct Circulation by Soil Dust Aerosols, *J. Atmos. Sci.*, *56*, 2403–3433.

Moore, C. M., M. M. Mills, A. Milne, R. Langlois, E. P. Achterberg, K. Lochte, R. J. Geider, and J. L. Roche (2006), Iron limits primary productivity during spring bloom development in the central North Atlantic, *Global Change Biology*, *12*, 626–634, doi: 10.1111/j.1365-2486.2006.01122.x.

Moulin, C., C. E. Lambert, F. Dulac, and U. Dayan (1997), Control of atmospheric export of dust from North Africa by the North Atlantic oscillation, *Nature*, *387*(6634), 691–694.

Moulin, C., C. E. Lambert, U. Dayan, V. Masson, M. Ramonet, P. Bousquet, M. Legrand, Y. J. Balkanski, W. Guelle, B. Marticorena, G. Bergametti, and F. Dulac (1998), Satellite climatology of African dust transport in the Mediterranean atmosphere, *J. Geophys. Res.*, *103*(D11), 13,137–13,144.

Murphy, E. A., R. B. D'Agostino, and J. P. Noonan (1982), Patterns in the Occurrences of Richardson Numbers Less Than Unity in the Lower Atmosphere, *J. Appl. Meteor.*, *21*, 321–333.

Nappo, C. J. (1991), Sporadic Breakdowns of Stability in the PBL over Simple and Complex Terrain, *Bound.-Layer Meteor.*, *54*, 69–87.

Neuer, S., M. E. Torres-Padrón, M. D. Gelado-Caballero, M. J. Rueda, J. Hernández-Brito, R. Davenport, and G. Wefer (2004), Dust deposition pulses to the eastern subtropical North Atlantic gyre: Does ocean's biogeochemistry respond?, *Global Biogeochem. Cycles*, *18*, GB4020, doi:10.1029/2004GB00228.

Nickovic, S., G. Kallos, A. Papadopoulos, and O. Kakaliagou (2001), A model for prediction of desert dust cycle in the atmosphere, *J. Geophys. Res.*, *106*(D16), 18,113–18,129.

Ott, S. T., A. Ott, D. W. Martin, and J. A. Young (1991), Analysis of a trans-Atlantic Saharan dust outbreak based on satellite and GATE data, *Mon. Wea. Rev.*, *119*(8), 1832–1850.

Pacyna, J. M. (1995), *Sources, Particle Size Distribution and Transport of Aerosol*, Springer-Verlag, Berling, Heidelberg.

Parker, D. J., R. R. Burton, A. Diongue-Niang, R. J. Ellis, M. Felton, C. M. Taylor, C. D. Thorncroft, P. Bessemoulin, and A. M. Tompkins (2005), The diurnal cycle of the West African monsoon circulation, *Quart. J. R. Met. Soc.*, *131*, 2839–2860, doi: 10.1256/qj.04.52.

Parker, M. D., and R. H. Johnson (2000), Organizational modes of midlatitude mesoscale convective systems, *Mon. Wea. Rev.*, *128*(10), 3413–3436, doi:10.1256/qj.04.52.

Payne, S. W., and M. M. McGarry (1977), The relationship of satellite inferred convective activity to easterly waves over West Africa and the adjacent ocean during phase III of GATE, *Mon. Wea. Rev.*, *105*, 413–420.

Peagle, J., M. McCorcle, and E. Miller (1984), Diagnoses and numerical simulation of a low-lewel jet during ALPEX, *Contirb. Atmpos. Phys.*, *57*, 419–430.

Pérez, C., S. Nickovic, J. M. Baldasano, M. Sicard, and F. Rocadenbosch (2003), A long Saharan dust event over the western Mediterranean: Lidar, Sun photometer observations, and regional dust modeling, *J. Geophys. Res.*, *111*, D15,214.

Perlwitz, J., I. Tegen, and R. L. Miller (2001), Interactive soil dust aerosol model in the GISS GCM: 1. Sensitivity of the soil dust cycle to radiative properties of soil dust aerosols, *J. Geophys. Res.*, *106*, 18,167–18,192.

Perry, K. D., T. A. Cahill, R. A. Eldred, D. D. Dutcher, and T. E. Gill (1997), Long-range transport of North African dust to the eastern United States, *J. Geophys. Res.*, *102*(D10), 11,225–11,238.

Pinzon, J. (2002), Using HHT to Successfully Uncouple Seasonal and Interannual Components in Remotely Sensed Data, in *SCI 2002 Conference Proceedings July 14-18*, edited by N. Huang, SCI Int., Orlando, Florida.

Pinzon, J., M. E. Brown, and C. J. Tucker (2005), *Satellite time series correction of orbital drift artefacts using empirical mode decomposition*, pp. 167–186, World Sci., Tokyo.

Poulos, G. S., W. Blumen, D. C. Fritts, J. K. Lundquist, J. Sun, S. P. Burns, C. Nappo, R. Banta, R. Newsom, J. Cuyart, E. Terradellas, B. Balsley, and M. Jensen (2002), CASES-99: A comprehensive investigation of the stable nocturnal boundary layer, *Bull. Amer. Meteor. Soc.*, *88*, 555–581.

Prata, A. J. (1989), Observations of volcanic ash clouds in the 10-12 μm window using AVHRR/2 data, *Int. J. Remote Sens.*, *10*, 751–761.

Prigent, C., I. Tegen, F. Aires, B. Marticorena, and M. Zribi (2005), Estimation of the aerodynamic roughness length in arid and semi-arid regions over the globe with the ERS scatterometer, *J. Geophys. Res.*, *110*(D9), D09,205.

Prospero, J. M. (1999), Long-term measurements of the transport of African mineral dust to the southeastern United states: Implications for regional air quality, *J. Geophys. Res.*, *D13*, 15,917–15–927.

Prospero, J. M., and P. J. Lamb (2003), African droughts and dust transport to the Caribbean: climate change implications, *Science*, *302*(5647), 1024–1027.

Prospero, J. M., and R. T. Nees (1986), Impact of the North African Drought and El-Nino on mineral dust in the Barbados trade winds, *Nature*, *320*(6064), 735–738.

Prospero, J. M., R. A. Glaccum, and R. T. Nees (1981), Atmospheric transport of soil dust from Africa to South America, *Nature*, *289*, 570–572.

Prospero, J. M., K. Barrett, T. Church, F. Dentener, R. A. Duce, J. N. Galloway, H. Levy, J. Moody, and P. Quinn (1996), Atmospheric deposition of nutrients to the North Atlantic Basin, *Biogeochemistry*, *35*, 27–73.

Prospero, J. M., P. Ginoux, O. Torres, S. E. Nicholson, and T. E. Gill (2002), Environmental characterization of global sources of atmospheric soil dust identified with the Nimbus 7 Total Ozone Mapping Spectrometer (TOMS) absorbing aerosol product, *Rev. Geophys.*, *40*(1), 1002, doi:10.1029/2000RG000095.

Prospero, J. M., E. Blades, G. Mathison, and R. Naidu (2005), Interhemispheric transport of viable fungi and bacteria from Africa to the Caribbean with soil dust, *Aerobiologica*, *21*(1), 1–19.

Psenner, R. (1999), Living in a dusty world: airborne dust as a key factor for alpine lakes, *Water, Air and Soil Pollution*, *112*(3-4), 217–227.

Pye, K. (1987), *Aeolian Dust and Dust Deposits*, Academic Press London.

Qian, W. H., L. S. Quan, and S. Y. Shi (2002), Variations of the dust storm in China and its climatic control, *J. Clim.*, *15*(10), 1216–1229.

Ramel, R., H. Gallée, and C. Messager (2006), On the northward shift of the West African monsoon, *Clim. Dyn.*, *26*(4), 429–440.

Redelsperger, J.-L., C. D. Thorncroft, A. Diedhiou, T. Lebel, D. J. Parker, and J. Polcher (2006), African monsoon multidisciplinary analysis: An international research project and field campaign, *Bull. Amer. Meteor. Soc.*, *87*(12), 1739–1746, doi:10.1175/BAMS-87-12-1739.

Riemer, N., O. M. Doherty, and S. Hameed (2006), On the variability of African dust transport across the Atlantic, *Geophys. Res. Lett.*, *33*(13), L13,814, doi: 10.1029/2006GL026163.

Rogora, M., R. Mosello, and A. Marchetto (2004), Long-term trends in the chemistry of atmospheric deposition in Northwestern Italy: the role of increasing Saharan dust deposition, *Tellus*, *56B*(5), 426–434.

Rosenfeld, D., Y. Rudich, and R. Lahav (2001), Desert dust suppressing precipitation: A possible desertification feedback loop, *PNAS*, *98*(11), 5975–5980.

Ryall, D. B., R. G. Derwent, A. J. Manning, A. L. Redington, J. Corden, W. Millington, P. G. Simmonds, S. O'Doherty, N. Carslaw, and G. W. Fuller (2002), The origin of high particulate concentrations over the United Kingdom, March 2000, *Atmos. Environ.*, *36*(8), 1363–1378.

Sarthou, G., A. R. Baker, S. Blain, E. P. Achterberg, M. Boye, A. R. Bowie, P. Croot, P. Laan, H. J. W. de Baar, T. D. Jickells, and P. J. Worsfold (2003), Atmospheric iron deposition and sea-surface dissolved iron concentrations in the eastern Atlantic Ocean, *Deep-Sea Research Part I*, *50*, 1339–1352, doi:10.1016/S0967-0637(03)00126-2.

Sarthou, G., A. R. Baker, J. Kramer, P. Laan, A. Laës, S. Ussher, E. P. Achterberg, J. H. W. de Baar, K. R. Timmermans, and S. Blain (2007), Influence of atmospheric inputs on the iron distribution in the subtropical North-East Atlantic Ocean, *Mar. Chem.*, *104*, 186–202, doi:10.106/j.marchem.2006.11.004.

Sassen, K., P. J. DeMott, J. M. Prospero, and M. R. Poellot (2003), Saharan dust storms and indirect aerosol effects on clouds: CRYSTAL-FACE results, *Geophys. Res. Lett.*, *30*(12), L1633.

Schepanski, K., I. Tegen, B. Laurent, B. Heinold, and A. Macke (2007), A new Saharan dust source activation frequency map derived from MSG-SEVIRI IR-channels, *Geophys. Res. Lett.*, *34*(18), L18,803, doi:10.1029/2007GL030168.

Schepanski, K., I. Tegen, and A. Macke (2008a), Saharan Dust Transport and Deposition towards the Tropical Northern Atlantic, *Atmos. Chem. Phys. Discuss.*, *8*, 16,061–16,096.

Schepanski, K., I. Tegen, M. C. Todd, B. Heinold, G. Bönisch, B. Laurent, and A. Macke (2008b), Meteorological processes forcing Saharan dust emission inferred from MSG-SEVIRI observations of sub-daily dust source activation, *J. Geophys. Res.*, revised.

Schmetz, J., P. Pili, S. Tjemkes, D. Just, J. Kerkmann, S. Rota, and A. Ratier (2002), An introduction to Meteosat Second Generation (MSG), *Bull. Amer. Meteor. Soc.*, *83*, 977–992.

Schütz, L. (1980), Long range transport of desert dust with special emphasis on the Sahara, *Ann. N. Y. Acad. Sci.*, *338*, 515–532.

Schwikowski, M., P. Seibert, U. Baltensperger, and H. W. Gaggeler (1995), A study of an outstanding Saharan dust event at the high-Alpine Site Jungfraujoch, Switzerland, *Atmos. Environ.*, *29*(15), 1829–1842.

Shao, Y. (2000), *Physics and Modelling of Wind Erosion*, Kluwer Academic Publishers.

Shao, Y. (2001), A model for mineral dust emission, *J. Geophys. Res.*, *106*(D17), 20,239–20,254.

Shao, Y., M. R. Raupach, and P. A. Findlater (1993), The effect of saltation bombardment on the entrainment of dust by wind, *J. Geophys. Res.*, *98*, 12,719–12,726.

Shao, Y., M. R. Raupach, and J. F. Leys (1996), A model for predicting aeolian sand drift and dust entrainment on scales from paddock to region, *Aust. J. Soil Res.*, *34*, 309–342.

Shenk, W. E., and R. J. Curran (1974), The detection of dust storms over land and water with satellite visible and infrared measurements, *Mon. Wea. Rev.*, *102*, 830–837.

Sijikumar, S., P. Roucou, and B. Fontaine (2006), Monsoon onset over Sudan-Sahel: Simulation by the regional scale model MM5, *Geophys. Res. Lett.*, *33*, L03,814, doi: 10.1029/2005GL024819.

Skammarock, W. C., and J. B. Klemp (1992), The stability of time-split numerical methods for the hydrostatic and the non-hydrostatic elastic equations, *Mon. Wea. Rev.*, *120*, 2109–2127.

Sokolik, I. N. (2002), The spectral radiative signature of wind-blown mineral dust: Implications for remote sensing in the thermal IR region, *Geophys. Res. Lett.*, *29*(24), 2154, doi:10.1029/2002GLR015910.

Sokolik, I. N., and O. B. Toon (1996), Direct radiative forcing by anthropogenic mineral aerosols, *Nature*, *381*, 681–683.

Sokolik, I. N., D. M. Winker, G. Bergametti, G. D. A, G. Carmichael, Y. J. Kaufman, L. Gomes, L. Schuetz, and J. E. Penner (2001), Introduction to special section: Outstanding problems in quantifying the radiative impacts of mineral dust, *J. Geophys. Res.*, *106*(D16), 18,015–18,027.

Solot, S. B. (1959), General circulation over the Angolo-Egyptian Sudan and adjacent regions, *Bull. Amer. Meteor. Soc.*, *31*, 85–94.

Sorbjan, Z. (2006), Local Structure of Turbulence in Stably Stratified Boundary Layers, *J. Atmos. Sci.*, *63*, 1526–1537.

Stensrud, D. J. (1996), Importance of Low-Level Jets to Climate: A Review, *J. Climate*, *9*, 1698–1711.

Steppler, J., G. Doms, U. Schättler, H. W. Bitzer, A. Gassmann, U. Damrath, and G. Gregoric (2003), Meso-gamma scale forecasts using the nonhydrostatic model LM, *Meteor. Atmos. Phys.*, *82*, 75–96.

Stull, R. B. (1988), *An Introduction to Boundary Layer Meteorology*, NATO Asi Series. Series C, Mathematical and Physical Science, 680 pp., Springer Verlag.

Sultan, B., and S. Janicot (2003), The West African monsoon dynamics. Part II: The "Preonset" and "Onset" of the summer monsoon, *J. Climate*, *16*, 3407–3427.

Sultan, B., K. Labadi, J. F. Guegan, and S. Janicot (2005), Climate drives the meningitis epidemics onset in West Africa, *Plos Medicine*, *2*(1), 43–49.

Sultan, B., S. Janicot, and R. Drobinski (2006), Characterization of the Diurnal Cycle of the West African Monsoon around the Monsoon Onset, *J. Climate*, *20*, 4014–4032.

Swap, R., M. Garstang, S. Greco, R. Talbot, and P. Kallberg (1992), Saharan dust in the Amazon Basin, *Tellus B*, *44*, 133–149.

Tegen, I., and I. Fung (1994), Modeling of mineral dust in the atmosphere: Sources, transport, and optical thickness, *J. Geophys. Res.*, *99*(D11), 22,896–22,914.

Tegen, I., and A. A. Lacis (1996), Modeling of particle size distribution and its influence on the radiative properties of mineral dust aerosol, *J. Geophys. Res.*, *101*(D14), 19,237–19,244.

Tegen, I., S. P. Harrison, K. Kohfeld, and I. C. Prentice (2002), Impact of vegetation and preferential source areas on global dust aerosol: Results from a model study, *J. Geophys. Res.*, *107*(D21), 4576, doi:10.1029/2001JD000963.

Tegen, I., B. Heinold, M. Todd, J. Helmert, R. Washington, and O. Dubovik (2006), Modelling soil dust aerosol in the Bodélé depression during the BoDEx campaign, *Atmos. Chem. Phys.*, *6*, 4345–4339.

Thomas, F. G. (1982), Saharan dust-fall in Dover, Kent, *J. Meteor.*, *7*, 92–93.

Thorncroft, C., and K. Hodges (2001), African easterly wave variability and its relationship to Atlantic tropical cyclone activity, *J. Climate*, *14*(6), 1166–1179.

Thorncroft, C. D., and M. Blackburn (1999), Maintance of the African easterly jet, *Quart. J. R. Met. Soc.*, *125*, 763–786.

Thorpe, A. J., and T. H. Guymer (1977), The nocturnal jet, *Quart. J. R. Met. Soc.*, *103*, 633–653.

Tiedtke, M. (1989), A comprehensive mass flux scheme for cumulus parametrisation in large-scale models, *Mon. Wea. Rev.*, *117*, 1779–1799.

Todd, M., R. Washington, J. V. Martins, O. Dubovik, G. Lizcano, S. M'Baimayel, and S. Engelstaedter (2007), Mineral dust emission from the Bodélé Depression, nothern Chad, during BoDEx 2005, *J. Geophys. Res.*, *112*(D6), D06,207, doi: 10.1029/2006JD007170.

Todd, M. C., R. Washington, S. Raghavan, G. Lizcano, and P. Knippertz (2008), Regional Model Simulations of the Bodélé Low-level Jet of Northern Chad during the Bodélé Dust Experiment (BoDEx 2005), *J. Climate*, *21*, 995–1012, doi: 10.1175/2007JCLI1766.1.

Tsai, F., G. T.-J. Chen, T.-H. Liu, W.-D. Lin, and J.-Y. Tu (2008), Characterizing the transport pathways of Asian dust, *J. Geophys. Res.*, *113*, D17,311, doi: 10.1029/2007JD009674.

Tsyro, S., and L. Erdman (2000), Parameterisation of aerosol deposition processes in EMEP MSC-E and MSC-W transport models, *EMEP/MSC-W Note 7/00*, Norwegian Meteorol. Inst., Oslo, Norway.

Tucker, C. J., J. E. Pinzon, M. E. Brown, D. Slayback, E. W. Park, R. V. E. Mahoney, and N. El Saleous (2005), An extend AVHRR 8-km NDVI data set compatible with MODIS and SPOT vegetation NDVI data, *Int. J. Remote Sens.*, *26*(20), 4485–4498.

Tulet, P., M. Mallet, V. Pont, J. Pelon, and A. Boone (2008), The 7-13 March 2006 dust strom over West Africa: Generation, transport, and vertical stratification, *J. Geophys. Res.*, *113*, D00C08, doi:10.1029/2008JD009871.

Van de Wiel, B. J. H., A. F. Moene, O. K. Hartogensis, H. A. R. D. Bruin, and A. A. M. Holtslag (2003), Intermittent Turbulence in the Stable Boundary Layer over Land. Part III: A Classification for Observations during CASES-99, *J. Atmos. Sci.*, *60*, 2509–2522.

VanCuren, R. A. (2003), Asian aerosols in North America: Extractin the chemical composition and mass concentration of the Asian continental aerosol plume from long-term aerosol records in the western United States, *J. Geophys. Res.*, *108*(D20), 4623, doi: 10.1029/2003JD003459.

Veihelmann, B., P. F. Levelt, P. Stammes, and J. P. Veefkind (2007), Simulation study of the aerosol information content in OMI spectral reflectance measurements, *Atmos. Chem. Phys.*, *7*, 3115–3127.

Wald, A. E., Y. J. Kaufman, D. Tanre, and B.-C. Gao (1998), Daytime and nighttime detection of mineral dust over desert using infrared spectral contrast, *J. Geophys. Res.*, *103*(D24), 32,307–32,313.

Walker, H. O. (1958), The Monsoon in West Africa, *Note*, Ghana Met. Dept., Accra.

Washington, R., and M. C. Todd (2005), Atmospheric controls on mineral dust emission from the Bodélé Depression, Chad: The role of the low level jet, *Geophys. Res. Lett.*, *32*, L17,701, doi:10.1029/2005GL023597.

Washington, R., M. Todd, N. J. Middleton, and A. S. Goudie (2003), Dust-Storm Source Areas Determined by the Total Ozone Monitoring Spectrometer and Surface Observations, *Annals of the Association of American Geographers*, *93*(2), 297–313.

Washington, R., M. C. Todd, S. Engelstaedter, S. Mbainayel, and F. Mitchell (2006a), Dust and the low-level circulation over the Bodele Depression, Chad: Observations from BoDEx 2005, *J. Geophys. Res.*, *111*(D3), D03,201.

Washington, R., M. C. Todd, G. Lizcano, I. Tegen, C. Flamant, I. Koren, P. Ginoux, S. Engelstaedter, C. S. Bristow, C. S. Zender, A. S. Goudie, A. Warren, and J. M. Prospero (2006b), Links between topography, wind, deflation, lakes and dust: The case of the Bodele depression, Chad, *J. Geophys. Res.*, *33*, L09,401, doi:10.1029/2006GL025827.

Weaver, C. J., P. Ginoux, N. C. Hsu, M.-D. Chou, and J. Joiner (2001), Radiative Forcing of Saharan Dust: GOCART Model Simulations Compared with ERBE Data, *J. Atmos. Sci.*, *59*(3), 736–747.

Wedepohl, K. H. (1995), The composition of the continental crust, *Geochemica et Cosmochimica Acta*, *59*(7), 1217–1232.

Weischet, W., and W. Endlicher (2000), *Regional Klimatologie, Teil 2: Die alte Welt*, Teubner Verlag, Stuttgart.

Westphal, D., O. Toon, and T. Carlson (1987), A Two–Dimensional Numerical Investigation of the Dynamics and Microphysics of Saharan Dust Storms, *J. Geophys. Res.*, *92*(D3), 3027–3049.

Wilkening, K. E., L. A. Barrie, and M. Engle (2000), Trans-Pacific air pollution, *Science*, *290*, 65–67.

Wolke, R., O. Hellmuth, O. Knoth, W. Schröder, B. Heinrich, and E. Renner (2004a), The chemistry-transport modeling system LM-MUSCAT: Description and CityDelta applications, in *Air Pollution Modeling and Its Application XVI*, edited by C. Borrego and S. Incecik, pp. 427–437, Proceedings of twenty-sixth NATO/CCMS international technical meeting on air pollution modeling and its application.

Wolke, R., O. Hellmuth, O. Knoth, W. Schröder, and E. Renner (2004b), The parallel model system LM-MUSCAT for chemistry-transport simulations: Coupling scheme, parallelization and application, *Parallel Computing: Software Technology, Algorithms, Architectures, and Applications*, pp. 363–370.

Wurzler, S., T. G. Reisin, and Z. Levin (2000), Modification of mineral dust particles by cloud processing and subsequent effects on drop size distribution, *J. Geophys. Res.*, *105*, 4501–4512.

Zender, C. S., and D. Newman (2003), Spatial heterogeneity in aeolian erodibility: Uniform, topographic, geomorphic, and hydrologic hypotheses, *J. Geophys. Res.*, *108*(D17), 4543, doi:10.1029/2002JD003039.

Zender, C. S., H. Bian, and D. Newman (2003), Mineral Dust Entrainment And Deposition (DEAD) model: Description and 1990s dust climatology, *J. Geophys. Res.*, *108*(D14), 4416, doi:10.1029/2002JD002775.

Zhang, L., S. Gong, J. Padro, and L. Barrie (2001), A size-segregated particle dry deposition scheme for an atmospheric aerosol module, *Atmos. Environ.*, *35*, 549–560.

Zhang, P., N. Lu, X. Hu, and C. Dong (2006), Identification and physical retrieval of dust storm using three MODIS thermal IR channels, *Global and Planetary Change*, *52*, 197–206, doi:10.1016/jgloplacha.2006.02.014.

Zhang, X. Y., S. L. Gong, Z. X. Shen, F. M. Mei, X. X. Xi, L. c. Liu, Z. J. Zhou, D. Wang, Y. Q. Wang, and Y. Cheng (2003), Characterization of soil dust aerosol in China and its transport and distribution during 2001 ACE-Asia: 1. Network observations, *J. Geophys. Res.*, *108*(D9), 4261, doi:10.1029/2002JD002632.

Zhao, T. L., S. L. Gong, X. Y. Zhang, J.-P. Blanchet, I. G. McKendry, and Z. J. Zhou (2006), A Simulated Climatology of Asian Dust Aerosol and Its Trans-Pacific Transport. Part I: Mean Climate and Validation, *JoCys*, *19*, 88–103.

Zobler, L. (1986), A world soil file for global climate modeling, *NASA Tech. Memo.*, NASA, Washington, D.C.

Acknowledgement

First of all, I want to thank all those people, who accompanied me but are not mentioned explicitly.

Many thanks to Prof. Dr. A. Macke and Dr. I. Tegen for supporting the development of this thesis, advice and discussion.

Thanks to Dr. Benoit Laurent for reading and critical discussion.

Furthermore, thanks to all colleagues of the "Modelling Department" at the IfT in Leipzig and the "Maritime Meteorologie" at the IFM-GEOMAR in Kiel for support and computing environment. The collaboration of both institutes allowed for an interesting and interdisciplinary view on Saharan dust.

Finally, I would like to thank my parents for their assistance and encouragement.

This work was performed in the frame of the network project TRACES (Ocean–Atmosphere–Land Impacts on TRopical AtlantiC EcoSystems) funded by the Wissenschaftsgemeinschaft Gottfried Willhelm Leibniz.

Erklärung

Hiermit bestätige ich, dass ich die vorliegende Dissertation selbstständig verfasst und keine anderen als die angegebenen Quellen und Hilfsmittel verwendet habe.
Ich versichere, dass diese Arbeit noch nicht zur Erlangung eines Doktorgrades an anderer Stelle vorgelegen hat.
Ich erkläre, dass die vorliegende Arbeit gemäß der Grundsätze zur Sicherung guter wissenschaftlicher Praxis der Deutschen Forschungsgemeinschaft erstellt wurde.

Kiel, Dezember 2008

(Kerstin Schepanski)